

UNIVERSITY OF NAVARRA
SCHOOL OF ENGINEERING
DONOSTIA-SAN SEBASTIÁN



IMPROVING THE PIPELINE OF AN OPTICAL
METROLOGY SYSTEM

DISSERTATION
submitted for the
Degree of Doctor of Philosophy
of the University of Navarra by

Desmond Kehinde Moru

under the supervision of

Diego Borro Yágüez

July, 2020

To:
My Parents

Acknowledgement

The years of the thesis have flown so fast, and have given me a lot of technical knowledge, but even more importantly, it has made me understand the value of a job well done, perseverance, patience, rest and even failure. I would not have come this far without the support of all those people who have been around me and who have helped me so much. To all of them millions of thanks, I will always owe you.

I would especially like to express my gratitude to the management and staff of TECNUN and CEIT for the trust, responsibility and opportunity given to me to carry out the doctoral thesis within the vision and robotics group. Many thanks.

To my director Diego Borro. Thank you! I am grateful for all the time and effort you have invested in me and in the projects, we have developed together. Always ready to discuss problems and give your honest opinion. Thank you for your trust, bringing me calm and tranquility in the most difficult moments, which have been many.

To my friends and colleagues, who have made the day to day more bearable. For the conversations at "coffee time", the laughter, the celebrations and the dinners. I am sure that the years of the thesis would have been more unbearable without you. It has been a pleasure to share these experiences with you. Also to all the people, I have worked with these years at the vision and robotic group, people who welcomed me and made me feel part of the team. I have met incredible people with whom I will surely continue sharing great moments.

I would also like to express my gratitude to the Colegio Mayor Ayete, where I have lived and have been cared for these years. The experience has been nothing short of a home full with warmth.

To the staff and colleagues at Pan Atlantic University (PAU), for all the support and concern that you have extended to me during these years. I express my gratitude and appreciation.

A special thanks to my family, especially my parents. Even though I have been far away, I have always felt your closeness and affection through the years. If I have come this far, it is undoubtedly to your support and prayers. Many thanks.

Abstract

Metrology is one of the many applications of machine vision, which has the advantage that allows for the analyzing of a total production batch that leaves an assembly line without supposing a bottleneck. As a result, quality control become a priority in the inspection processes of industrial manufacturing. Due to the advancement of technology and the realizations of Industry 4.0, smart factories demand high precision and accuracy in the measurements and inspection of industrial products. Machine vision technology provide image-based inspection and analysis for such demanding applications. With the use of software, sensors, cameras and robot guidance, such integrated systems can be realized. Machine vision highlights a growing trend in industrial systems. As camera sensors become smarter, the quality of data produced offers accuracy into the systems operations.

This thesis is a study of the typical vision system pipeline, in the different phases, necessary to achieve optimal inspection in an industrial operation. The first step is the study of the light alignment to monitor and achieve an optimal light alignment system, in order to eliminate the effects of misalignment. The algorithm was tested with a not-optimal system to ascertain its efficiency and effectiveness. In the second phase, a deep study of the calibration process is carried out to address the effect of different parameters as the camera focus among others. Endocentric and telecentric lenses are used in the image acquisition and a comparative analysis is obtained using a multivariable statistical analysis to study the influence of each parameter in the calibration process: camera focus, exposure time, calibration plate tilt and number of images used. In the third proposal, an object alignment algorithm is developed to address the challenge of object alignment during a measurement process. Object plane alignment is key point for achieving good repeatability of object measurements in all orientations. A complete study of the impact of every single pipeline

phase is carried out in the proposals validation chapter. Finally, a complete 2D machine vision application is developed to determine the precise measurement of gears, at subpixel level, with the potential to improve quality control, reduce downtime and optimize the inspection process. The calibrated vision system was verified by measuring a ground-truth sample gear in a Coordinate Measuring Machine (CMM), using the parameter generated as the nominal value of the outer diameter. A methodical study of the global uncertainty associated with the process is carried out in order to know better the admissible zone for accepting gears.

This thesis try to reach the optimal values in every single phase of the pipeline in order to improve the accuracy of the inspection. The different studies and algorithms developed in this thesis show that it is worthwhile to invest on achieving the optimal values during the different phases of an industrial inspection process.

Contents

I	Introduction	1
1	Introduction	3
1.1	Machine Vision System	4
1.2	The Benefits of Machine Vision Technology	6
1.3	Research Objectives	7
1.4	Dissertation Organization	9
2	State of the art	11
2.1	Introduction	11
2.2	Machine Vision and Metrology	15
2.2.1	Mechanical devices	16
2.2.1.1	Caliper type	16
2.2.1.2	Micrometer	16
2.2.1.3	Coordinate Measurement Machine (CMM)	17
2.2.2	Optical methods	18
2.2.2.1	Microscopy	19
2.2.2.2	Profile projector	19
2.2.2.3	Laser Tracker	20
2.2.2.4	Camera-based systems	20
2.3	Error in Measurement	22
2.4	Cameras	23
2.5	Machine vision software	23

2.5.1	iNspect	23
2.5.2	Sherlock	25
2.5.3	Halcon	26
2.5.4	Merlic	27
II Proposal		29
3 Proposal I: Optimal Light Alignment		31
3.1	Introduction	31
3.1.1	Standard or endocentric lenses	32
3.1.2	Telecentric lenses	33
3.1.2.1	Magnification constancy	34
3.1.2.2	Low distortion	35
3.1.2.3	Perspective errors limitation	36
3.2	Optical Axis Alignment	37
3.3	Experiment and Analysis	38
3.4	Discussion	43
4 Proposal II: Optimal Camera Focus and Calibration Parameters Study		45
4.1	Introduction	45
4.2	Focus computation algorithm	47
4.3	Camera Model Representation	48
4.3.1	Calibration Process	49
4.4	Experiments and Analysis	52
4.4.1	Endocentric experiments	56
4.4.1.1	Focus parameter	56
4.4.1.2	Exposure time parameter	58
4.4.1.3	Tilt angle parameter	58
4.4.1.4	Number of images parameter	59
4.4.2	Telecentric experiments	60
4.5	Discussion	62

5	Proposal III: Optimal Object Alignment	65
5.1	Introduction	65
5.2	Setup Configuration	66
5.3	The Alignment Algorithm	68
5.4	Data Analysis	70
5.5	Discussion	73
6	Proposals Validation	75
6.1	Analysis of Experiments	75
6.2	Discussion	78
7	Measurement and uncertainty analysis	81
7.1	Introduction	81
7.2	The Proposed System	82
7.3	The Algorithms	84
7.3.1	Image Segmentation	87
7.3.2	Edge Detection Sub Pixel	87
7.3.3	The Outer Diameter Algorithm	89
7.3.4	The Inner Diameter Algorithm	90
7.3.5	The Tooth Number Algorithm	92
7.3.6	The Other Parameters	93
7.4	Inspection Process	93
7.5	Measurement Error and Uncertainty Analysis	95
7.5.1	Resolution uncertainty	97
7.5.2	Pattern uncertainty	98
7.5.3	Calibration uncertainty	98
7.5.4	Measurement uncertainty	100
7.6	Validation and Analysis	101
7.7	Discussion	106

III	Conclusions	107
8	Conclusions	109
8.1	Future research lines	110
IV	Appendices	113
A	Optical Set-Up Definitions	115
A.1	Understanding Focal Length and Field of View	115
A.2	Working Distance (WD) and Field of View (FOV)	116
A.3	Lens Specifications and Resolution	118
A.4	Vignetting within a Lens	120
A.5	Depth of Field and Depth of Focus	121
A.6	Distortion	122
A.7	Telecentric and Perspective Error	125
A.8	Telecentric Lenses and Depth of Field	126
A.9	Telecentricity and Distortion	128
B	Generated Publications	131
	Index	133
	References	133

List of Figures

1.1	An outline of a machine vision system	5
1.2	Pipeline of an optical set-up	7
2.1	Overview of typical machine vision systems	12
2.2	Architecture of a smart camera	14
2.3	Digital caliper	16
2.4	Micrometer	17
2.5	Gauge Blocks	17
2.6	Coordinate Measurement Machine	18
2.7	Microscopy	19
2.8	Profile Projector	19
2.9	Laser Tracker from FARO	20
2.10	Different hardware involved in a camera-based system	21
2.11	Gocator products catalog from LMI	22
2.12	iNspect software	24
2.13	Tools in iNspect	24
2.14	Sherlock main window	26
2.15	Halcon software	27
2.16	Merlic development interface	28
3.1	Optical distortions	32

3.2	On the left an image of an internal spline on a cylindrical object taken with a telecentric lens (top) and the same object viewed by an ordinary lens (bottom). On the right an image of two identical machine screws set 100mm apart, taken with a telecentric lens (top) and with an ordinary lens (bottom)	34
3.3	on the left an image of a distortion pattern taken with a telecentric lens, where no radial or trapezoidal distortion is present. In the middle the image of the same pattern showing strong radial distortion. On the right an example of trapezoidal distortion.	35
3.4	On the left endocentric lens showing image perspective error. On the right, a telecentric lens is able to cancel any perspective effect.	36
3.5	Comparison between standard and telecentric lenses	37
3.6	Scheme of the optical axis alignment	38
3.7	Flowchart of the light algorithm	39
3.8	Devices and instruments used for the light alignment experiments	40
3.9	Devices' specifications used for the light alignment experiments	40
3.10	Not-optimal light alignment setup	41
3.11	Optimal light alignment setup	41
3.12	(a) Optimal light alignment. (b) Not-optimal light alignment	42
3.13	Chart of the experimental	43
4.1	The relationship between field of view, focal length and image plane	48
4.2	Perspective projection model	51
4.3	Calibration plate in Halcon development framework. Note the white marks, useful to know the orientation of the plate.	52
4.4	Optimal calibration plate alignment setup	53
4.5	Not-optimal calibration plate alignment setup	53
4.6	Comparison between cumulative distribution functions of the data and the standard normal distribution)	55

4.7	Box diagrams of endocentric experiments. First and second rows show focus level and exposure time comparisons respectively (the line inside the rectangles represents the median values, and the asterisks the outliers). Third row shows experiments studying the tilt degree (g), and number of images (h) and (i)	57
4.8	Box diagrams of telecentric experiments. First row shows exposure time comparisons (the line inside the rectangles represents the median values, and the asterisks the outliers). Second row shows experiments studying the number of images	61
4.9	Box diagram of telecentric experiments studying the tilt angle parameter (the line inside the rectangles represents the median values, and the asterisks the outliers)	61
5.1	Object alignment scheme	66
5.2	a) Compact 5-Axis Pitch, Yaw, and Translation Stage. b) The Mounting Base.	67
5.3	Devices and instruments used for the object alignment experiments	67
5.4	Object alignment setup configuration	68
5.5	Object alignment algorithm flowchart.	69
5.6	(a) Object at optimal alignment. (b) Object at an angular tilt of 20°.	70
5.7	The object alignment experiments for endocentric lens . . .	71
5.8	The object alignment experiments for telecentric lens	72
6.1	Flow of the experiments	76
6.2	Calibration experiment chart	79
6.3	Alignment experiment chart	79
7.1	The proposed system configuration. a) Robot and telecentric lens configuration. b) The inspection belt. c) The vision2D application interface.	82
7.2	Devices used for the measurement experiment	84
7.3	Nomenclature of gear	84
7.4	Flowchart of the Vision2D application.	86

7.5	The edge detection details. a) The edge pixel detection of the gear tooth. b) The edge sub-pixel detection of the gear tooth. c) The outer edge detection of gear. d) The intersection points to determine the diameter of tooth.	88
7.6	Flowchart of outer diameter algorithm.	90
7.7	Flowchart of inner diameter algorithm.	91
7.8	Flowchart of tooth number algorithm.	92
7.9	The main interface of the Vision2D application.	95
7.10	Graph to check the minimum system error	100
7.11	Computation of the admissible zone	103
7.12	The Verification Chart	105
A.1	Focal length of AFOV	116
A.2	Relationship between HFOV, sensor size, and WD for a given angular FOV	118
A.3	Resolving two squares. If the space between the squares is too small (a) the camera sensor will be unable to resolve them as separate objects	119
A.4	A 16mm lens design at a) f/1.8 and b) f/4. At f/1.8 vignetting occurs where light rays are clipped by the edges of the lens.	120
A.5	Geometric representation of DOF for high and low f/# lenses.	121
A.6	Distortion plot showing the variance of distortion with respect to wavelength	122
A.7	An illustration of positive and negative distortion	123
A.8	Calibrated target (red circles) vs. imaged (black dots) dot distortion pattern.	124
A.9	Field of view comparison of a conventional and Telecentric Lens. Note the conventional lens's angular field of view and the Telecentric Lens's zero angle field of view.	126
A.10	The angular field of view of the Fixed Focal Length Lens translates to parallax error in the image and causes the two cubes to appear to be different sizes.	126
A.11	The same pin imaged both in and out of focus. Note that the transition from white to black covers many more pixels when the lens is slightly out of focus (b), which can be advantageous.	127

-
- A.12 Plot showing the difference in slope between a focused and defocused edge. The defocused edge takes up many more pixels; finding the edge becomes easier without relying on sub-pixel interpolation. 128
- A.13 Comparison of jumpers on a circuit board. a) shows an image that has been taken with a Fixed Focal Length Lens. b) shows an image that has been taken with a Telecentric Lens. Note that the pins do not appear bent in the telecentric image.129

List of Tables

3.1	Summary of the light alignment experiments	42
4.1	Number of images used in each calibration configuration . .	55
4.2	p -values of the experiments. Gray cells indicate that the experiment is meaningless and white cells without data that the experiment was not done because of few available data .	56
4.3	Three-way ANOVA analysis in endocentric experiments . .	59
5.1	Object Alignment Experiments (Endocentric)	71
5.2	Object Alignment Experiments (Telecentric)	72
6.1	Experiments configurations and results. The color gradient indicates the level of optimized set-up pipeline phases (red none, orange several phases optimized, green pipeline optimized). The last column is the % of improvement with respect to the not-optimal experiment, 1A or 2A.	78
7.1	The gear nomenclature and formulas	94
7.2	Coverture factor for different probability distributions . . .	97
7.3	Summary of involved uncertainties	101
7.4	Summary of involved uncertainties with numerical values .	102
7.5	Inspection details of accepted Gear 1	104
7.6	Inspection details of rejected Gear 12	104
7.7	The Inspection Results	105

Part I

Introduction

Chapter 1

Introduction

Metrology and machine vision are two fields that have been considered jointly by other authors, due to the versatility of artificial vision to solve industrial problems. Metrology is one of the many applications of machine vision, which has the advantage that allows for the analyzing of a total production batch that leaves an assembly line without supposing a bottleneck in production. These topics are the basis for the elaboration of this dissertation, as well as to understand the need for a good metrology system based on artificial vision. The advancement of technology and the realizations of Industry 4.0 in modern world applications has amplified the research possibilities in the field of machine vision and industrial inspections. Image-based inspection and automatic applications analysis, such as robot guidance, process control and automatic inspection are the mainstream technologies of machine vision in today's industries (Sanz, 2012) (Steger et al., 2018). These conventional technologies usually involves a stream of integrated systems, hardware products, methodologies and expertise that uses software algorithms across sensors, cameras and hardware processing to automate mundane and complex inspections that guides the precise handling of tasks and equipment during the assembly of products. The distinctions of such applications vary from verification, positioning, flaw detection, identification and measurement. In the bit to improve control quality, low production cost and higher yields, a machine vision system can work pertinaciously accomplishing very low error rates during inspection processes (Pedreschi et al., 2006). The system configuration involves diverse components, ranging from the sensor cameras to image acquisitions for inspection, critical to the processing framework that provides and communicates the outcome. With the rapid development

of image processing and pattern recognition, machine vision technology has attracted more attentions. In addition, it is widely used in the industrial field, for its simplicity, non-contact and robustness (Jurkovic et al., 2005). It is a pre-eminent tool for quality control inspection of a variety of products such as industrial components and manufacturing tools.

1.1 Machine Vision System

Machine vision is the technology and method used to provide imaging-based automatic inspection and analysis for applications such as automatic inspection, process control, and robot guidance, usually in the industry (Sanz, 2012). It integrates image capture systems with digital input/output devices and computer networks to provide real time quality control and for general control of manufacturing equipment such as robots. Manufacturing industries favour machine vision for visual inspections that require high-speed, high-magnification, 24-hour operation, and repeatability of measurements. A typical machine vision system will be a part of an automated production process consisting of the following components:

- One or more digital cameras (monochrome or color) with suitable optics for acquiring images, such as lenses to focus the desired field of view onto the image sensor, suitable light sources and where necessary filters, to help minimize glare and reflections, enhance colors, reduce light coming into the lens.
- A synchronizing sensor for part detection to trigger image acquisition and processing and some form of actuators to sort, route or reject defective parts.
- A computer program to process images, detect, measure and compare in order to confirm that a quality criterion has been met to provide type verification or robot control to another control system.
- Input/Output hardware or communication links to report results and to automatically reject components.

Figure 1.1 illustrates the components of a typical machine vision system.

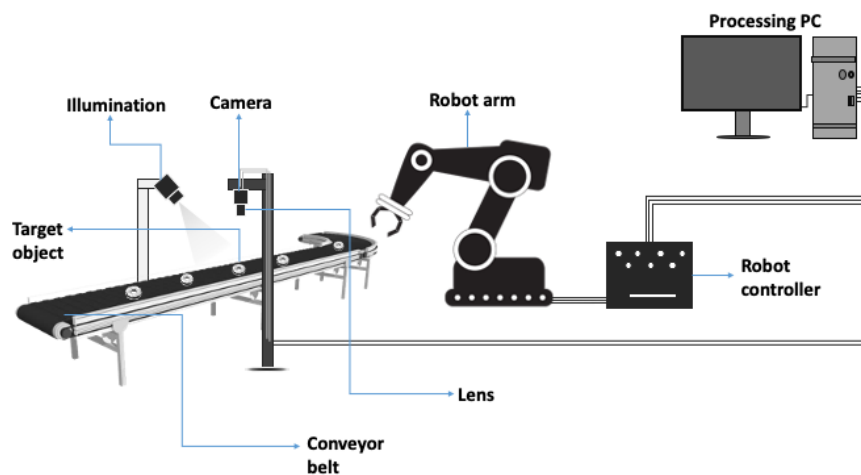


Figure 1.1: An outline of a machine vision system

A machine vision system can work tirelessly performing 100% inspection, resulting in improved product quality, higher yields and lower production costs (Pedreschi et al., 2006). It consists of several critical components, from the sensor camera that captures a picture for inspection, to the processing engine itself (vision application) that renders and communicates the result (Peng et al., 2016). It is an excellent tool for inspecting a variety of items such as industrial components, and machine tools. Machine vision traditionally refers to the use of Computer Vision in an industrial or practical application or process where it is necessary to execute a certain function or outcome based on the image analysis done by the vision system. The vision system uses software to identify pre-programmed features. The system can be used to trigger a variety of set actions based on the findings (Beyerer et al., 2015).

Often thought to be one in the same, Computer Vision and Machine Vision are different terms for overlapping technologies: Computer Vision refers in broad terms to the capture and automation of image analysis with an emphasis on the image analysis function across a wide range of theoretical and practical applications (Szeliski, 2010). Machine Vision methods has been implemented to develop specific quality control application and algorithms in a manufacturing industry process.

In inspection tasks (measures, check gaps) and metrology (dimensional inspection of parts) it is very important to study the best technology to inspect the element (camera, optics, illumination) and machine vision brings benefits with respect to other mechanical solutions (for example, probe clocks, three-dimensional machines, etc.). There are many solutions in the market and companies dedicated to implementing solutions. However, there are still niches where machine vision solutions are not applied for several reasons:

- Ignorance of current hardware and software and its possibilities and limitations.
- Too complex problem and/or ignorance of the underlying theory in technology.
- Accuracy requirements too high.
- Knowledge gap in evaluating and performing uncertainty analysis.

1.2 The Benefits of Machine Vision Technology

The following are some of Machine Vision Technology benefits:

- Machine vision inspection is widely recognised as a key technology for the automation of production lines. Utilising the correct camera system with optics and lighting together with a proven vision analysis software package can provide the solution for the most challenging inspection requirements, be it high speed or difficult image components.
- The adoption of inline inspection increases customer satisfaction and reduces waste. It is key to product and batch integrity, as well as batch mix prevention.
- Vision systems improve product quality. Machine Vision technology enables the manufacturer to replace sample testing with one hundred percent quality checks done via a camera system. This means that every single batch produced can be reliably checked for flaws during the production process and without interruption. A rapid and thorough inspection that guarantees a superior product.

- Vision systems reduce the cost of production. By employing a vision inspection system in the early production stages, defective parts are immediately removed from the process. Faulty products never continue to subsequent manufacturing stages and therefore incur no further costs. Defected products can be re-introduced back into the production process at a later stage, thus saving materials. Through analysis, problems can be rectified at the point of origin, resulting in increased system productivity and availability.

Machine vision technology is unique in its ability to enhance quality whilst simultaneously cutting costs and protecting the brand from recalls, fines and adverse negative publicity. For these opportunities, current hardware may not meet required performance requirements, but in-depth knowledge of machine vision theory may result in new methods that achieve greater accuracy than existing ones.

1.3 Research Objectives

When preparing an optical set-up for an inspection system, there is usually a pipeline (Figure 1.2) that many times the process has to follow, sometimes quickly, sometimes subjectively, and not much attention is paid because the measurement results are good enough for the application. However, it is possible to achieve better results optimizing every single step of this pipeline.

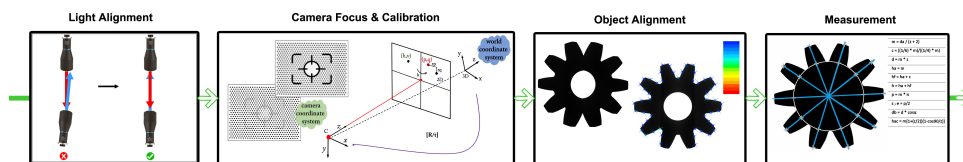


Figure 1.2: Pipeline of an optical set-up

The main objectives of this dissertation was to investigate the following research questions associated to each of the identified phases:

- *How does light alignment affect and influence the accuracy of measurement? (Chapter 3)*

The effects of lens misalignment can be highly pronounced. If the lens is not mounted correctly then the result will be an image that is not perfectly focused. If the lens is tilted, part of the image captured by the sensor may be in focus while another part of the image will be blurred. Proposal 1 presents a light alignment algorithm to track and monitor acquired image planes to verify an optimal light alignment system.

- *How do different calibration parameters influence the calibration process? (Chapter 4)*

Due to the importance and complex nature of an efficient calibration process, several factors are involved for a successful calibration. Each of these factors play a significant role in determining the accuracy of the error generated. The level of accuracy of the calibration process determines to a large extent the accuracy of the measurement results desired. Proposal 2 presents the results from this study, in which the effects of the different parameters, such as camera focus, exposure time, calibration plate tilt and number of images, were analysed to determine how they influence the calibration process.

- *How does an object alignment affect the measurement? (Chapter 5)*

As a result of adjustments and motions during a measuring process, it becomes important to have an alignment system to avoid any possible errors that may result from a lack of alignment. In order to obtain the best possible alignment conditions, it is necessary to check if the object to be measured is well placed. Proposal 3 presents the results from this study, in which an algorithm was developed to determine the challenges of object alignment in a measurement system.

- *Does quality control inspection play a role in determining industrial production process? Is the uncertainty of the machine vision system known? (Chapter 6)*

Quality control has become a priority in the inspection processes of industrial manufacturing. Chapter 6 presents the results in which an improved machine vision application is developed to perform a precise measurement of industrial gears (at subpixel level), and making a deep study of the uncertainty of the measurement.

1.4 Dissertation Organization

The rest of this thesis is organized as follows.

Chapter 2 reviews the most relevant studies presented about this topic. It briefly summarizes the post-process and on-process dimensional measurement tools. It discusses the implications of error in a measurement system. And finally, it introduces the various cameras and softwares that were used in the experiments for the realization of the dissertation.

Chapter 3 presents an optimal light alignment algorithm, developed to monitor and achieve an optimal light alignment, in order to eliminate the effects of misalignment and its consequences. This proposal aims to demonstrate the effects of using an optimal light alignment algorithm against a not-optimal light aligned system.

Chapter 4 performs a deep study of the influence of different parameters in the calibration process.

Chapter 5 discusses an optimal object alignment algorithm, developed to address the challenges of object alignment during measurement.

Chapter 6 discusses the experiments performed for each of the proposed algorithms, comparing the impact of optimizations accomplished to every single pipeline phase.

In Chapter 7, a 2D machine vision application is developed to determine the precise measurement of gears, at subpixel level, with the potential to improve quality control, reduce downtime and optimize the inspection process. A deep study of the uncertainty of the measurement is carried out in order to evaluate the goodness of the algorithm.

Finally, Chapter 8 discusses the conclusions of this thesis as well as its possible future works.

Chapter 2

State of the art

2.1 Introduction

Visual inspection is to identify whether a particular attribute is present or properly located in a predetermined area (Dowling et al., 2006). As described in (Newman and Jain, 1995), inspection is to determine whether an object deviates from a given set of specifications. Machine vision systems are designed to release human operators in industrial inspection process and achieve a more robust and high quality of performance of manufacturing process and quality control. Different from computer vision, which refers to a broad terms of the capture and automation of image analysis, machine vision needs an engineering to system design with additional hardware I/O and computer networks to transmit information (Batchelor, 1999). One of the most common applications of machine vision is the inspection of products, such as integrated circuits, vehicle parts and components, food and pharmaceuticals (Sanz, 2012). An early survey reported automated visual inspection systems and techniques from 1988 to 1993 (Newman and Jain, 1995). Both the benefits and challenges on using of CAD data or models, which contain exact specifications of an object, in inspection are highlighted and discussed. Based on the inspected features, the inspection tasks can be categorized into four basic groups: dimensional characteristics, surface characteristics, structural quality, and operational quality (Newman and Jain, 1995). A variety of software and hardware solutions for the machine vision system development are reviewed in the year 2003 (Malamas et al., 2003). In the review (Thomas et al., 1995), real-time performance and verification of industrial machine vision systems as well as the temporal reliability were discussed and described. The flexibility and complexity

of modern manufacturing process brings challenges for the assurance of speed of production and quality of product. The increasing demands on constant precision and reliability need sophisticated machine vision systems to take significantly varied inspection tasks. Machine vision systems are evolving with the technology advances, such as imaging sensors, digital interfaces, illumination, computational capability, artificial intelligence, communication, and network. The emerging of low-cost and high-efficient embedded vision systems and smart cameras makes it possible to build a scalable machine vision system for varied industrial applications. The integration of multiple cameras and multi-modal imaging systems offers a more robust solution for the difficulties in industrial inspection. Fusing the visual information and those beyond visual spectrum can achieve a comprehensive inspection with less uncertainty. Industrial inspection is benefiting from such advances for improved accuracy and performance.

Modern machine vision system consists of digital input/output devices and computer networks for automatic operation of equipment or quality control systems. There are basically three categories: PC-based vision system, embedded vision system, and smart cameras. Figure 2.1 shows the three types of machine vision systems. The smart camera-based systems cover a wider range of applications, while embedded vision and PC-based systems offer less flexibility and higher performance due to the increased complexity of the overall system.

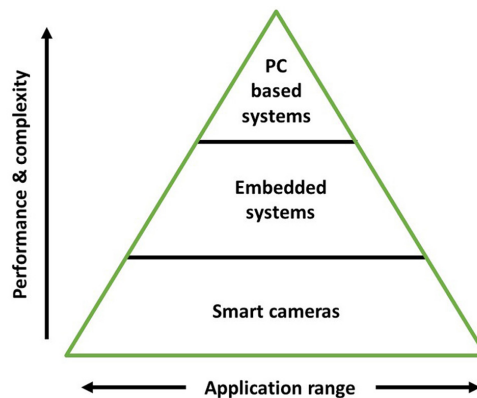


Figure 2.1: Overview of typical machine vision systems

A typical PC-based machine vision system consists in several

components illustrated in Fig. 1.1 (Gregory, 2015):

- Cameras and optics
- Lighting
- Frame grabber
- PC platform
- Inspection software
- Digital I/O and network connection

The PC-based machine vision system employs one or more cameras and lenses to capture a picture of the object under inspection (Gregory, 2015). Different types of cameras can be used, such as monochrome camera, RGB color camera, and progressive-scan or line-scan camera. To assure a better quality of the image, the object is illuminated with the lighting device. The lighting of high-frequency fluorescent, light-emitting diode (LED), incandescent, and quartz-halogen fiber optic can be configured in various shapes, colors and sizes with a variety of intensities (Gregory, 2015). Frame grabbers or video capture cards provide low-level interface capabilities with other system components and host computer (Malamas et al., 2003). It can also control the camera by setting the triggering, exposure/integration time, shutter speed, etc. The PC platform runs the inspection software to process acquired image data and even make a binary decision, e.g., accept/reject. For varied inspection tasks, algorithms need to be tailored with proper software tools. The data exchange and communication with outside systems and databases are done through the digital I/O interface and/or network connection. The PC-based machine vision system should be configured based on the specific requirements and goal of the inspection task.

Embedded vision is the merging of computer vision and embedded systems. The low-cost, powerful, and energy-efficient processors makes it possible to incorporate vision capabilities into a wide range of embedded systems for using of visual inputs (Bier, 2011) (Gardner, 2015). Embedded vision becomes a key technology for the automated inspection in manufacturing and quality control systems. Embedded vision is usually implemented with a combination of processing elements, such as CPU,

high-performance digital signal processor (DSP), and highly parallel engine. The popular types of processors used in embedded vision system include high-performance embedded CPU, graphics processing unit (GPU) + CPU, DSP + accelerators + CPU, field-programmable gate array (FPGA) + CPU, and application-specific standard product (ASSP) + CPU (LIVE et al., 2014). As described in (Gardner, 2015), embedded vision systems are facing a number of challenges and constrains in the compute resources. Embedded vision has been widely adopted in the industrial inspection applications and is proliferating broad markets with the emergence of high-performance, low-cost, energy-efficient programmable processors (LIVE et al., 2014) (Dibert and Khan, 2013).

Smart cameras integrate lenses, sensors, processors, camera-to-computer interfaces, and software in one camera system. As described by Wolf et al. in (Wolf et al., 2002), smart cameras output processed image data with high-level descriptions of a scene and perform real-time analysis of what they see. The overall architecture of a smart camera is illustrated in Figure 2.2. The application-specific processing (ASP) is performed by embedded algorithms on a per channel basis (Shi and Lichman, 2005)(Bramberger et al., 2003).

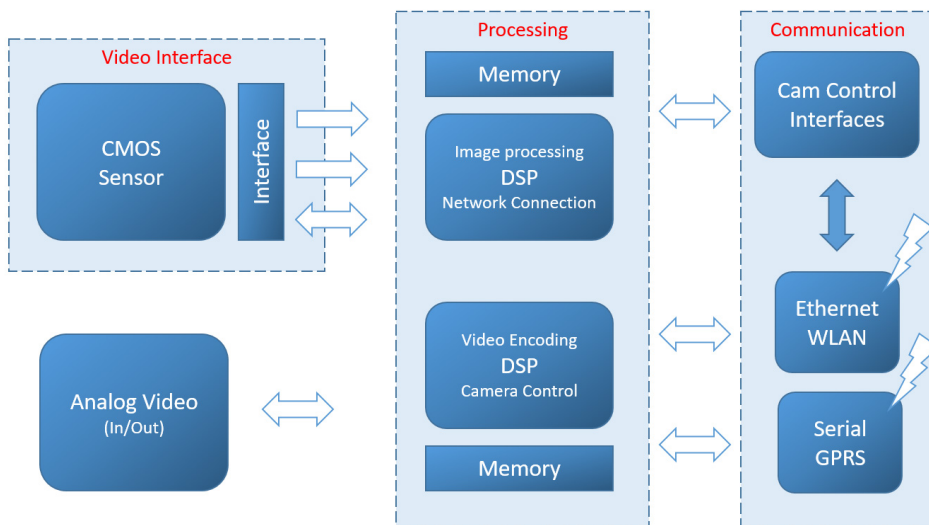


Figure 2.2: Architecture of a smart camera

Generally, in vision industry, conventional PC-based vision systems are being replaced by smart cameras due to its relatively low cost, simplicity, integration, and reliability (Bramberger et al., 2003) (Nair et al., 2013). The smart camera-based systems can carry out real-time processing operations within the camera at high speeds and lower cost (Bramberger et al., 2003). In (Malik et al., 2013), an investigation was conducted to compare three smart camera architectures for real-time machine vision system. Processing speed and power consumption appear to be the most important metrics. Vision-systems-on-chip is the trend for the future (Elouardi et al., 2006)(Rodríguez-Vázquez et al., 2010).

2.2 Machine Vision and Metrology

Metrology is one of the many applications of machine vision. It is an advance analysis of a production line without becoming a bottleneck in the process (Batchelor, 2012). It is the science of calibrating and using physical measurement equipment to quantify the physical size or distance of any given object. It requires the use of a variety of physical scales to determine dimension and distance based on a combination of touch and/or optics. Traditionally, there are two kind of dimensional metrology techniques: post-process and on-process dimensional measurement.

In the called post-process, the measurements are made after the part has been produced. The inspection can be made over a percentage of the production or over the 100% of the parts. On the first case, if the dimensions are not within the given tolerance zone, correction actions (modifications or even rejections) have to be made over the whole batch. On the other hand, 100% inspection ensures the non-zero defects production modifying or rejecting just the single defective parts. The inconvenience of the 100% inspection is that the inspection has to ensure the production cycle time as well as the required accuracy.

When the manufactured parts are big, with higher material cost and longer cycle times, on-process measurement is required to monitor the process, improve the productivity and reduce the cost. In the on-process measurement, parts are measured while they still are on the manufacturing process.

In the next subsections, there is a brief summary of the most classical

metrology systems:

2.2.1 Mechanical devices

2.2.1.1 Caliper type

A caliper is a device used to measure the distance between two opposite sides of an object. A caliper can be as simple as a compass with inward or outward-facing points. The tips of the caliper are adjusted to fit across the points to be measured, the caliper is then removed and the distance read by measuring between the tips with a measuring tool, such as a ruler. The measured work piece diameter range with this method reaches 5-190mm.



Figure 2.3: Digital caliper

2.2.1.2 Micrometer

The micrometer is commonly used for measuring the thickness and inside or outside diameters of parts. It is a gauge which measures small distances or thicknesses between its two faces, one of which can be moved away from or towards the other by turning a screw with a fine thread. Micrometers

are also available for measuring depths. Micrometers can be equipped with digital readout to reduce errors in reading.



Figure 2.4: Micrometer

Both calipers and micrometers are used to be calibrated with gauge blocks. They are individual square, rectangular, or round metal blocks of various sizes. Their surfaces are lapped and are flat and parallel within a range of 1-5 micro inch. Gauge blocks are available in sets of various sizes. The blocks can be assembled in many combinations to obtain desired lengths. The gauge block assemblies are used as an accurate reference length to measure the part's length.



Figure 2.5: Gauge Blocks

2.2.1.3 Coordinate Measurement Machine (CMM)

Today it is the most accurate and widely used mechanical device in the manufacturing industry. A coordinate measurement machine (CMM) is an advanced, multi-purpose quality control system used to help inspection keep pace with modern production requirements. It replaces long, complex and inefficient conventional inspection methods with simple procedures. A CMM provides instant measurement results without complicated setup and operating procedures. It combines surface plate, micrometer and Vernier type inspection methods into one easy to use machine. CMM can check the dimensional and geometric accuracy of everything from small engine blocks, to sheet metal parts, to circuit boards.



Figure 2.6: Coordinate Measurement Machine

2.2.2 Optical methods

An optical method measurement is defined as one in which the transmitter module produces and emits a light, which is collected and photo electrically sensed through the object to be measured, by a receiver module. This produces the signals which can be converted into a convenient form and displayed as dimensional information. The principal advantages of optical methods are:

- Direct mechanical contact between the sensor and the object to be measured is not required.
- The distance from the object to be measured to the sensor can be large.
- The response time is limited only to the electronics used in the sensor.
- The light variations can be directly converted into electrical signals.

2.2.2.1 Microscopy

Microscopy is the technical field of using microscopes to view objects and areas of objects that cannot be seen with the naked eye (objects that are not within the resolution range of the normal eye).



Figure 2.7: Microscopy

2.2.2.2 Profile projector

The profile projector, also known as an optical comparator, or even called a shadow-graph, is used for measuring two-dimensional contours of precision specimens and other work pieces produced. The part to be measured is magnified by an optical system and projected on a screen. The reading on the screen gives the dimension of the part.



Figure 2.8: Profile Projector

2.2.2.3 Laser Tracker

Laser trackers are instruments that accurately measure large objects by determining the positions of optical targets held against those objects. The targets are known as "retro-reflective" because they reflect the laser beam back in the same direction it came from (in this case, back to the laser tracker). One type of target in common use is called a spherically mounted retro-reflector (SMR), which resembles a ball bearing with mirrored surfaces cut into it. The accuracy of laser trackers is of the order of few microns even in distances of several meters. It is considered one of the best optical systems.



Figure 2.9: Laser Tracker from FARO

2.2.2.4 Camera-based systems

This classification would include all machine vision systems composed of a set of cameras, lenses and lighting systems. Depending on the used sensors and the object size, the accuracy of these systems can be close to the laser tracker. Machine Vision necessarily involves the harmonious integration of mechanical handling, lighting, optics, video cameras, image sensors (visible, UV, IR and X-ray sensor arrays, as well as laser scanners), digital, analogue and video electronics, signal processing, image processing, computer systems architecture, software, industrial engineering,

human-computer interfacing, control systems, manufacturing, existing work practices and quality assurance methods. Machine Vision is not a scientific endeavor; it is a branch of Systems Engineering. Hence, consideration of application requirements pays a key role in the design of practical vision systems.



Figure 2.10: Different hardware involved in a camera-based system

In many situations, one of the most common task of vision systems is achieving dimensional measure on a 2D plane. In a broad range of applications 2D measuring is applied to get spatial information about planar objects or object parts that are extracted from images. In this case, a single camera with the suitable optic and light can be used (Figure 2.10). Measuring in images corresponds to the extraction of specific features of objects. 2D features that are often extracted comprise:

- the area of an object, i.e., the number of pixels representing the object
- the orientation of the object
- the angle between objects or segments of objects
- the position of an object
- the dimension of an object, i.e., its diameter, width, height, or the distance between objects or parts of objects
- the number of objects

However, 3D inspection systems are currently being used every time due to their lower cost, accuracy and compactness of the solution. In these cases, the 3D information is reconstructed by means of projecting a structured

light (laser, light pattern,...) and visualizing that light with a pre-calibrated camera (or several cameras) with respect to the projector.



Figure 2.11: Gocator products catalog from LMI

2.3 Error in Measurement

In any measurement, there is always a degree of uncertainty resulting from measurement error, i.e. all measurements are inaccurate to some extent. Measurement error is the difference between a reference value and actual values of the measurand. The error can be expressed either as an absolute error or on a relative scale, most commonly as a percentage of full scale. It is important to examine fully the errors in measurement systems that cause these uncertainties, the meaning and interpretations of these errors and methods of reducing or circumventing of errors. Each component of the measuring system has sources of errors that can contribute to measurement error. Instrument or indication errors may be caused by defects in manufacture or adjustment of an instrument, imperfections in design, etc.

It is important to bear in mind the measurement error, as it is going to be the decisive factor when choosing the best hardware, software, illumination conditions, etc. In addition to measurement error, the tolerances are also important. Tolerance is the total amount a dimension may vary and it's the difference between the upper (maximum) and lower (minimum) limits. Tolerances are used to control the amount of variation inherent in all manufactured parts.

2.4 Cameras

Machine vision systems has one or more digital cameras that record color, monochrome, or wide-spectrum images. Just like consumer cameras, the optics/lenses attached deliver a specific field of view and available light. To pick the proper lens it is prior to know the field-of-view (FOV) and the working distance. The FOV is the size of the area to be captured. The working distance is approximately the distance from the front of the camera to the part being inspected. A more detail of parameters related to camera sensors and lens can be found in Appendix A.

2.5 Machine vision software

There is a wide range of Machine Vision software aimed at inspection applications. Depending on the user requirements, the software can be simpler, with a straightforward user interface, or software designed for more advanced users. As there is a wide range of software, it is important to analyze each software, focusing on those features that are useful for the present project. Some example of different softwares from MVTec company are: iNspect, Sherlock, Merlic and Halcon. iNspect and Sherlock come as embedded software with the BOA cameras, while Merlic and Halcon are external softwares for which a license is required.

2.5.1 iNspect

iNspect is a vision application software specifically designed to simplify the design and deployment of automated inspection on the factory floor. iNspect offers new and experienced users alike a practical tool delivering uncompromising functionality that can be readily applied to a wide range of manufacturing tasks. iNspect's simple, straightforward setup allows users to quickly configure and deploy an application. Each of the inspection tools have been carefully designed to extract the relevant information from the object image. No programming or extensive training is required.

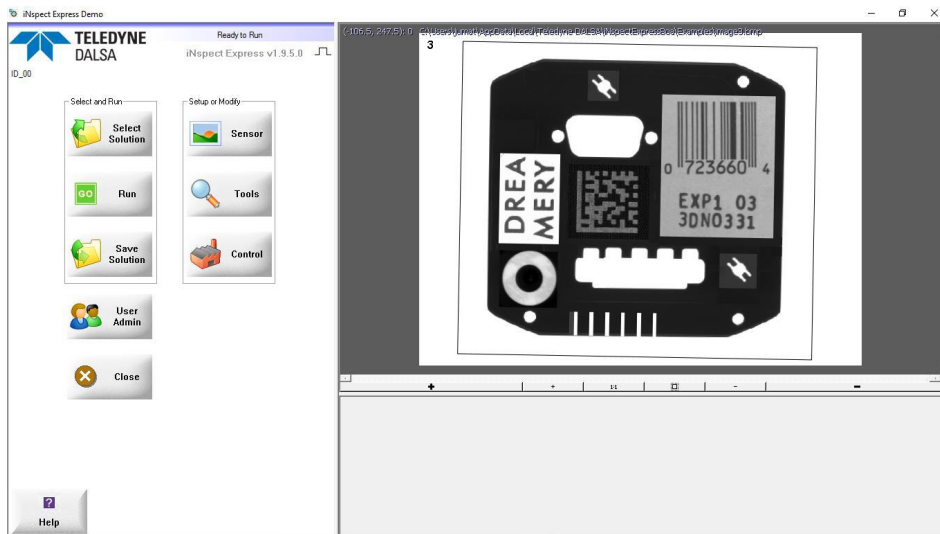


Figure 2.12: iNspec software

In Figure 2.12 the main window of iNspec can be seen. There is a left panel where the many actions can be selected. There are several tools that can be applied to the live image, as it can be seen in Figure 2.13.



Figure 2.13: Tools in iNspec

All these tools, like caliper measurement, circle detection or angle measurement, can be applied to the image grabbed from the camera, and the user can see immediately the effect on the image. iNspect offers the tools and the ideal features for inspection applications. It is interesting to note the extensive literature provided by the manufacturer. There are several tutorials and examples of the different tools, all well documented. Thanks to the fact that there is also an offline emulator, the programmer can familiarize himself and train with these examples. A program developed from the emulator can be saved and run later with the camera connected to the software. There is also a light version of the software, called iNspect IDR, that has a selection of tools focused only in identification.

2.5.2 Sherlock

Sherlock is an advanced machine vision software interface that can be applied to a wide variety of automated inspection applications. It offers maximum design flexibility and provides a rich suite of proven tools and capabilities that have been deployed in thousands of installations worldwide. Like iNspect, this software comes embedded in some BOA cameras. In this case, Sherlock is more advanced software than the previous one, being able to develop more complex applications and covering a wider range of them. Unlike iNspect, this software is based on floating windows, so the user can resize, hide and move them to suit its liking. This system makes the software very easy to any inexperienced user. The way in which the program works is by defining regions of interest (ROI) and applying different tools on that regions. One can also use the script window, customizing the code wanted to be run. The predefined functions existing in Sherlock make up a complete language (with loops, conditions, etc.) and in most applications, it's more than enough to cover the needs of most users. The fact that this program includes two different ways of working (by graphical tools and by scripting/programming) makes it ideal to any kind of application, either simple or advanced. As in iNspect, the user has the option to save the images and to work offline thanks to an emulator. Similarly, there is the possibility of establishing a user registration system to protect the level of access under passwords. Sherlock also offers the option to save backups.

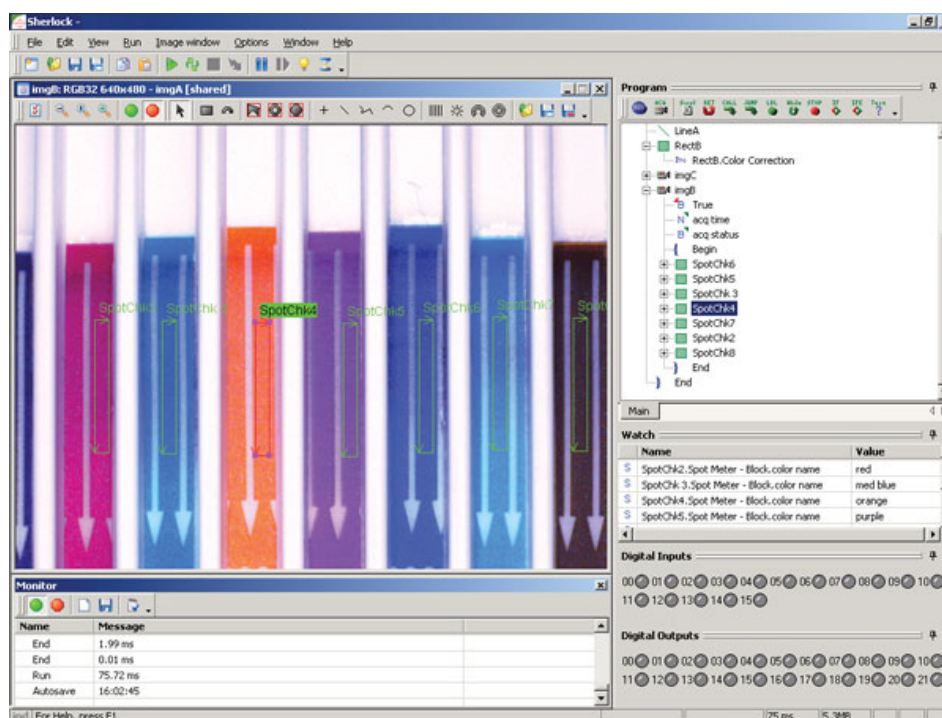


Figure 2.14: Sherlock main window

2.5.3 Halcon

Halcon is the programming library for machine vision application development most well-known worldwide. Its flexibility enables rapid development of applications at a reduced cost. As an easily configurable software, it provides solutions for both the needs of industrial machine vision and image processing. The diversity of Halcon libraries includes more than 2000 image processing functions and more than 1000 examples in HDevelop (Halcon's integrated development environment), it allows to develop vision applications for the morphological analysis of objects, pattern recognition, bar codes / matrix, OCR, applications of color classification, as well as a complete 3D application analysis library. Unlike other visual programming softwares, Halcon's open software architecture allows to access defined data structures and thus to integrate Halcon with further software components such as a user interface. Halcon offers various

interfaces to access all its operators from programming languages like C, C++, and .NET languages like C# or VB.NET.

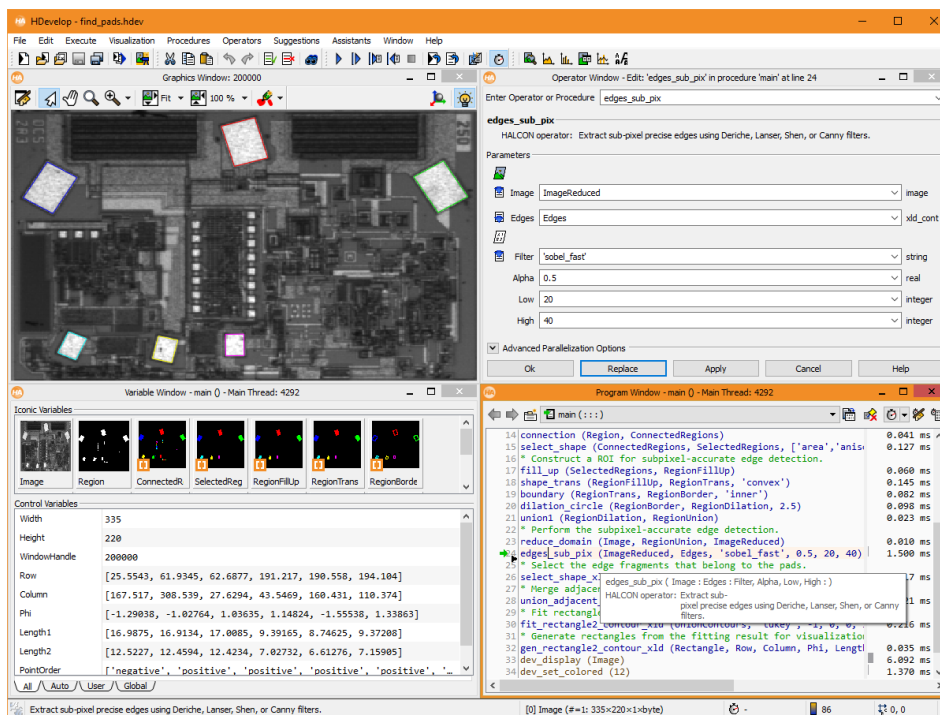


Figure 2.15: Halcon software

2.5.4 Merlic

Merlic is an all-in-one software for quickly building machine vision applications without programming. It is based on MVTec's extensive machine vision expertise and combines reliable, fast performance with ease of use. The vision engine of Merlic is based on Halcon so, it is a good choice if the application is not very complex thanks to its visual approach programming.

An image-centered user interface and intuitive interaction concepts like easy-touch provide an efficient workflow, which leads to time and cost savings. The very clear and reduced interface presents a large view on the processed image in the center of the program. The tool library on the left

side provides many standard vision tools such as acquisition, calibration, alignment, measuring, counting, checking, reading, position determination, and defect detection. It can also be extended with customized tools. Each tool has its own graphical representation in the workspace, which allows you to see and review every step of your vision application. The image-centered design allows you to configure the application directly via the image without the need to write source code or to adjust lots of parameters. While most common machine vision programs require extensive programming knowledge, Merlic was created to build a machine vision application without programming a single line of code. So instead of coding line by line, you can simply step through your application and rely on the many standard machine vision tools. The vision tools in the Merlic are connected automatically. Alternatively, you can simply reconnect them by drag and drop. Figure 2.16 shows the software interface.

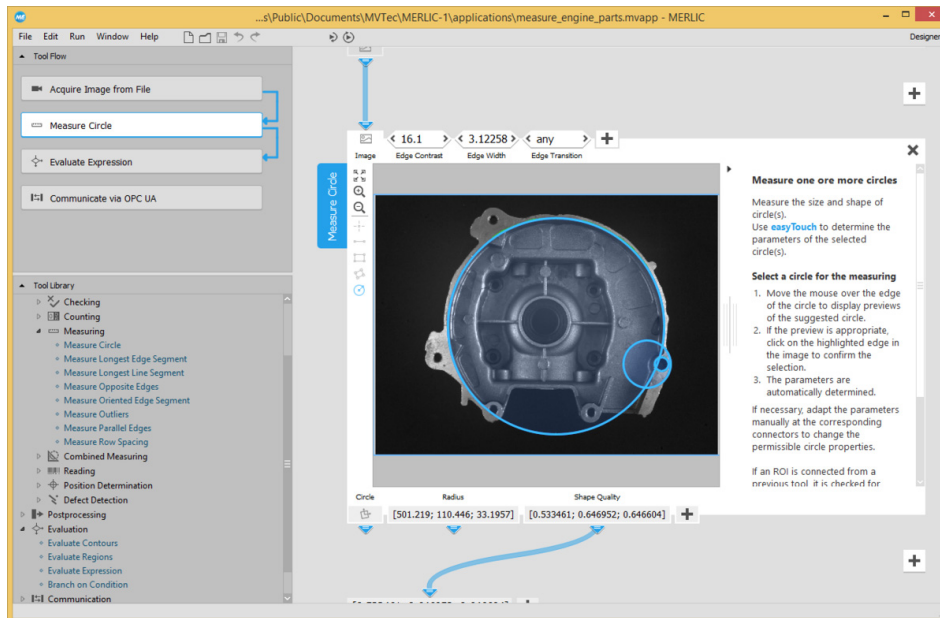


Figure 2.16: Merlic development interface

Part II

Proposal

Proposal I: Optimal Light Alignment

3.1 Introduction

Usually an industrial camera does not have its own lens. Instead, they come with a standardized mount and a wide range of lenses available for that mount. However, it is fundamental to ask the question; how is a suitable lens chosen? There are three main factors that affect this choice notably: the camera sensor size, the working distance and the field of view of the camera. The illumination setup is also an aspect to take into consideration. The focal length can be determined directly from the field of view and the working distance, as shown in Equation 3.1, where h is the horizontal sensor dimension (number of horizontal pixels multiplied by the pixel size) and f is the focal length of the lens, the horizontal field of view (HFOV) and the working distance (WD). Some amount of flexibility to the system's working distance should be factored in, as the above equation is only a first-order approximation and does not take distortion into account.

$$f = \frac{h * WD}{HFOV} \tag{3.1}$$

There are a lot of manufacturers who sell industrial lenses, so one must be clear about what lens is appropriate for each application. Even so, it is not easy to choose the best lens. In fact, many times the choice of the lens does not lead to the expected or optimal results. The only detail to

be considered is that most of the industrial lenses that are marketed are fixed focus lenses. There are various types of lenses: standard or endocentric lenses, telecentric lenses, lenses with motorized zoom capability, autofocus lenses, macrolenses, and perferic lenses, among others. In this thesis we focus our studies on endocentric and telecentric lenses.

3.1.1 Standard or endocentric lenses

Standard lenses are the most often used in machine vision systems. They have a wide range of focal distance, ranging from around 3mm to 200mm. They are optimized to focus the desired object from very close distances to very far distances. In this kind of lenses, a minor distortion or aberration effect is present. This distortion can affect the image in three ways:

- Barrel distortion: image magnification decreases with distance from the optical axis. The apparent effect is that of an image which has been mapped around a sphere (or barrel), as shown in Figure 3.1(a).

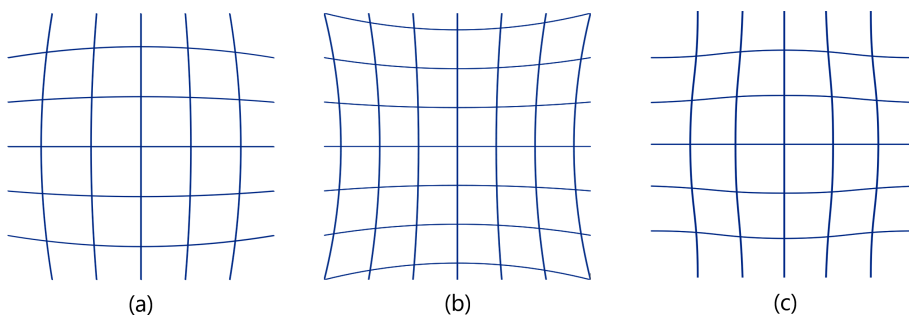


Figure 3.1: Optical distortions

- Pincushion distortion: image magnification increases with the distance from the optical axis. The visible effect is that lines that do not go through the center of the image are bowed inwards, towards the center of the image, like a pincushion, as shown in Figure 3.1(b).
- Mustache distortion: a mixture of both types, sometimes referred to as mustache distortion or complex distortion, is less common but not rare. It starts out as barrel distortion close to the image center and gradually turns into pincushion distortion towards the image

periphery, making horizontal lines in the top half of the frame look like a handlebar mustache, as shown in Figure 3.1(c).

Distortion is a key effect to take into account in Computer Vision applications, because it can lead to completely wrong results or measurements. The degree of distortion of each lens is often specified by the manufacturer. Moreover, there are distortion correction techniques that can be applied by the use of software, which are discussed a little further.

3.1.2 Telecentric lenses

Software engineers requiring precise measurement of mechanical parts need high contrast images with the lowest possible geometrical distortion. Perspective effects, causing change of magnification when the object is not precisely positioned or is highly 3-dimensional, must also be minimized or canceled. Besides image processing problems, vision system designers must take into account that common endocentric optics introduce several factors, which limit measurement accuracy and repeatability such as:

- non-constant magnification with object displacement
- image distortion
- perspective errors
- poor image resolution
- uncertainty in determining object edge position

Telecentric lenses reduces or even cancel most of these problems, and for this reason have become a key component for developing high accuracy gauging applications. A telecentric lens is a compound lens that has its entrance or exit pupil at infinity; in the prior case, this produces an orthographic view of the subject. This means that the chief rays (oblique rays that pass through the center of the aperture stop) are parallel to the optical axis in front of or behind the system, respectively. This kind of lenses help a great deal in reducing the level of perspective distortion.

3.1.2.1 Magnification constancy

In measurement applications, an orthonormal view of the object is frequently needed so that correct linear measurements may be performed. As often is the case, because of vibration, many mechanical parts cannot be precisely positioned, or a measurement must be performed at different depths or the object thickness may vary. Nevertheless, there is the need to do a perfect correlation between imaged and real dimensions, as shown in Figure 3.2.

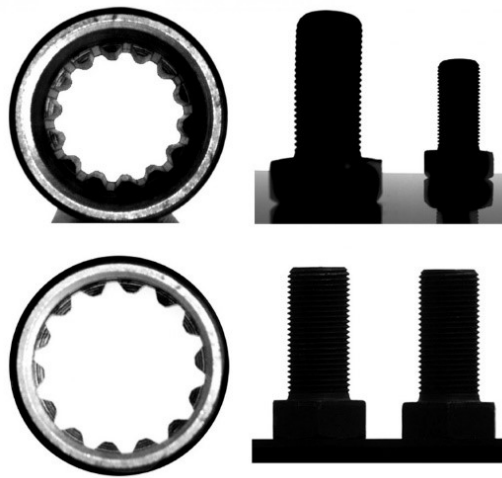


Figure 3.2: On the left an image of an internal spline on a cylindrical object taken with a telecentric lens (top) and the same object viewed by an ordinary lens (bottom). On the right an image of two identical machine screws set 100mm apart, taken with a telecentric lens (top) and with an ordinary lens (bottom)

Common lenses give different magnifications at different conjugates, such as when the object is displaced, the size of its image changes almost proportionally with the object distance. With telecentric lenses the image size is left unchanged with object displacement, provided the object stays within a certain range often referred to as depth of field or telecentric range.

3.1.2.2 Low distortion

Distortion is one of the worst problems limiting measurement accuracy, even the best performing optics are affected by some grade of distortion, while often even a single pixel of difference between the real image and the expected image could be critical. Distortion is simply defined as the percentage difference between the distance of an image point from the image center and the same distance as it would be measured in a distortion-free image; it can be thought of as a deviation between the imaged and the real dimensions of an object. High quality telecentric lenses normally show a very low distortion degree, in the range of 0.1%, although this amount seems to be very small it would actually result into measurement errors approaching the size of one pixel of a high-resolution camera. For this reason, in most applications, distortion has to be software calibrated.

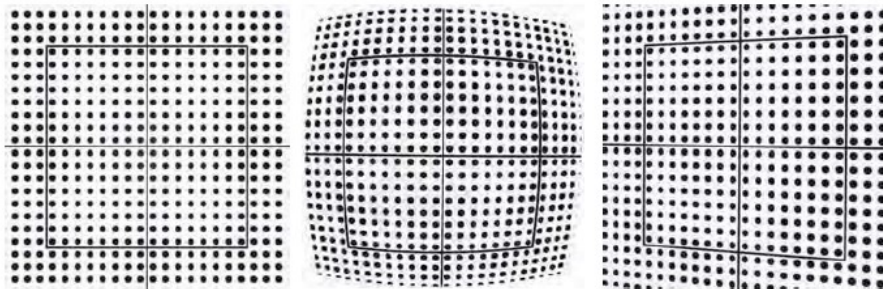


Figure 3.3: on the left an image of a distortion pattern taken with a telecentric lens, where no radial or trapezoidal distortion is present. In the middle the image of the same pattern showing strong radial distortion. On the right an example of trapezoidal distortion.

Figure 3.3 shows the effect of an image of a distortion pattern taken with a telecentric lens.

3.1.2.3 Perspective errors limitation

When using common optics to image objects, far objects will look smaller than closer objects. As a consequence, when objects like a cylindrical cavity are imaged, the top and the bottom crown edges will appear to be concentric although the two circles are perfectly identical. On the contrary, by means of a telecentric lens, the bottom crown edge will disappear because the two crown edges are perfectly overlapping. Figure 3.4 shows the distortion effect of endocentric lenses against the same effect present in telecentric lenses. It can be seen the improvement of the telecentric lenses in terms of distortion.

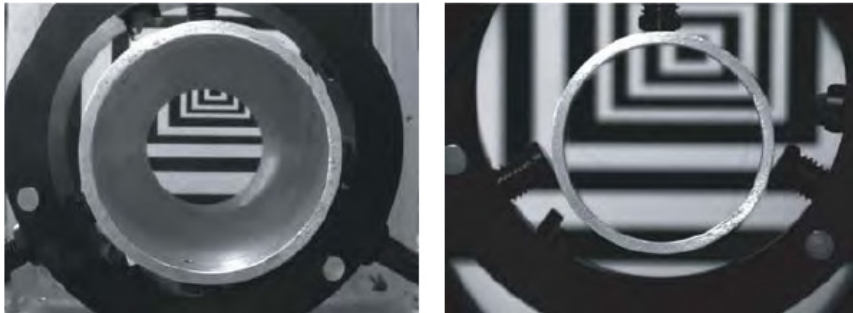


Figure 3.4: On the left endocentric lens showing image perspective error. On the right, a telecentric lens is able to cancel any perspective effect.

However, telecentric systems also have some disadvantages: as only light that enters in parallel can reach the image plane, and only objects placed directly in front of the lens are visible. Also, telecentric lenses are usually significantly more expensive than regular endocentric lenses. Furthermore, as the light rays are parallel to the optical axis, there is a need to have larger lens diameters, which makes them considerably larger and heavier than standard lenses.

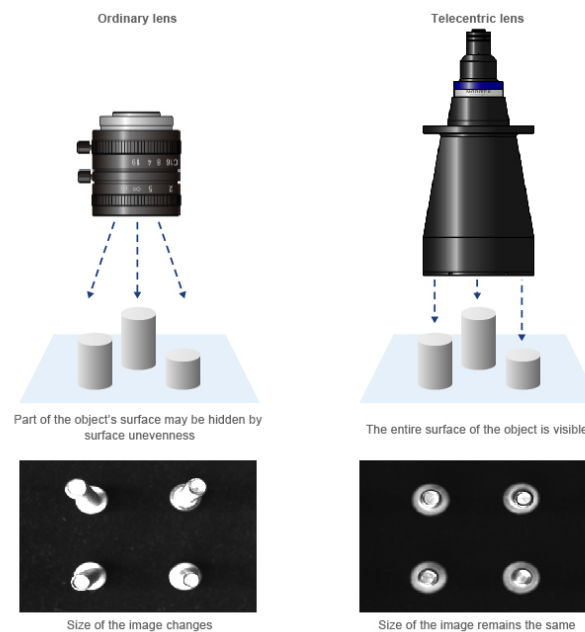


Figure 3.5: Comparison between standard and telecentric lenses

3.2 Optical Axis Alignment

The performances of a lens setup is achieved when working with high contrast not-saturated images. To achieve optimal illumination, there is the need to change the exposure time on the camera panel and/or light intensity on the back-light. Optical axis alignment is conducted by tilting the lens illuminator around the X and Y axis, assuming the optical axis corresponds with the Z axis. Figure 3.6 shows a scheme of the tilt. The effects of lens misalignment can be highly pronounced. If, for example, the lens is shifted in the x, y plane from its optimum position, the image captured by the sensor will also be shifted by a corresponding amount. If the lens is not mounted correctly in the z plane, then the result will be an image that is not perfectly focused. If the lens is tilted, part of the image captured by the sensor may be in focus while another part of the image will be blurred. The alignment process increases the homogeneity in order to achieve image improvement.

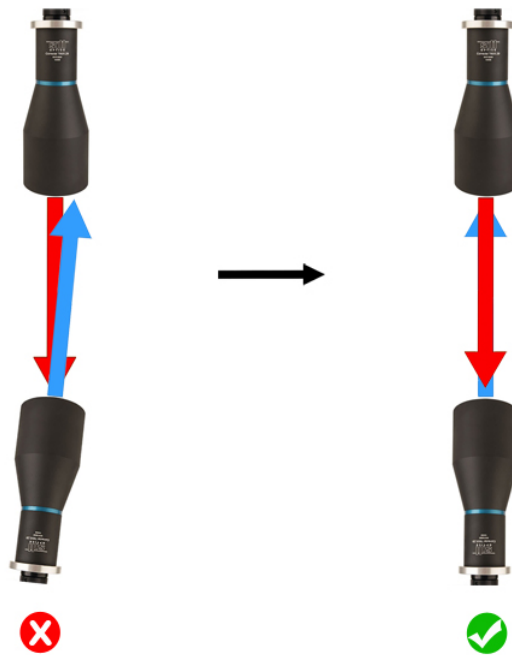


Figure 3.6: Scheme of the optical axis alignment

3.3 Experiment and Analysis

In this proposal, we have developed a light alignment algorithm using Halcon development framework to track different regions of interest (ROI) of an acquired image plane to verify if the image plane reaches an optimal or a not-optimal light alignment. This observation is necessary because, often times, the effect of light alignment is taken for granted, or not taken into consideration at all. It is often assumed that there is little or no error derived from this consideration. However, the experiments revealed that the effects of a badly aligned lighting system can have an impact on the calibration process, and hence on the measurement result. Several experiments were performed to determine the effects of a well aligned lighting system against the other parameters, like calibration error and object alignment (see Chapter 6 for more details of the proposals validation experiments). Figure 3.7 shows the flowchart process of the algorithm.

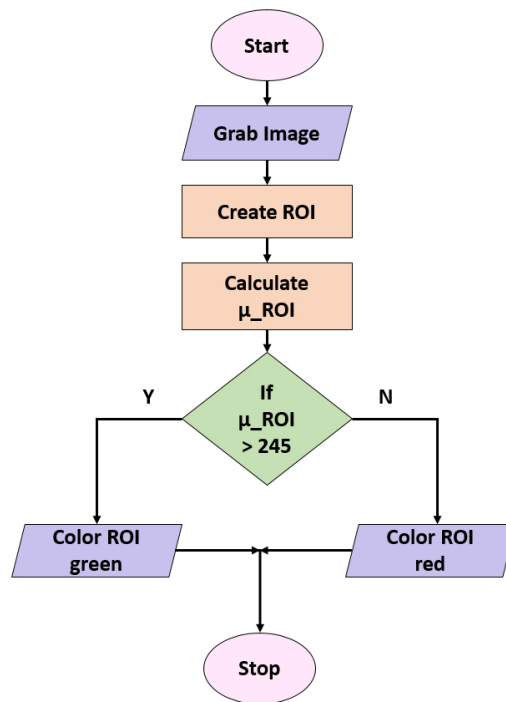


Figure 3.7: Flowchart of the light algorithm

The light alignment algorithm creates different ROIs in the acquired image. The pixel intensity mean of each of the ROI is calculated. If the mean of the ROI is greater than a specific threshold, a decision is made on whether to color the borders of the ROI green or red for giving a user feedback. A good exposure value is set when the average indicator on the lens-light alignment interface is green. This process is applied to all the created ROIs. The best position is achieved when most of the region rectangles are maximizing their mean values.

The experiments were performed using the endocentric and telecentric lenses to ascertain for optimal light alignment and observing that the results are exactly the same for both kind of lens. Figure 3.8 shows the instrumentation used to perform the experiments and Figure 3.9 shows a summary of the hardware specifications.


EXPERIMENT\DEVICE	CAMERA	OPTICS	LIGHT
Endocentric		 Goyo Optical GM31614MCN	
Telecentric	Allied Vision Manta G-504B	 Opto Engineering TC12056	Backlight IBL-W130- 110

Figure 3.8: Devices and instruments used for the light alignment experiments

DEVICE	Specifications																		
 Allied Vision Manta G-504B	<table border="1"> <tr> <td>Interface</td> <td>IEEE 802.3 1000baseT</td> </tr> <tr> <td>Resolution</td> <td>2452 x 2056</td> </tr> <tr> <td>Sensor</td> <td>Sony ICX655</td> </tr> <tr> <td>Type</td> <td>CCD Progressive</td> </tr> <tr> <td>Sensor Size</td> <td>Type 2/3</td> </tr> <tr> <td>Cell size</td> <td>3.45 μm</td> </tr> <tr> <td>Lens mount</td> <td>C</td> </tr> <tr> <td>Max frame rate at full resolution</td> <td>9 fps</td> </tr> </table>	Interface	IEEE 802.3 1000baseT	Resolution	2452 x 2056	Sensor	Sony ICX655	Type	CCD Progressive	Sensor Size	Type 2/3	Cell size	3.45 μ m	Lens mount	C	Max frame rate at full resolution	9 fps		
Interface	IEEE 802.3 1000baseT																		
Resolution	2452 x 2056																		
Sensor	Sony ICX655																		
Type	CCD Progressive																		
Sensor Size	Type 2/3																		
Cell size	3.45 μ m																		
Lens mount	C																		
Max frame rate at full resolution	9 fps																		
 Goyo Optical GM31614MCN	<table border="1"> <tr> <td>Focal Length</td> <td>16mm</td> </tr> <tr> <td>Iris Range</td> <td>f/1.4-Close</td> </tr> <tr> <td>Lens Format</td> <td>2/3"</td> </tr> <tr> <td>Resolution</td> <td>100 lp/mm</td> </tr> <tr> <td>MOD</td> <td>400mm</td> </tr> <tr> <td>Mount</td> <td>C</td> </tr> <tr> <td>Filter Thread</td> <td>M27xP0.5</td> </tr> <tr> <td>Angle of View (HxVxD) 1/2"</td> <td>22.2° x 16.5° x 27.58°</td> </tr> <tr> <td>Angle of View (HxVxD) 2/3"</td> <td>30.22° x 23.0° x 38.6°</td> </tr> </table>	Focal Length	16mm	Iris Range	f/1.4-Close	Lens Format	2/3"	Resolution	100 lp/mm	MOD	400mm	Mount	C	Filter Thread	M27xP0.5	Angle of View (HxVxD) 1/2"	22.2° x 16.5° x 27.58°	Angle of View (HxVxD) 2/3"	30.22° x 23.0° x 38.6°
Focal Length	16mm																		
Iris Range	f/1.4-Close																		
Lens Format	2/3"																		
Resolution	100 lp/mm																		
MOD	400mm																		
Mount	C																		
Filter Thread	M27xP0.5																		
Angle of View (HxVxD) 1/2"	22.2° x 16.5° x 27.58°																		
Angle of View (HxVxD) 2/3"	30.22° x 23.0° x 38.6°																		
 Opto Engineering TC12056	<table border="1"> <tr> <td>Magnification</td> <td>0.114</td> </tr> <tr> <td>Working Distance</td> <td>157.8 mm</td> </tr> <tr> <td>Sensor Size</td> <td>1/2</td> </tr> <tr> <td>Vision Area</td> <td>62.58 mm x 46.75 mm (with sensor 1/1.8")</td> </tr> <tr> <td>Mount</td> <td>C</td> </tr> <tr> <td>Distortion Typical</td> <td><0.04 %</td> </tr> <tr> <td>Field depth</td> <td>51 mm</td> </tr> <tr> <td>Length</td> <td>205 mm</td> </tr> <tr> <td>Diameter</td> <td>80 mm</td> </tr> </table>	Magnification	0.114	Working Distance	157.8 mm	Sensor Size	1/2	Vision Area	62.58 mm x 46.75 mm (with sensor 1/1.8")	Mount	C	Distortion Typical	<0.04 %	Field depth	51 mm	Length	205 mm	Diameter	80 mm
Magnification	0.114																		
Working Distance	157.8 mm																		
Sensor Size	1/2																		
Vision Area	62.58 mm x 46.75 mm (with sensor 1/1.8")																		
Mount	C																		
Distortion Typical	<0.04 %																		
Field depth	51 mm																		
Length	205 mm																		
Diameter	80 mm																		

Figure 3.9: Devices' specifications used for the light alignment experiments

The first set of experiments to this effect was to test the effect of a not-optimal light alignment system. The illuminator was set at certain angles to cause an angular light deflection. Figure 3.10 shows the not-optimal system configuration.

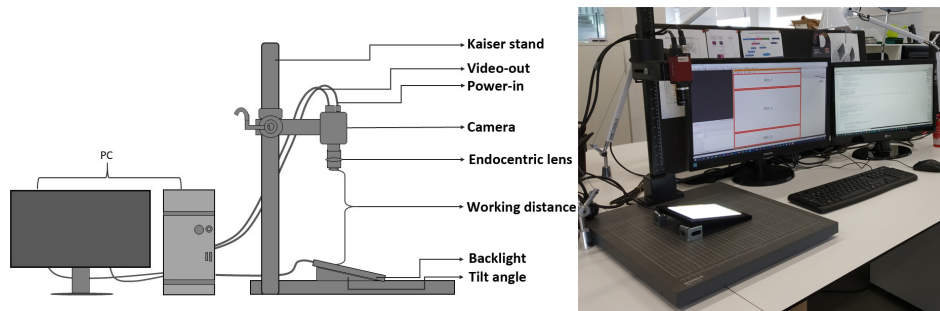


Figure 3.10: Not-optimal light alignment setup

The second set of experiments was performed to test the effect of an optimal alignment system. In these experiments, the light illumination was set at a perfect alignment with the lenses. The level of alignment was achieved with the aid of the developed light alignment algorithm. Figure 3.11 shows the optimal light alignment configuration. The effect of the deflection is observed in Figure 3.12(a).

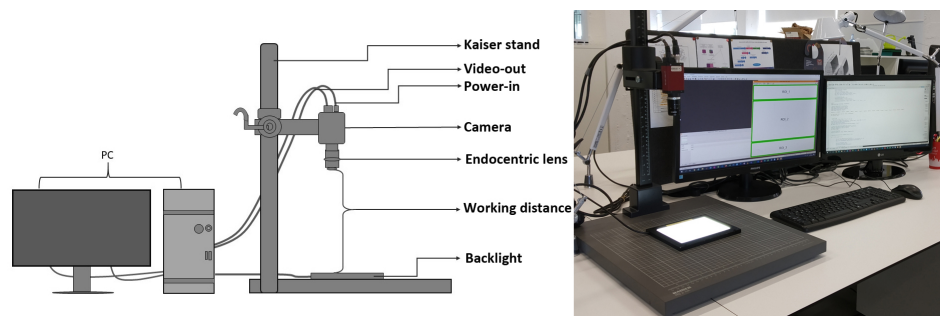


Figure 3.11: Optimal light alignment setup

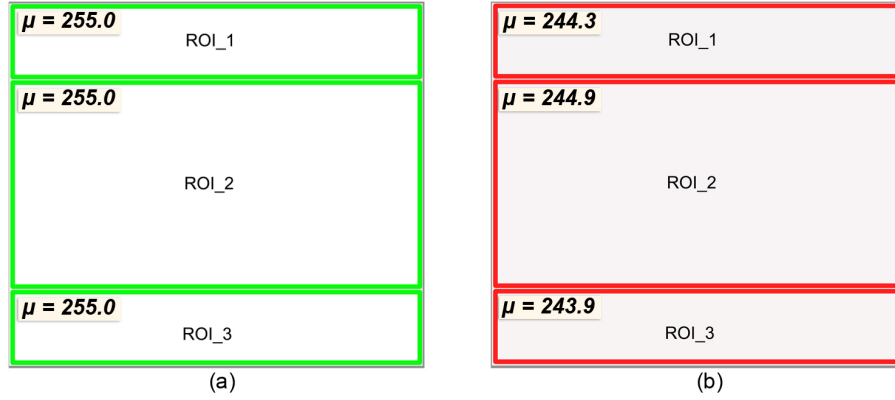


Figure 3.12: (a) Optimal light alignment. (b) Not-optimal light alignment

Three ROIs have been used for the purpose of the experiments. The number of ROIs used could depend on the particular interest of the research, as the same algorithm is implemented for each ROI. For the purpose of this proposal, we considered three ROIs sufficient to track and monitor the effects of the tilt angles and light deflection on the image plane for the calibration process. Table 3.1 shows the summary of the experiments performed with the algorithm to test the ROIs.

Table 3.1: Summary of the light alignment experiments

ROI\Tilt Angle	0°	10°	15°	20°
1	255.000	253.984	251.829	245.999
2	255.000	252.655	251.758	234.958
3	255.000	252.995	251.965	244.996
Average	255.000	253.211	251.851	244.984

Figure 3.13 shows some examples of the light alignment experiments. The figure shows the mean pixel values of the three ROIs and the corresponding tilt angle of the back-light.

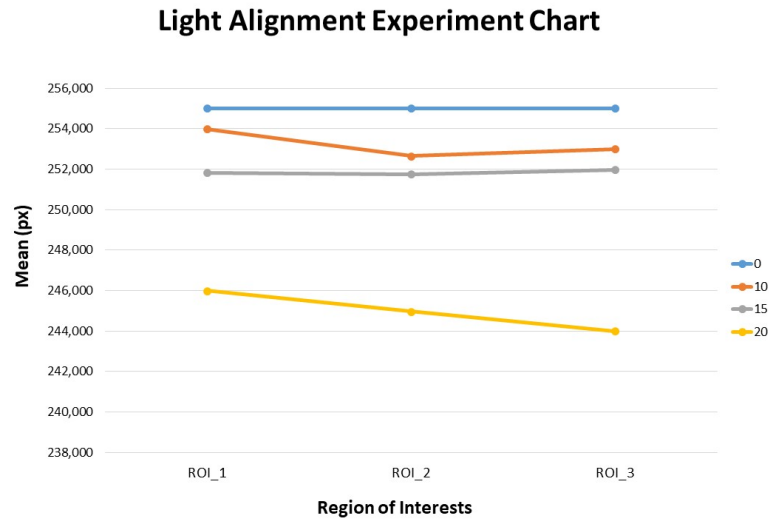


Figure 3.13: Chart of the experimental

3.4 Discussion

The light alignment algorithm was developed to monitor and achieve an optimal alignment system, in order to eliminate the possible effects of misalignment, which could lead to significant errors in the calibration process and measurement system. The impact that misalignment have on the calibration and measurement process is described in detail in Chapter 6. However, several observations can be made so far:

- It is observed that the mean value of the pixel at the ROIs have no significant difference at 0° , 10° and 15° tilt angles respectively. However, a notable decline is observed at 20° tilt angle. This could be a result of a significant change in the working distance between the camera and the illuminator.
- Although 0° , 10° and 15° tilt angles seem to have similar alignment values, the fact is that they don't. Even these small changes could produce differences in the measurement process.
- The light alignment algorithm performs equally for both the telecentric and endocentric lens. This is as a result of the sensor

exposure of the camera and the principal calculations of the mean and the standard deviation of the ROIs, which has the same tolerance regardless of the lenses.

The goal of Chapter 6 is to proof that although visually a misalignment of 10° or 15° is good enough, it is worth looking for the optimal in order to demonstrate the effects of an optimal and a not-optimal light alignment system in the calibration process and measurement system.

Proposal II: Optimal Camera Focus and Calibration Parameters Study

A synthesis of this chapter is under review in:

Moru, D. K. and Borro, D. "Analysis of different parameters of influence in industrial cameras calibration processes". Measurement 2020. (Quartil Q1).

4.1 Introduction

The effect of a good calibrating procedure cannot be over-emphasized enough, due to the benefits it gives to the system. In machine vision, calibration is used to convert dimensions in the image coordinate plane to the world coordinate plane. This conversion primarily affects the metrological system. For accurate and precise measurement to be taken, the calibrated system has to possess very little or no error. However, as this is almost impossible to achieve, due to several factors, the evaluation of the degree of uncertainty is used to determine the accuracy of the calibrated system (Moru and Borro, 2020).

Image formation process has been a trending research for over 20 years. This process is intrinsic to the end target of image processing. It

is important to understand the different techniques often used to form digital images. The processing advances and their affiliated algorithms when reviewing digital image techniques, are highlighted in (Ekstrom, 2012). The determination of light exposure from a point on an image to the observer is vital to understanding how images are composed. Camera sensor exposure can be perplexing to comprehend but it is fundamental to pay attention to how lighting affect the acquisition of the image, because the most essential precondition for a camera system is to give consistent image quality (Shirvaikar, 2004). The proper understanding of exposure makes possible the acquisition of images of ideal brightness, high levels of details in shadows, translation and rotation, where applicable.

Automatic camera focus revolutionized the digital image world. With automatic focus, quality images can be acquired from a wider range of camera quality specification. This has proven to be reliable in a non-industrial setting. However, in industrial inspections, automatic focused cameras are not broadly used because most applications have a fixed working distance. Although there are lens products with programmable focus, the use of a manual camera focus has been mainly adopted. With a manual camera focus, more control can be achieved regardless of the change or random nature of the working distance. Nevertheless, this option poses a great challenge in the achievement of a good-focused image. The human eye is visually capable of determining when a camera image is well-focused but it is not capable of determining the optimal one. This proposal addresses the challenge to discover the effects of four parameters in the determining the error in a calibration process.

There are previous works that study the influence of different parameters in the calibration process. For instance, (Chen et al., 2014) study the influence of corner detection, noise, and number of used pattern image; and (Muruganantham et al., 2008) study factors like illumination intensity, length of extender tube, number of control points, and region of interest. However, in this proposal other different parameters have been taken into account like camera focus, exposure time, calibration plate tilt and number of images used. The experiment performs calibration on the images taken with endocentric and telecentric lenses. A sample of 2176 images was used to generate the population analysis.

The analysis of the camera focus on the calibration process shows that the human eye cannot visually determine an optimal focus of an image.

This means that it is difficult to visually determine when an image is 100% focused from when it is 95% focused for example. However, the existence of a difference, even if negligible, plays a vital role and has an effect in the calibration error, and therefore in the measurement error. In this proposal, we determine the comparative difference in the calibration results among the focus of 95%, 97% and 99%. The experiments show that the calibration error reduces, with a statistically significant effect, as the focus tends toward 100%. The difference, even though small, has an impact in the accuracy of the calibration process. The paper also study other calibration parameters like exposure time, tilt angle of the calibration plate and number of images used. A multivariable statistical analysis was performed to study the influence of each parameter in the calibration error.

4.2 Focus computation algorithm

In an industrial calibration process, where the working distance is constant, the use of a manual focus camera is necessary due to several factors such as, the distance between the object and the camera, which usually affects the focus and focal length of the lens, the size of the object, which determines the field of view (FOV), the camera exposure, which determines how the lighting can be controlled or if the object is luminous or not (Kepf, 2016). These parameters make selecting the proper lens a challenge. A focused lens manifests the manner in which the image from the world is reproduced on the sensor, which could be adjusted manually or automatically, as shown in Fig.4.1.

The criteria for quantifying the focus of an image are usually based on the evaluation of the gradient function (Chern et al., 2001). In the past, several experimental evaluation on focus measures have been researched (Shirvaikar, 2004) (Li et al., 2004) (Zhang et al., 2000). D. Wang et al. (Wang et al., 2013a) demonstrated a fast auto-focusing technique, which employed internal optical elements to directly sense the deviations in back focal distance of the lens and restore the imaging system to a best-available focus. Y. Tian (Tian, 2011) proposed a focus measure using phase congruency, by addressing the key issue in passive autofocus, choosing robust focus measures to judge optical blur in defocused images. W. Martin (Martin, 2019) developed a system and method for installing security cameras on a security network. The cameras include an autofocus routine,

with manually adjustable lenses, and a feedback mechanism. The autofocus routine calculates the degree to which the field of view is out of focus and the feedback mechanism provides feedback to the installer during installation.

For our experiments, we follow the well-known approach of measuring the sharpness of an image using edge gradients (Chern et al., 2001). For the edge detection, the Sobel operator is used and the sharpness quantity is computed as the standard deviation of the grey values of the image. Moving the focus ring of the lens, the most focused image will be the one with the highest sharpness value.

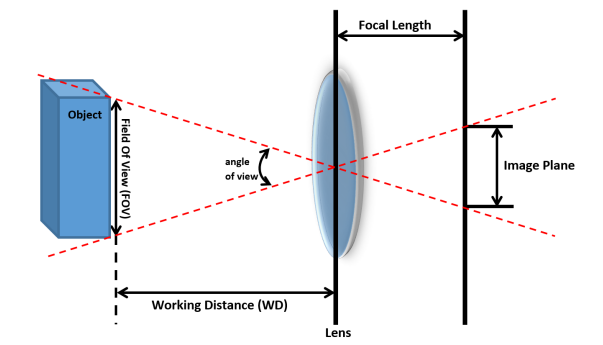


Figure 4.1: The relationship between field of view, focal length and image plane

From now on, when the term "focus level" is used, it implies to the percentage of the maximum value computed with the edge gradient algorithm.

4.3 Camera Model Representation

The pinhole (Wang et al., 2013b) (Chen et al., 2012) (Hartley and Zisserman, 2003) is the most common camera model. It projects a 3D point $\mathbf{P}(x_w, y_w, z_w)$ on an image plane $\mathbf{p}(u_u, v_u)$ in the given mathematical equation:

$$s \begin{bmatrix} u_u \\ v_u \\ 1 \end{bmatrix} = \begin{bmatrix} f_x & 0 & c_x & 0 \\ 0 & f_y & c_y & 0 \\ 0 & 0 & 1 & 0 \end{bmatrix} \begin{bmatrix} \mathbf{R} & \mathbf{t} \\ \mathbf{O}^T & 1 \end{bmatrix} \begin{bmatrix} x_w \\ y_w \\ z_w \\ 1 \end{bmatrix} \quad (4.1)$$

where s is a non-zero scale factor (Liu et al., 2015), (f_x, f_y) are the scale factors along the image axes u and v , and (c_x, c_y) is the principal point. (f_x, f_y, c_x, c_y) are the four intrinsic parameters. While the extrinsic parameters \mathbf{R} and \mathbf{t} , are the rotation matrix and the translation vector from the world coordinate system to the camera coordinate system.

Within a camera, distortion of the lens, especially radial distortion, is often present. Many digital cameras are made from lenses with spherical surfaces, and the latent radial distortions serves as unique identification within the images (San Choi et al., 2006). Camera calibration determines the intrinsic parameters, extrinsic parameter and the lens distortion coefficient.

Let $\mathbf{p}_u(x_u, y_u)$ and $\mathbf{p}_d(x_d, y_d)$ be the distortion-free image and the distorted image coordinates respectively:

$$\begin{cases} x_u = x_d(1 + k_1r^2 + k_2r^4 + k_3r^6 \dots) \\ y_u = y_d(1 + k_1r^2 + k_2r^4 + k_3r^6 \dots) \end{cases} \quad (4.2)$$

where $r = \sqrt{x_d^2 + y_d^2}$; $k_{1,2}, k_3 \dots$ are the coefficients of radial distortion.

The analysis of a computer vision system often leads to a decision on the type of lens to be used for acquisition of the image. There are three categories of lens options: endocentric, telecentric and hypercentric. The endocentric lens captures images with the same perspective as the human eye. It is commonly referred to as the standard fixed-focal-length lens. The telecentric lens erases the perspective errors. The hypercentric lens reverses the usual perspective to see nearly the entire surface of a tridimensional object. However, this proposal does not consider the hypercentric lens.

4.3.1 Calibration Process

Camera calibration is an estimation method for generating the intrinsic and extrinsic parameters (Zhang, 2000). As a result of different calibration

processes, the intrinsic parameters of the camera are determined to define the concept of imaging. There are different calibration techniques, but all of them have a common objective, they try to minimize projection errors. The perfect calibration of a camera would guarantee that the projected points coincide with the points detected. In reality, however, there is a certain projection error that is calculated as the Euclidean distance between the two points. Therefore, the objective of the calibration process is to minimize these errors to ensure the highest possible accuracy.

A distinctive feature of a calibration process is based on matching specific measured positions on the camera sensor with the specific real world position on a calibration target. A calibration target with accurately known metrics properties is chosen to fill approximately 80% of the field of view. Before calling the actual calibration, a series of images of the calibration object in different orientations is obtained and care is taken to make sure that the whole field of view or measurement volume is covered.

Figure 4.2 shows a point in space with known coordinates (X, Y, Z) . For that 3D point, a point (h, v) is detected in the image plane. In addition, 3D points are projected through several initial intrinsic parameters. The point detected (h, v) and the projected point do not occupy the same position in the plane. In such a way that it is necessary to apply the correction of distortions in order to obtain the point (p, q) .

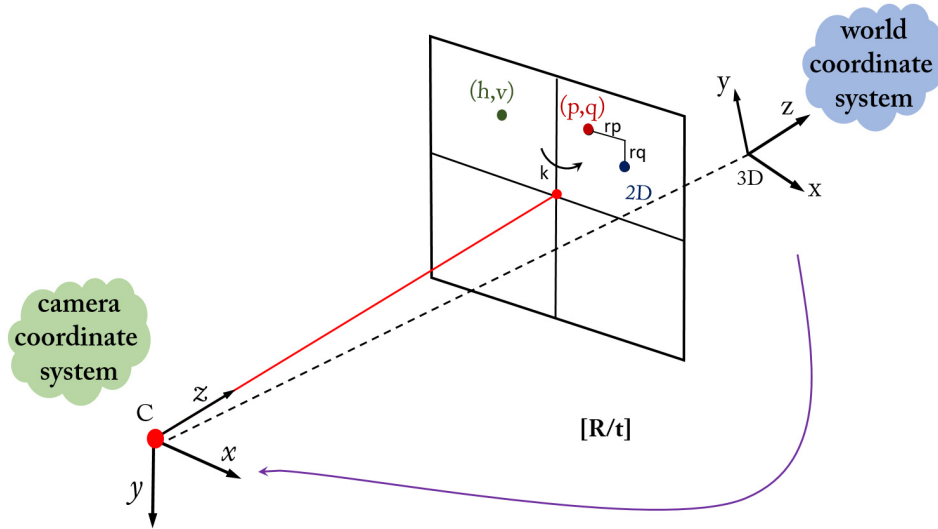


Figure 4.2: Perspective projection model

After applying the correction to the detected points, it does not occupy yet the same position in the image. Therefore, the difference between the horizontal and vertical coordinates of the corrected points (p, q) and the 2D projected points, define the residual error terms (r_p, r_q) according to Equation (4.3).

$$\begin{aligned} r_p &= (p_i - 2D_{X_i}) \\ r_q &= (q_i - 2D_{Y_i}) \end{aligned} \quad (4.3)$$

By grouping the terms of residual errors in a vector (Equation (4.4)), the vector that is intended to be minimized by calibration is achieved.

$$[r] = \begin{bmatrix} r_{11} \\ r_{21} \\ \cdot \\ r_{1N} \\ r_{2N} \end{bmatrix} = \begin{bmatrix} (p_1 - 2D_{X1}) \\ (q_2 - 2D_{Y2}) \\ \cdot \\ (p_N - 2D_{XN}) \\ (q_N - 2D_{YN}) \end{bmatrix} \quad (4.4)$$

In this proposal we use HALCON software (Halcon HDevelop 13) and its calibration procedure. For this, the known 3D model points are

projected into the image and the sum of the squared distances between the projected 3D-coordinates and their corresponding image point coordinates is minimized (Equation (4.4)). For a successful calibration, at least one calibration object with accurately known metric properties is needed (a HALCON calibration plate like the one shown in Figure 4.3), taking a series of images of the calibration object in different orientations and making sure that the whole field of view or measurement volume is covered.

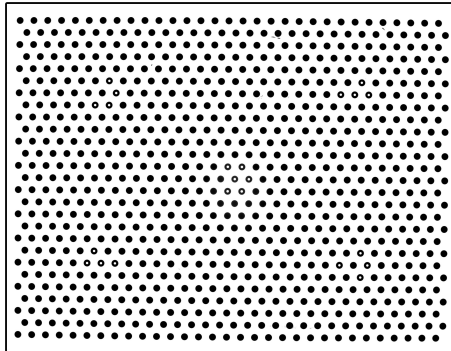


Figure 4.3: Calibration plate in Halcon development framework. Note the white marks, useful to know the orientation of the plate.

As a direct result, only the calibration error is returned by the HALCON calibration process. It corresponds to the average distance (in pixels) between the back-projected calibration points and their extracted image coordinates. HALCON documentation points out that an error of up to 0.1 pixels indicates that the calibration is successful.

4.4 Experiments and Analysis

The devices of the experiments are the same as the ones of previous chapter (Figure 3.8). All images have been taken from a 145.1 mm and 157.8 mm of working distance for endocentric and telecentric respectively, both using a transparent calibration pattern of 80x60 mm.

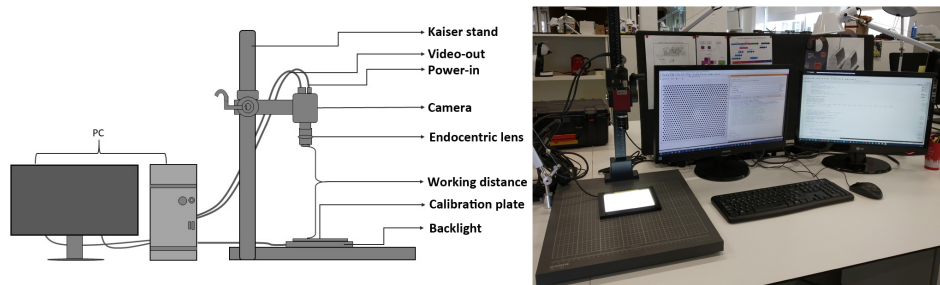


Figure 4.4: Optimal calibration plate alignment setup

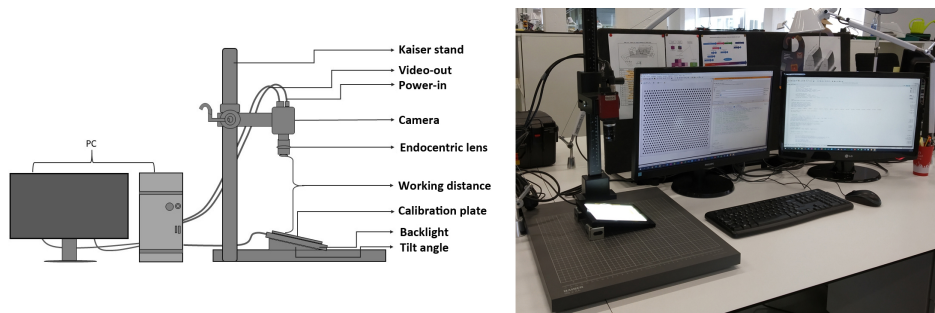


Figure 4.5: Not-optimal calibration plate alignment setup

Figure 4.4 and Figure 4.5 show the optical set-up configuration. To perform the calibration experiment, a total of 2176 image samples were acquired from both endocentric and telecentric lenses. The images acquired with endocentric lens are grouped into three categories:

- **Center plate no tilt:** In this experiment, 8 positions of the calibration images were acquired with no angular tilt (i.e., flat with the table), rotating each time 45° over the camera axis. The camera exposures range between 5000:1000:8000, and the focus level at 95%, 97% and 99% respectively. A total number of 96 images are acquired.
- **Corner plate 20° degree tilt:** In this experiment, the angular tilt of the calibration plate with respect to the table plane is 20° , changing the tilt in each of the four corners and between corners. For each position of the tilt, 8 images of the calibration plate, using the corresponding plate rotation are acquired. Besides, for each position

of the tilt, the camera exposures range between 5000:1000:8000, and the focus level at 95%, 97% and 99% respectively. A total number of 768 images are acquired.

- **Corner plate 30° tilt:** This experiment is exactly as the previous one but with an angular tilt of the calibration plate of 30°. A total number of 768 images are acquired.

The images acquired with the telecentric lens are grouped into three categories:

- **Center plate no tilt:** In this experiment, 8 positions of the calibration plate was acquired with no angular tilt, rotating 45° over the camera axis. The camera exposures range between 6000:1000:9000. No focus level is required. A total number of 32 images are acquired.
- **Corner plate 20° tilt:** In this experiment, the angular tilt of the calibration plate is 20°. For each position of the tilt, 8 images of the calibration plate, using the corresponding plate rotation (previous point) are acquired. The camera exposures range between 6000:1000:9000. No focus level is required. A total number of 256 images are acquired.
- **Corner plate 30° tilt:** This experiment is exactly as the previous one but with an angular tilt of the calibration plate of 30°. A total number of 256 images are acquired.

A summary of the number of images used for each calibration process can be observed in Table 4.1. Note that for each number of images that appear in the cells, the exposure time and focus level values have also been varied with the ranges described above.

After the acquisition of the images, different calibration processes were performed using the Halcon development framework. The camera focus level was measured (following the method described in Section 4.2) by three levels of focus percentages: 95%, 97% and 99% respectively. These focus levels are visually well targeted and impossible to differentiate by the human eye. The camera exposure is controlled and measured by changing the sensor exposure within the Halcon framework for each percentage degree of focus.

Table 4.1: Number of images used in each calibration configuration

Lens	No tilt	Tilt (for 20° and 30°)											
		Corner 1	Corner 2	Corner 3	Corner 4	Corner 5	Corner 6	Corner 7	Corner 8	Corner 1,3,5,7	Corner 2,4,6,8	All corners	
Endocentric	8	8	8	8	8	8	8	8	8	8	32	32	64
Telecentric	8	8	8	8	8	8	8	8	8	8	32	32	64

The main goal of the experiment is to verify the analysis that searching the real optimal focus gets better results than the "visual-search" optimal focus. To determine the quality and effectiveness with which the experiment is carried out, the calibration error (in pixels) is taken as the evaluation parameter. The lower this value, the better the calibration, which subsequently imply a measurement closer to the real one.

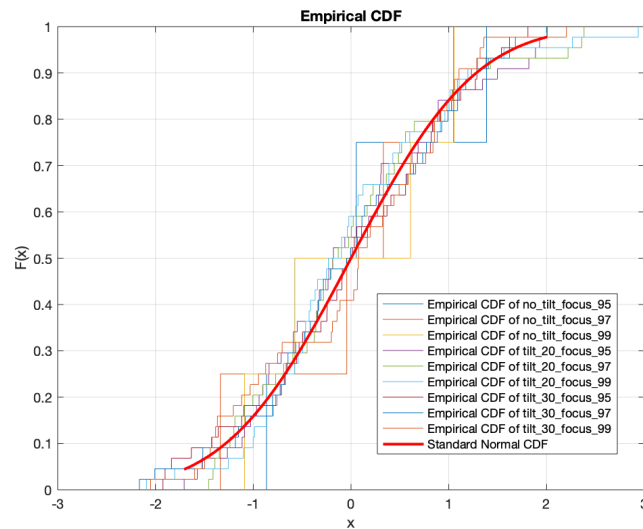


Figure 4.6: Comparison between cumulative distribution functions of the data and the standard normal distribution)

Table 4.2: p -values of the experiments. Gray cells indicate that the experiment is meaningless and white cells without data that the experiment was not done because of few available data

	Focus	Exposure	Tilt	#images
Endocentric			< 0.001	
No tilt	0.0034	0.7609		
Tilt 20	< 0.001	0.2329		0.0065
Tilt 30	< 0.001	0.7491		0.0027
Telecentric			< 0.001	
No tilt				
Tilt 20		0.1638		0.1788
Tilt 30		0.938		< 0.001

For further statistical studies, all data has been normalized centering the data to have a mean 0 and scaled to have a standard deviation 1. A one-sample Kolmogorov-Smirnov test is used to verify adjustment to a normal distribution. Fig. 4.6 proves the similarity between the empirical cumulative distribution function (cdf) of the centered and scaled data and the cdf of the standard normal distribution.

In continuation, endocentric and telecentric lens experiments were carried out and different variables were taken into consideration so that their influence could be studied. Table 4.2 shows a summary of the results.

4.4.1 Endocentric experiments

4.4.1.1 Focus parameter

Figure 4.7a, Figure 4.7b and Figure 4.7c show the average calibration error values for endocentric lens. In addition, it shows a graphical representation of these results by means of a box diagram, that allows a comparison at a glance of the distribution of the values obtained for each focus level. Each box represents the ranges where 50% of the selected data is concentrated,

whose ends come through quartiles 1 and 3. The inner line to the boxes represents the medians of the data set. The 95% confidence interval of the medians are represented by the notches. The lines that leave each box indicate the position of the maximum and the minimum value of the distribution (extreme values) eliminating the atypical values.

After an analysis of the results obtained, it can be concluded that in general, focus level at 99% results considerably improve the calibration error compared to the results obtained with the other two focus levels.

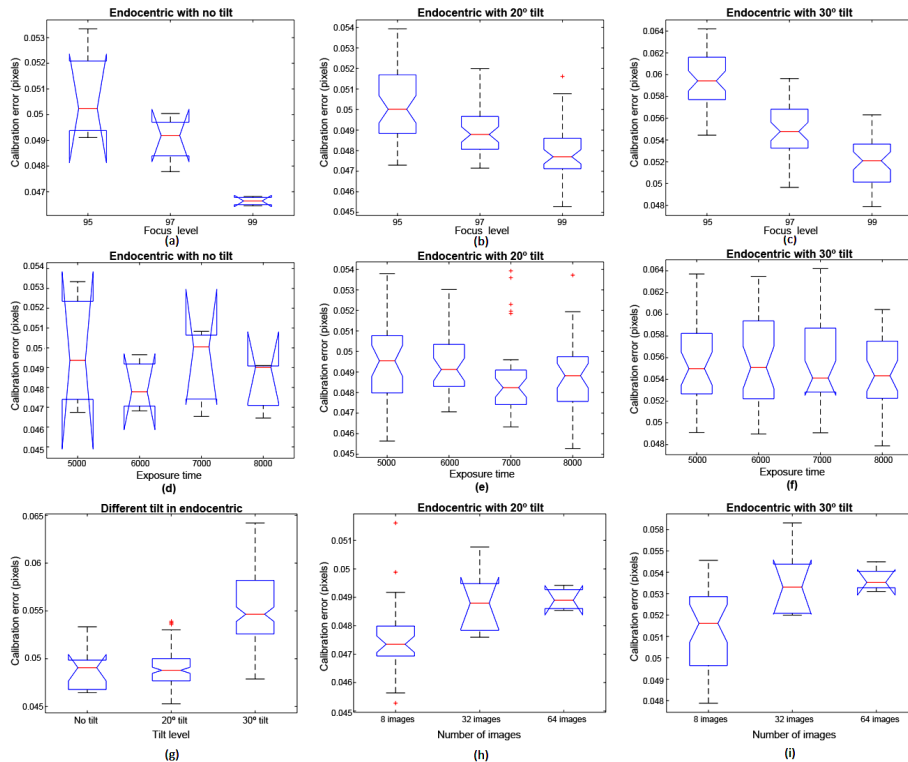


Figure 4.7: Box diagrams of endocentric experiments. First and second rows show focus level and exposure time comparisons respectively (the line inside the rectangles represents the median values, and the asterisks the outliers). Third row shows experiments studying the tilt degree (g), and number of images (h) and (i)

As can be seen in Figure 4.7a, when the sample size is small, notches

may extend beyond the end of the box. In the 20° tilt experiment, as the box diagram shows, the range of values of the results obtained with a 95% focus level is much wider than the other two remaining modalities. In this case, the uncertainty of the calibration error is bigger due to worse focus. On the contrary, it is observed that the size of the boxes in the other modalities are smaller, indicating a more uniform distribution of the results obtained. From this data, it follows that the two remaining modalities provides a lower uncertainty error.

To find statistically significant differences, a one-way ANOVA analysis has been performed. With no tilt option, the test result shows that 99% focus level does have a statistically significant effect on the average calibration error ($p=0.0034$). For the 20° and 30° tilt, 99% focus level does have a statistically high significant effect on the average calibration error ($p<0.001$). A post-hoc Tukey's Honestly Significant Difference procedure has been carried out on the results. It is observed that there are significant differences among all focus levels, although in no tilt option the significant difference is only between 99% focus level and the other two levels.

4.4.1.2 Exposure time parameter

Figure 4.7d, Figure 4.7e and Figure 4.7f show the average calibration error values for endocentric lens by comparing each exposure time. In this case, a one-way ANOVA analysis did not have statistically significant results. That means that the exposure time parameter does not change significantly and therefore it is not possible to choose an optimal value.

Moreover, a two-way ANOVA analysis was performed as well in order to verify if there is any statistically significant interaction between focus level and exposure time. All results (for no tilt, 20° tilt and 30° tilt) were negative with p values greater than 0.05.

4.4.1.3 Tilt angle parameter

Figure 4.7g shows the box diagram comparing all data for no tilt (12 calibration processes), 20° tilt (132 calibration processes) and 30° tilt (132 calibration processes). The one-way ANOVA analysis gives statistically high significance ($p<0.001$) between 30° tilt and the other two groups.

Table 4.3: Three-way ANOVA analysis in endocentric experiments

Source	Sum Sq.	d.f.	Mean Sq.	F	Prob >F
Focus	0.00034	2	0.00017	43.48	0
Exposure	0.00001	3	0	1.14	0.3318
Tilt	0.00279	2	0.00139	360.97	0
Focus*Exposure	0.00001	6	0	0.35	0.912
Focus*Tilt	0.0003	4	0.00007	19.27	0
Exposure*Tilt	0.00001	6	0	0.6	0.7277
Focus*Exposure*Tilt	0.00002	12	0	0.49	0.9214
Error	0.00093	240	0		
Total	0.00522	275			

That means that high plate inclination is bad for the calibration process. Meanwhile, it seems like there is no difference between the calibration with no tilt and 20° tilt.

4.4.1.4 Number of images parameter

Taking the 20° tilt data with 99% focus level, a one-way ANOVA analysis was performed in order to verify the effect of calibration processes using 8 images, 32 images and 64 images. Looking at the p -values of the results, there is a statistical significance ($p < 0.05$) between the 8 images group and the other two groups. The same result is obtained performing the one-way ANOVA analysis over the 30° tilt data with 99% focus level. Figure 4.7h and Figure 4.7i show the box diagrams of both experiments.

Previous experiments studied the impact of individual variables. Table 4.3 shows the result of the three-way ANOVA analysis (studying focus level, exposure and tilt parameters) performed in order to test the effects of multiple factors on the mean in the calibration errors. The interaction terms are represented by '*' symbol in the ANOVA table.

The ANOVA table shows the between-groups variation and within-groups variation (*Error* row). 'Sum Sq' is the sum of squares and

'*d.f.*' is the degrees of freedom. '*Mean Sq.*' is the mean squared error, which is $Sum Sq/d.f.$ for each source of variation. The '*F*-statistic' is the ratio of the mean squared errors. The last column is the *p*-value.

4.4.2 Telecentric experiments

A similar study was carried out for telecentric data and Figure 4.8 shows the box diagrams. In this case, it did not make sense to study focus level parameter due to the fact that telecentric lenses always work at a fixed focus.

As it can be seen in Figure 4.8a and Figure 4.8b, and also in Table 4.2, the one-way ANOVA analysis performed for the exposure time parameter did not have statistically significant results. That means that the exposure time parameter does not change significantly and is therefore not possible to choose an optimal value. Concerning the number of images parameter, Figure 4.8c and Figure 4.8d show no statistically significant results in 20° tilt configuration, while there is a statistically high significant effect on the average calibration error ($p < 0.001$) in 30° tilt configuration between the 8 images group and the other two groups.

Studying the tilt level, Figure 4.9 shows the box diagram comparing all data for no tilt (4 calibration processes), 20° tilt (44 calibration processes) and 30° tilt (44 calibration processes). The one-way ANOVA analysis gives a statistically high significant ($p < 0.001$) value. The post-hoc Tukey's Honestly Significant Difference procedure indicates that the significant differences are only between no tilt and 30° tilt. It seems like there are no differences between doing the calibration with no tilt and 20° tilt. However, looking at the box diagrams it seems that there are differences in the medians. The reason can be (as it has been observed previously) that when the sample size is small (no tilt configuration case), the uncertainty is bigger and the range of the values is wider causing an overlap with the 20° tilt group and therefore, causing a non-significant result in the ANOVA.

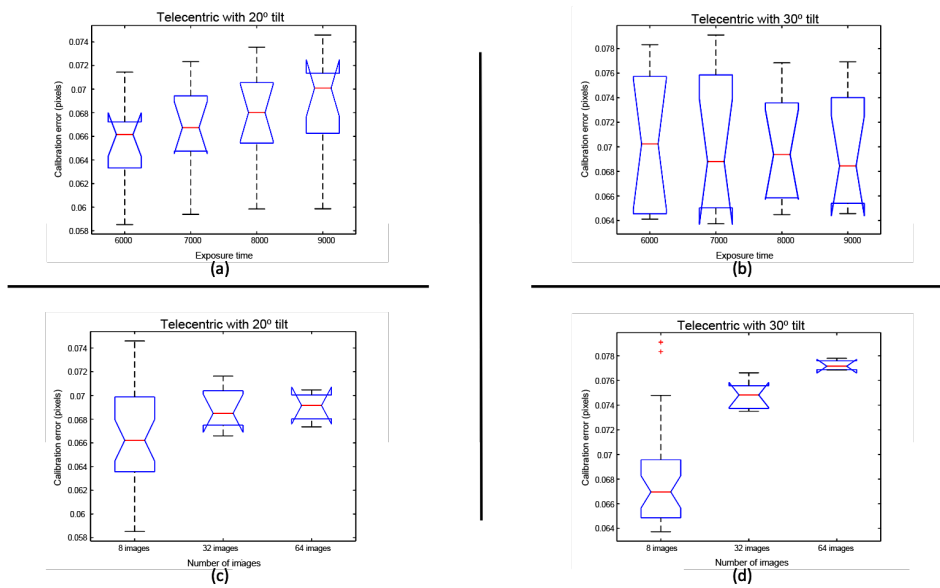


Figure 4.8: Box diagrams of telecentric experiments. First row shows exposure time comparisons (the line inside the rectangles represents the median values, and the asterisks the outliers). Second row shows experiments studying the number of images

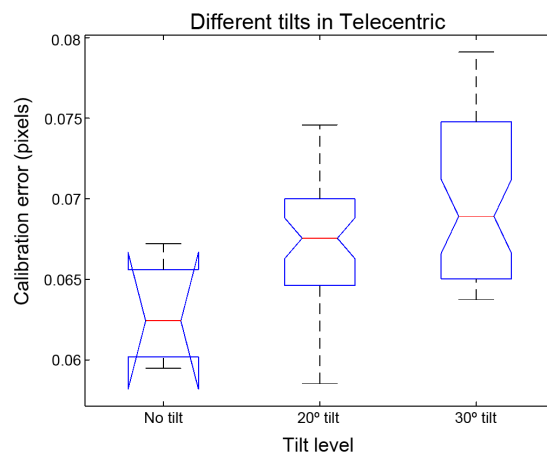


Figure 4.9: Box diagram of telecentric experiments studying the tilt angle parameter (the line inside the rectangles represents the median values, and the asterisks the outliers)

4.5 Discussion

Looking at all the results for endocentric and telecentric experiments, the following conclusions can be drawn:

- Box plots show that the 99% focus level is always the best in terms of calibration error and Table 4.2 shows that in all cases there are statistical significant differences (p -values lower than 0.05).
- It is not clear that there exists an exclusive optimal exposure time value (no significant differences). This could mean that the chosen range is good enough for these experiments, as this parameter is very dependent of every single application and configuration.
- The tilt angle is very important in the calibration process. Specifically, it seems that the more flat and perpendicular the plate is, the lower the calibration error will be. This result clarifies the way HALCON recommends the calibration procedure, since a priori, it is said that images should be obtained at different angles of rotation.
- In both endocentric and telecentric lenses, it seems that it is better to perform the calibration process with fewer images. This goes beyond what is suggested by HALCON documentation (that does not specify any number of images to use).

This proposal studies the effect of different parameters in the calibration error, specifically, camera focus, exposure time, tilt angle and number of images. Endocentric and telecentric lenses are used for the experiments. A sample of 2176 images is used to generate the population and the calibration errors are obtained varying the parameters of interest. A multivariable statistical analysis is performed to study the influence of each parameter in the calibration error. The experiments show which parameters have statistically significant results and the ones that do not.

In particular, special attention has been paid to the focus parameter, as currently the procedure to find the focused image is done visually by the user. However, in this work we demonstrate that using an algorithm that detects the optimal focus, results in lower (and statistically different) calibration errors.

Although the results for the exposure time seem to be inconclusive, the experiments have proven that HALCON calibration standard instructions can be improved upon, concerning the tilt level and the number of images used.

Proposal III: Optimal Object Alignment

5.1 Introduction

Industrial dimensional metrology is the science of calibrating and using physical measurement equipment to quantify the physical size of or distance from any given object. An industrial metrology process is used on industrial systems, components and objects to perform inspections, alignment and measurement. Metrological systems are based upon the principle of a good alignment system. Due to changes and movements during a measurement process, the need to have an alignment system becomes imperative, in order to avoid all possible errors that may arise from a lack of alignment. In the effort to obtain the best possible conditions for alignment, it is necessary to check whether the object to be measured is well-positioned. Good alignment reduces down-time and should be part of the quality control process and preventive maintenance program.

For the purpose of this proposal, an algorithm was developed to determine the gray intensity pixel on the region of the acquired object. An aligned region would be sharp and possess fewer or no gray pixels. An unaligned region, on the other hand, would be unfocused, and would possess more numbers of gray level pixels. Figure 5.1 shows the object alignment scheme.

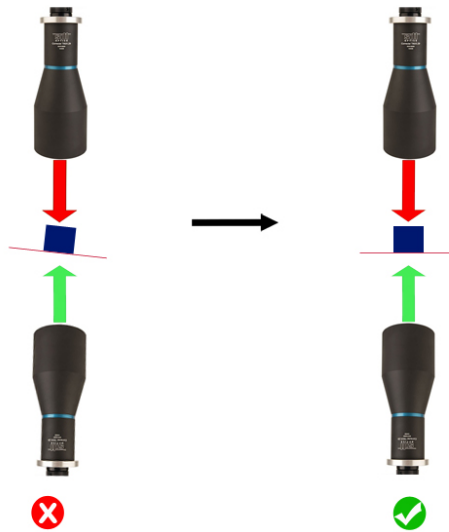


Figure 5.1: Object alignment scheme

5.2 Setup Configuration

In order to have a stable control of the object tilting effect, a 5-Axis compact stage setup configuration was used to mount the object for acquisition and alignment experiment. The 5-Axis compact stage provides five axes of adjustment in a package measuring 2.36" x 2.15" x 1.08" (59.9 mm x 54.7 mm x 27.3 mm). It has five 100 TPI actuators for adjusting the top platform's pitch, yaw, X, Y, and Z positions. Two actuators together control the yaw and Y-axis position, two actuators together control the pitch and Z-axis position, and a single actuator controls the X-axis position. The actuators have a 5/64" (2 mm) hex for adjustments with a hex key thumbscrews. The base of the compact stage has two counter-bored 1/4" (M6) slots for mounting the stage to an optical table as shown in Figure 5.2.

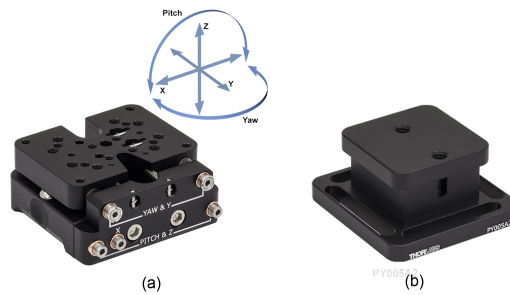


Figure 5.2: a) Compact 5-Axis Pitch, Yaw, and Translation Stage.
b) The Mounting Base.

The translating top platform of the compact stage has a variety of mounting holes and taps for compatibility with many mechanical components. These holes allow the platform to be used for many different applications. For instance, the eight 8-32 (M4) tapped holes and the 8 (M4) counter-bore on the underside of the top platform, accessible from the bottom of the stage, allow optic mounts and other mechanical components to be mounted on the platform. The eight 6-32 (M4) tapped holes are compatible with our several clamping arms. The holes are positioned so that the setscrew of the clamping arm is centered over the top platform. Figure 5.3 shows the rest of the devices used for the experiments. Figure 5.4 shows the setup configuration for the object alignment.

EXPERIMENT\DEVICE	CAMERA	OPTICS	LIGHT
Endocentric		 Goyo Optical GM31614MCN	 Backlight IBL-W130- 110
Telecentric	Allied Vision Manta G-504B	 Opto Engineering TC12056	 Opto Engineering LTCLHP056-G

Figure 5.3: Devices and instruments used for the object alignment experiments

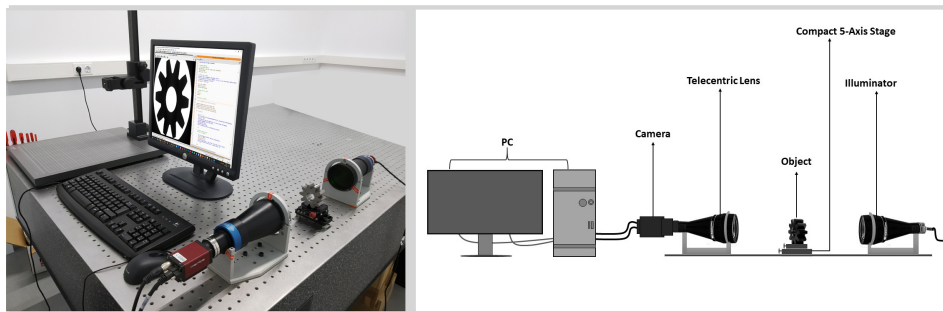


Figure 5.4: Object alignment setup configuration

5.3 The Alignment Algorithm

The object alignment algorithm uses the gray value intensity function of Halcon to calculate the mean and the standard deviation of the image acquired. The mean value is used to evaluate the effect of tilting in the acquired object. Fig.5.5 shows the flowchart. The algorithm works as follows:

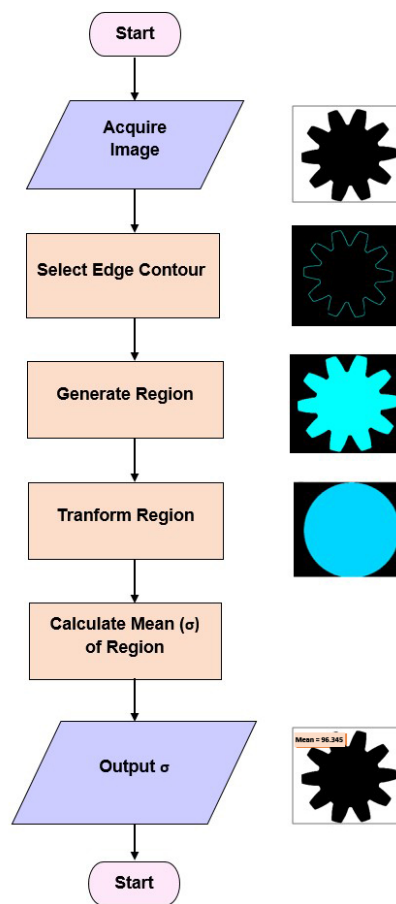


Figure 5.5: Object alignment algorithm flowchart.

- Acquire image: The image is acquired from the camera configuration.
- Select edge contour: The select contours algorithm selects edges as contours from the input image specified. Contours whose length are far away from the parameter specified are not returned.
- Generate region: The generate region algorithm creates a region from the selected contour. Open contours are closed before converting them to regions.
- Transform region: Transforms the shape of the region to derive the largest circle fitting into the region.

- Intensity function: Uses the the gray value of each pixel of the region to calculate the mean and the standard deviation of the transformed region. The mean is used to determine the output.

5.4 Data Analysis

The experiment performed for this analysis entails the capture of images, at different orientations, with a degree of tilt achieved by the use of the compact 5-axis setup configuration. The algorithm calculates the mean and standard deviation of the image pixels at each particular tilt orientation. When the object is well aligned the mean of the pixels reaches its maximum value. As the object experiences a tilt orientation away from the perfect state, it begins to experience a loss in the mean-pixel value. Figure 5.6(a) shows the object in the optimal alignment state. Figure 5.6(b) shows that as the object experiences an angular tilt, it begins to gain more gray pixels, and hence the mean value begins to reduce.

The experiments were performed several times to ascertain the repeatability of the configuration and the algorithm. To implement this, the 5-Axis compact configuration was setup to mount the gear object at different angles, ranging from -20° to 20° . When the gear was mounted on the configuration at a particular angle, the vision application runs the algorithm, several images are acquired, the mean and deviation is calculated and stored.

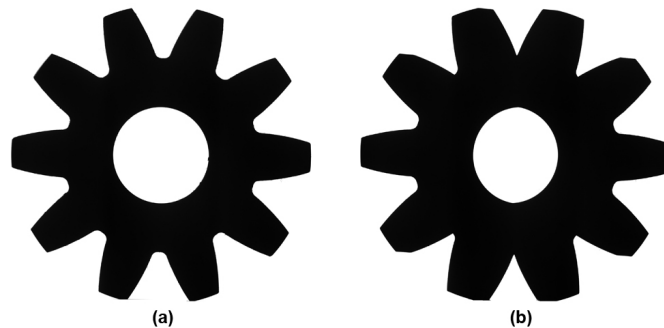


Figure 5.6: (a) Object at optimal alignment. (b) Object at an angular tilt of 20° .

Table 5.1 shows the data generated from the experiments on the

Table 5.1: Object Alignment Experiments (Endocentric)

Image Mean (pixels)									
Exps	-20°	-15°	-10°	-5°	0°	5°	10°	15°	20°
1	83.543	87.454	91.123	94.025	96.354	94.444	92.111	88.011	84.323
2	83.344	87.015	91.252	93.885	96.535	94.040	91.985	88.001	84.122
3	83.294	87.204	90.112	94.114	97.375	94.114	92.045	87.961	84.032
4	83.453	87.774	91.342	94.005	96.445	93.541	92.125	87.891	83.923
5	82.903	87.640	90.022	93.775	96.647	93.984	91.885	88.018	83.873
6	83.111	87.414	91.443	93.654	97.365	94.134	92.345	88.161	84.002
7	83.266	87.054	92.003	94.113	96.945	94.004	92.065	88.205	84.111
8	83.432	87.140	91.332	94.004	96.775	93.884	91.903	88.189	84.025
9	82.943	87.254	91.923	94.565	96.847	94.314	92.205	88.102	83.803
10	83.109	87.754	90.882	94.615	97.575	94.034	91.915	87.788	84.100

different angles when using the endocentric lens. Figure 5.7 shows the graphical representation of the results.

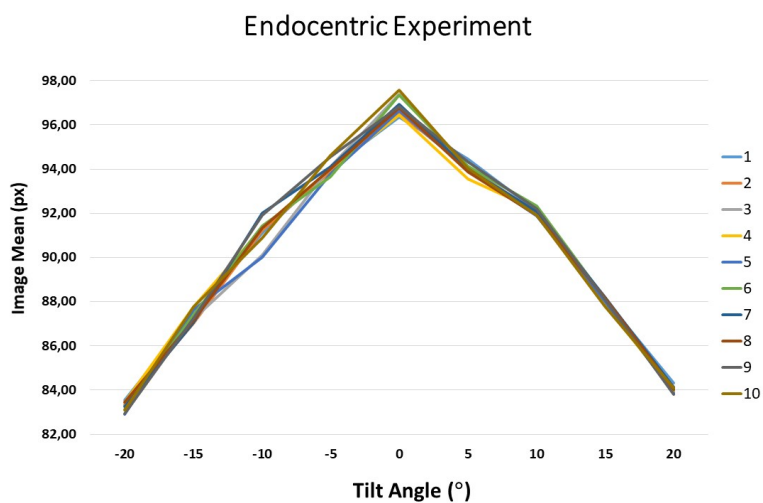


Figure 5.7: The object alignment experiments for endocentric lens

Table 5.2: Object Alignment Experiments (Telecentric)

Image Mean (pixels)									
Exps	-20°	-15°	-10°	-5°	0°	5°	10°	15°	20°
1	81.202	85.102	89.891	93.544	99.823	94.192	91.491	87.850	83.145
2	82.025	84.002	88.192	92.847	99.621	93.133	90.112	88.123	84.076
3	82.173	85.222	87.911	93.322	98.793	92.102	91.292	86.168	85.500
4	83.991	84.443	88.122	93.111	99.923	94.016	91.001	88.343	84.212
5	84.173	85.100	90.112	94.432	100.12	95.111	89.349	87.123	83.122
6	81.307	86.332	90.001	94.121	99.133	93.001	90.422	86.120	82.099
7	83.200	85.222	89.543	92.113	97.556	93.144	91.122	88.129	83.002
8	80.011	83.115	88.151	93.434	100.22	94.213	91.331	87.142	80.115
9	83.654	86.002	90.190	92.115	99.982	95.165	90.487	87.001	82.155
10	82.212	85.121	89.231	93.010	98.323	94.912	91.276	86.281	81.046

Table 5.2 shows the data generated from the experiments on the different angles using the telecentric lens on the mounted configuration. Figure 5.8 shows the graphical representation of the experiments.

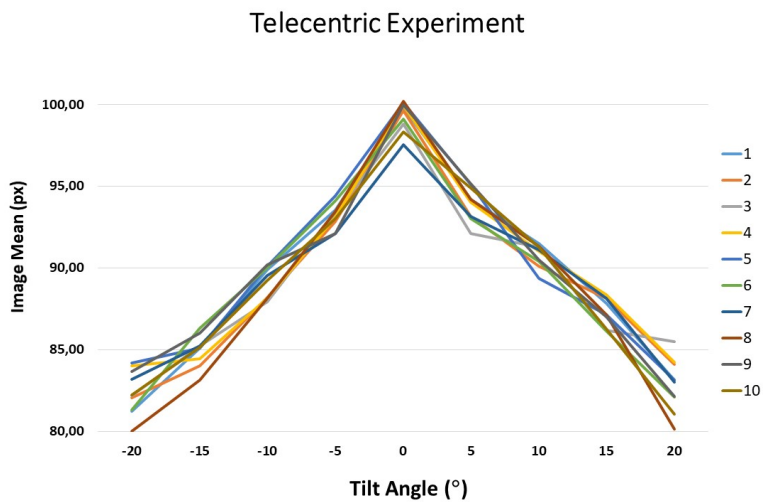


Figure 5.8: The object alignment experiments for telecentric lens

5.5 Discussion

The results from the experiments performed using the object alignment algorithm proves that the algorithm based on gray intensity level is able to detect when the object peaks at 0° . The experiments also exposes the effects of misalignment on the object when there is an angular tilt. Several images were acquired at different angles to demonstrate the effect. The angles range between -20° and 20° . The gray value intensity of the image is used to derive the mean. When the object peaks at its optimal alignment, the mean of the gray value reaches its maximum value. When the image begins to experiences an angular tilt, the gray value of the image begins to decline. This experiments demonstrates that the developed algorithm can be used to obtain the desired optimal value for a successful object alignment.

Proposals Validation

6.1 Analysis of Experiments

The experiments performed for each of the proposed algorithms culminates with the measurements of the gear piece. The nominal diameter acquired from a CMM with the ground-truth sample gear (62,014 mm) is used to verify the values generated by the experiments. To verify the functionality of the algorithms, two groups of experiments were performed (endocentric and telecentric). For both groups, four different experiments were carried out to track and measure the independent effects of every single proposed algorithm in the previous chapters. Figure. 6.1 shows the flow of the experiments of the proposals and Table 6.1 summarizes all configurations and results. Note in the flow that in the case where a telecentric optic is used, the focus stage is not considered due to the fact that telecentric optics have a fixed focus distance.

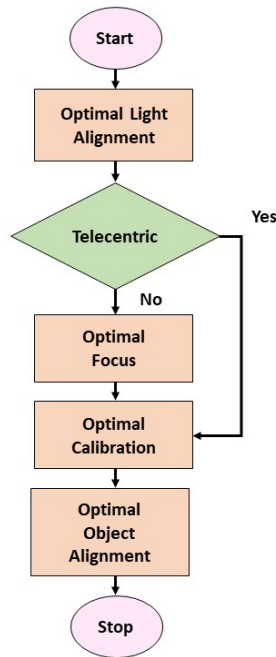


Figure 6.1: Flow of the experiments

The first group of experiments was performed using an endocentric lens:

- **Experiment 1A:** The purpose of the experiment was to simulate a not-optimal scenario. A not-optimal scenario is mostly common in industrial inspections, because many of the details are not always put into consideration when inspection processes are on-going. Sometimes, this could be as a result of workload and the urgency of production. In this experiment, a not-optimal light alignment, a not-optimal focus, a not-optimal calibration and a not-optimal object alignment method was applied to the measurement process.
- **Experiment 1B:** These experiments were performed to achieve an optimal measurement scenario. However, in this experiment an attempt was put to differentiate the various conditions that could affect the achievement of an optimal system. This experiment was hence divided into three sub experiments:
 - **Experiment 1Bi:** In this experiment, the endocentric optimal

light alignment with not-optimal focus, not-optimal calibration (32 images) and not-optimal object alignment was evaluated.

- **Experiment 1Bii:** In this experiment, the endocentric optimal light alignment, optimal calibration (focus and 8 images), not-optimal object alignment were evaluated.
- **Experiment 1Biii:** In this experiment, the optimal configuration is set-up: endocentric optimal light alignment, optimal calibration (focus and 8 images) and optimal object alignment.

The second group of experiments was performed using a telecentric lens:

- **Experiment 2A:** Like experiment 1A, the purpose of the experiment was to simulate a not-optimal scenario. In this experiment, a not-optimal light alignment, a not-optimal calibration and a not-optimal object alignment method was applied to the measurement process.
- **Experiment 2B:** These experiments were performed to achieve an optimal measurement scenario. This experiment was divided into three sub experiments:
 - **Experiment 2Bi:** In this experiment, the telecentric optimal light alignment, not-optimal calibration (32 images), not-optimal object alignment were evaluated.
 - **Experiment 2Bii:** In this experiment, the telecentric optimal light alignment, optimal calibration (8 images), not-optimal object alignment algorithms were evaluated.
 - **Experiment 2Biii:** In this experiment, the optimal configuration is set-up: telecentric optimal light alignment, optimal calibration (8 images) and optimal object alignment.

Table 6.1: Experiments configurations and results. The color gradient indicates the level of optimized set-up pipeline phases (red none, orange several phases optimized, green pipeline optimized). The last column is the % of improvement with respect to the not-optimal experiment, 1A or 2A.

Exp.	Light Align.	Focus (%)	Calib. Error (px)	Object Align.	Meas. (mm)	Error (mm)	Improv. (%)
1A	No	95	0.0582	No	62,258	0.244	-
1Bi	Yes	95	0.0506	No	62,120	0.106	56.56
1Bii	Yes	100	0.0275	No	62,109	0.095	61.07
1Biii	Yes	100	0.0273	Yes	62,019	0.005	97.95
2A	No	-	0.1784	No	62,175	0.161	-
2Bi	Yes	-	0.0987	No	62,065	0.051	68,32
2Bii	Yes	-	0.0547	No	62,039	0.025	84,47
2Biii	Yes	-	0.0515	Yes	62,012	0.002	98,76

6.2 Discussion

Figure. 6.2(a) and Figure. 6.2(b) show the result from the calibration experiments performed using both the endocentric and telecentric lenses. When the developed optimal algorithms are implemented with the endocentric optics, it could be observed that the calibration error is as low as 0.027 pixels, as opposed to the calibration error achieved at 0.058 pixels, without using the algorithms. When the optimal algorithms are implemented with the telecentric optics, it could be observed that the calibration error is as low as 0.052 pixels, as opposed to the calibration error achieved at 0.1784 pixels, without using the algorithms. These differences, even though it could be further improved, clearly demonstrate that the proposed algorithms provide a clear pathway for the achievement of a preferred and improved calibration process.

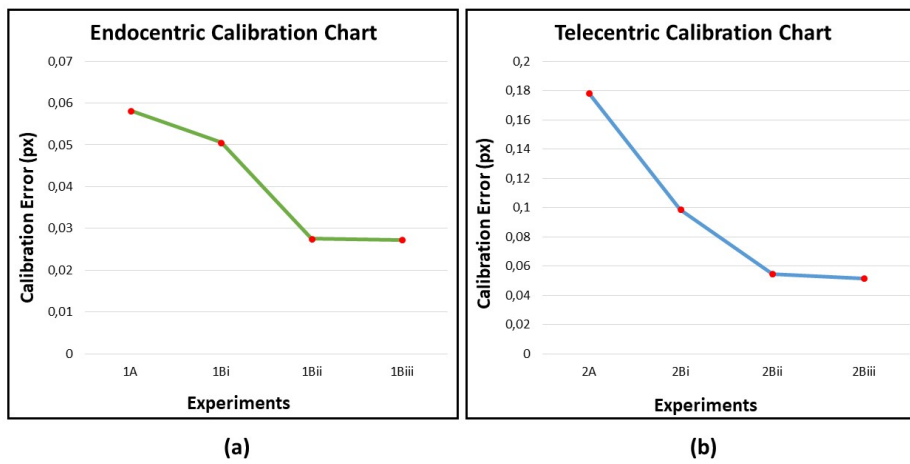


Figure 6.2: Calibration experiment chart

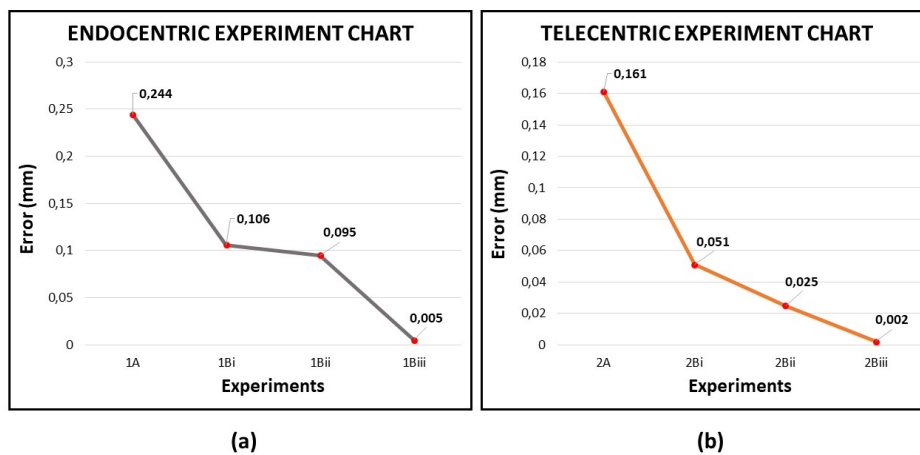


Figure 6.3: Alignment experiment chart

Figure 6.3(a) and Figure 6.3(b) show the summary of results from the measurement experiments for both the endocentric and telecentric optics. It could be observed that when the optimal algorithms are applied for

the endocentric lens, the error value reduces to a minimum of 0.005 mm, as opposed to the error value of 0.244 mm when no optimal algorithms are considered. With the telecentric optics, it could be observed that with the application of the optimal algorithms, the error value reaches a minimum of 0.002 mm, as opposed to the error value of 0.161 mm when no optimal algorithms are considered. The consistency of the results generated by the proposed algorithms is obviously seen in the different phases of implementation in improving the pipeline of an optical metrology system.

Therefore, given the number of experiments performed to verify the different stages of the proposed algorithms, it can be evidently confirmed that the implementation of the developed algorithms in a quality inspection process is worth the while.

Chapter 7

Measurement and uncertainty analysis

A synthesis of this chapter has been published in:

Moru, D. K. and Borro, D. "A machine vision algorithm for quality control inspection of gears". The International Journal of Advanced Manufacturing Technology, Vol. 106, N. 1-2, pp. 105-123. January 2020. (Quartil Q2).

7.1 Introduction

Most industrial and haulage application use gears as common mechanism for conveying power and motion. This element is important and frequently used as fundamental component (Amarnath et al., 2009). As current methodologies of gear measurement are expensive and time consuming, precision and accuracy becomes evidently crucial in the measurement and inspection of industrial products. There are very few methods available of measuring gear parameters accurately, and at the same time, minimizing error and production cost (Gadelmawla, 2004). As a key to production and inspection, the utilization of machine vision applications to develop accurate and precise measurement system with the ability to perform appropriate inspection and measurement is fundamental to any manufacturing process (Gadelmawla, 2017).

The aim of this chapter is to deploy an improved machine vision application to determine the precise measurement of gears, at subpixel

level, with the potential to improve quality control, reduce downtime and optimize the inspection process.

7.2 The Proposed System

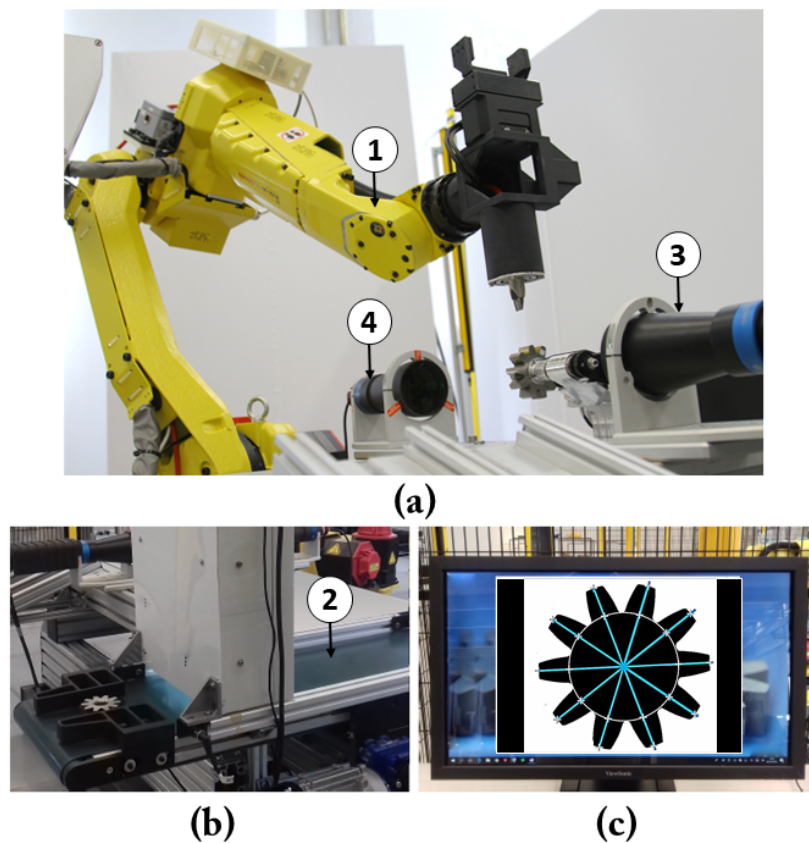


Figure 7.1: The proposed system configuration. a) Robot and telecentric lens configuration. b) The inspection belt. c) The vision2D application interface.

The Vision2D application has been developed to perform inspections and measurements to determine the precise and accurate measurement of the gear parameters to enhance quality inspection control. Fig.7.1(a) shows the

proposed system configuration. The flow of the running system is as follows:

1. The gear was placed in a mechanical system configuration by an M-10iA Fanuc robot. The robot is a six-axis, high performance industrial robot. It weighs 130kg and provides 10kg payload with the highest wrist moments and inertia in its class. The M-10iA can be floor or wall mounted at any angle. For this experiment, the robot was floor mounted.
2. A dynamic inspection belt was used to convey the gear piece from a start state, during the inspection (Fig.7.1b). The belt configuration is setup with a sensor. The sensor triggers when the gear is detected. The robot receives the trigger signals from the sensor, automatically picks the gear from the dynamic belt and places it on the mechanical system.
3. When the gear has been placed on the mechanical system, a Manta G-504 camera acquires the image of the gear. It is attached to a telecentric lens TC12056 that can take advantage of high-resolution detectors such as 5 MP - 2/3", acquiring images with exceptional fidelity and precision maximizing the performance of the proposed system.
4. A high-performance telecentric illuminator specifically designed to back illuminate objects imaged by telecentric lenses was used. The telecentric illuminator offer higher edge contrast when compared to diffused back light illuminator and therefore higher measurement accuracy. This type of illumination is especially recommended for high accuracy measurement of round or cylindrical parts where diffusive back lighting would offer poor performances because of the diffuse reflections coming from the edges of objects under inspection. Figure 7.2 shows the devices used for the experiment.

The Vision2D application was developed in-house in C# programming and Visual Studio 2015, incorporating the Halcon 13 integration libraries. C# programming was used to develop the user interface for a better touch and feel. To perform the measurement process, several image processing and machine vision algorithms are applied (explained in next Section) to the acquired images.

EXPERIMENT/DEVICE	CAMERA	OPTICS	LIGHT
Telecentric	 Allied Vision Manta G-504B	 Opto Engineering TC12056	 Opto Engineering LTCLHP056-G

Figure 7.2: Devices used for the measurement experiment

In this chapter, a calibration target of 80 mm is used to generate the coordinates of the calibration marks in the acquired image and to calculate the estimation for the camera parameters. A root mean square error of 0.06 pixels (calibration error) was obtained.

7.3 The Algorithms

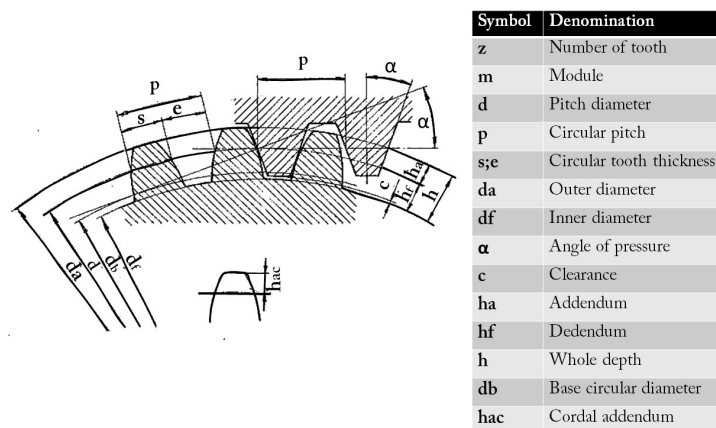


Figure 7.3: Nomenclature of gear

The Vision2D application interface performs the measurement of all gear parameter, as shown in Fig.7.3, by calculating only three parameters: the outer diameter, the inner diameter (also called root diameter) and the number of tooth. These three parameters are the most necessary values needed to calculate the rest of the gear parameters. Many of the gear parameters are well known to be correlated to each other by known equations (Goch, 2003). For example, the pitch diameter is correlated to the number of teeth and the module, while the module is correlated to the pitch diameter and the number of teeth. In this situation, computer vision algorithms were developed to calculate the outer diameter, the inner diameter and the number of teeth of the gear to be measured, then the rest of the gear parameters are calculated using their equations based on these three parameters.

The image processing starts with the camera acquiring the image, and several algorithmic steps are used for thresholding, segmentation, detection and measurement of the gear. Fig.7.4 shows a block diagram of the algorithms used. The next sections describes the algorithms in details.

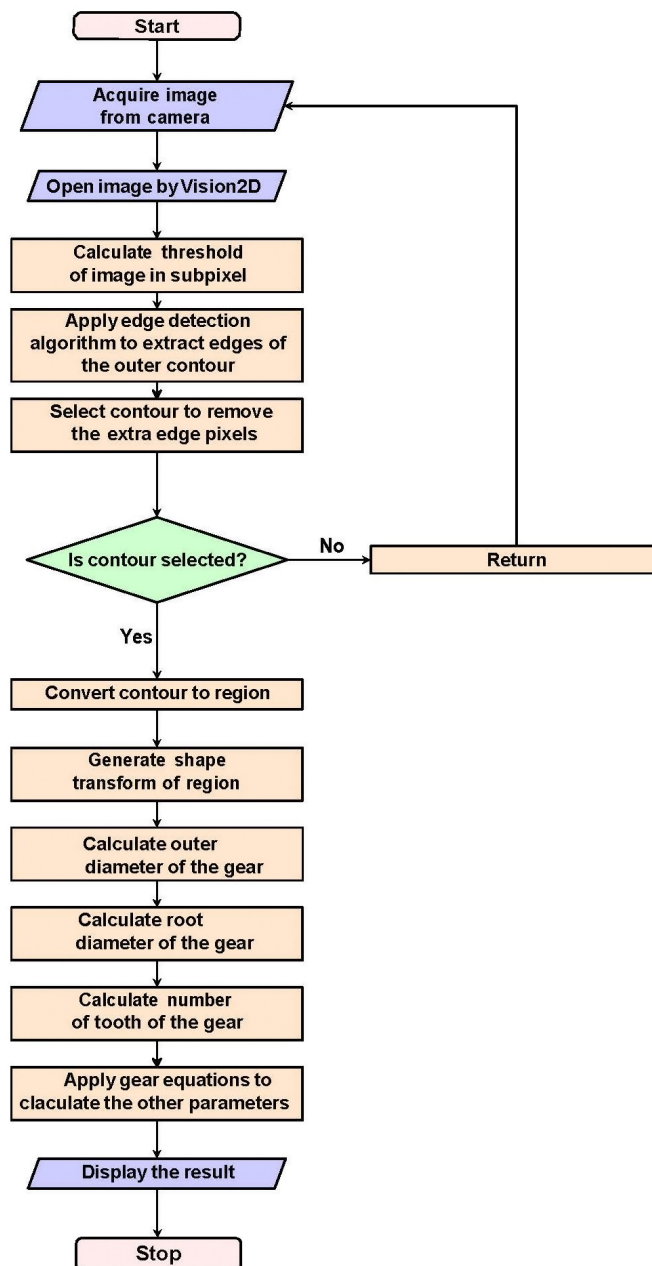


Figure 7.4: Flowchart of the Vision2D application.

7.3.1 Image Segmentation

A. Bali et al (Bali and Singh, 2015) describes segmentation as a method of partitioning an image or picture into different regions which has same attributes like texture, intensity and gray level with the motive to yield object of interest from the background. Image segmentation methods has been extensively used in the identification of images and classification of image in numerous fields (Zhang et al., 2008). Thresholding, because of its clarity and direct nature, and clustering, because of its ability to categorize images efficiently, are the very well known method for image segmentation between image segmentation techniques (Cheng et al., 2001). K. Singh et al further discussed the different types of image segmentation thresholding techniques for the different application areas: pixel based, edge based and region based segmentation techniques (Singh and Singh, 2010). Pixel based segmentation is conceptually the simplest approach used for segmentation. In this approach, information from the input image fuses in a pixel-by-pixel basis either in the transform or in spatial domain. Edge based segmentation is based on the fact that the position of an edge is given by an extreme of the first-order derivative or a zero crossing in the second-order derivative. Region based method focus attention on an important aspect of the segmentation process missed with pixel based techniques: it classifies a pixel as an object pixel judging solely on its gray value independently of the context. This dissertation implements thresholding at sub-pixel level using the edge base method.

7.3.2 Edge Detection Sub Pixel

In industrial applications, like measurement of gears with high precision, it is sometimes necessary to detect edges with sub-pixel precision. The need of sub-pixel accuracy in image processing and analysis was firstly pointed out in the late 1970s (Nevatia, 1978). Since then, the issue of edge detection at the sub-pixel level has gained attention of approaches of many scientists and researchers (Fabijańska, 2012). Detection of edges with sub-pixel accuracy improves the measurement accuracy and reduce hardware cost.

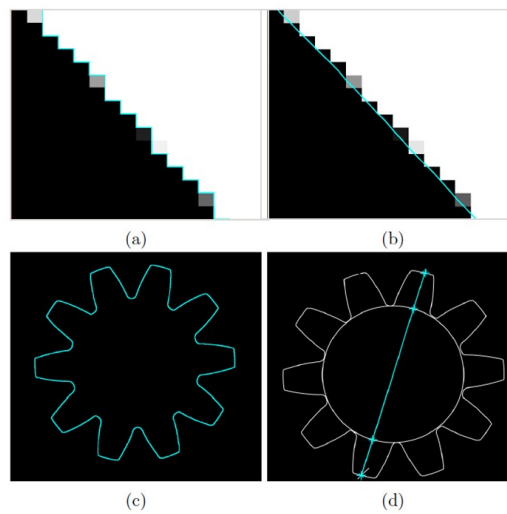


Figure 7.5: The edge detection details. a) The edge pixel detection of the gear tooth. b) The edge sub-pixel detection of the gear tooth. c) The outer edge detection of gear. d) The intersection points to determine the diameter of tooth.

M. Hagara et al (Hagara and Kulla, 2011) describes that most edge detectors at sub-pixel level fall in three groups: fitting, moment-based and interpolation-based methods. Fitting method use continuous functions, such as hyperbolic tangent (Nalwa and Binford, 1986), to fit samples of image function. Moment-based methods apply moment to determine unknown edge model parameters. For example, gray level moments tangent (Da and Zhang, 2010), spatial moments (Baozhang and Yanping, 2010), Fourier-Mellin moments (Bin et al., 2008) or Zernike moments (Zhang et al., 2010). Interpolation based methods achieve the sub-pixel accuracy by interpolating the image data to obtain a finer grid of pixels. Thresholding at the sub-pixel extracts segments from the image with sub-pixel accuracy. A segmentation process develops with the analysis of the input image as a surface, where the gray values are bi-linearly interpolated amid the centers of the individual pixels. Each pixel is thus extracted forming a segmented line, consistent with the image surface and then associated into intact topological contours. The segmentation contours therefore are accurately divided at intersecting points. Only image borders of areas containing extended gray values are generated. Figures 7.5 (a), (b), (c)

and (d) show the edge detection at different levels. Figure 7.5a shows the edge pixel detection of the gear tooth. Figure 7.5b shows the edge sub-pixel detection of the gear tooth. Figure 7.5c shows the principal outer edge detected applying the threshold sub-pixel algorithm. Figure 7.5d shows the diametric intersections generated to calculate the distance between two points of the outer tooth edge across the area center. It also shows the intersecting distance between two points in the inner circle across the area center.

7.3.3 The Outer Diameter Algorithm

To calculate the external diameter of the gear from the extracted edge of the outer contour, the outer diameter algorithm was developed. Figure 7.6 shows the flow process.

- Threshold the acquired image: The threshold sub-pixel algorithm extracts segments of the input image with sub-pixel accuracy.
- Select edge contour: The select contours algorithm selects contours from the input image according to a contour length specified. All contours whose length is far away from the parameter specified are not returned.
- Fit circle contour: The fit circle contour algorithm approximates the contours by a circle. The operator returns the area center, and the radius.
- For five tooth, generate a radius line from two points: the tooth edge and the area center of the circle contour.
- Extending the radius lines, the intersection points at the edge contour are generated for each teeth, and the corresponding distance diameter computed.

$$Distance = \sqrt{((R1 - R2)^2 + (C1 - C2)^2)}$$

where $R1$ and $R2$ are the row coordinates of the first and second point respectively, and $C1$ and $C2$ are the column coordinates of the first and second point respectively.

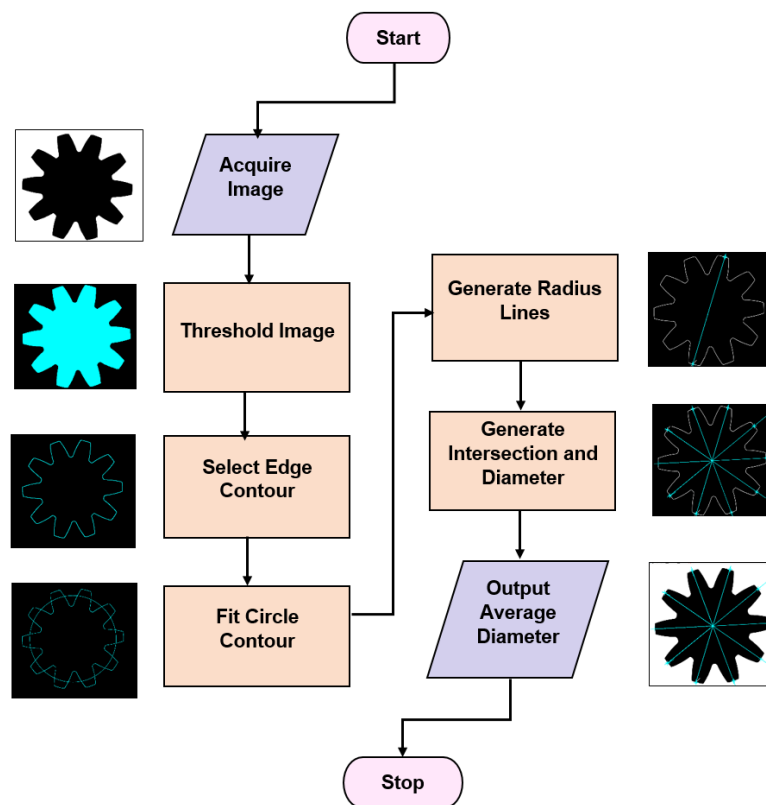


Figure 7.6: Flowchart of outer diameter algorithm.

- The average of all the computed distances is reserved as the outer diameter.

7.3.4 The Inner Diameter Algorithm

The root diameter algorithm calculates the inner diameter from the extracted edge pixels. Figure 7.7 illustrates the flow process.

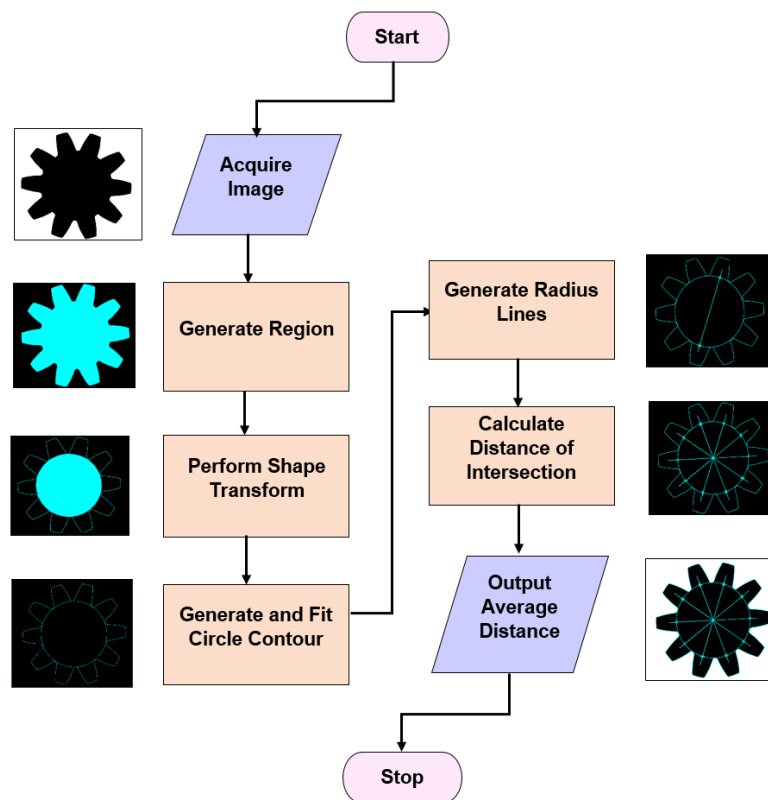


Figure 7.7: Flowchart of inner diameter algorithm.

- Generate region from contour: The generate region contour algorithm creates a region from a sub-pixel contour. The contour is sampled according to the Bresenham algorithm (Jia et al., 2008). Open contours are closed before converting them to regions.
- The shape transform is used to transform the shape of the input regions to derive the largest circle fitting into the region.
- Generate contour of region: The generate contour region algorithm generates contours from the regions.
- Fit circle contour approximates the contours by circles. The operator returns the contour area center and radius.
- Arbitrary lines are generated from the area center to intersect with the circle contours.

- The average of all intersection points are then used to calculate the inner diameter across the area center of the circle contour.

7.3.5 The Tooth Number Algorithm

The tooth number algorithm counts the number of tooth in the gear image. Figure 7.8 shows the flowchart. The algorithm works as follows:

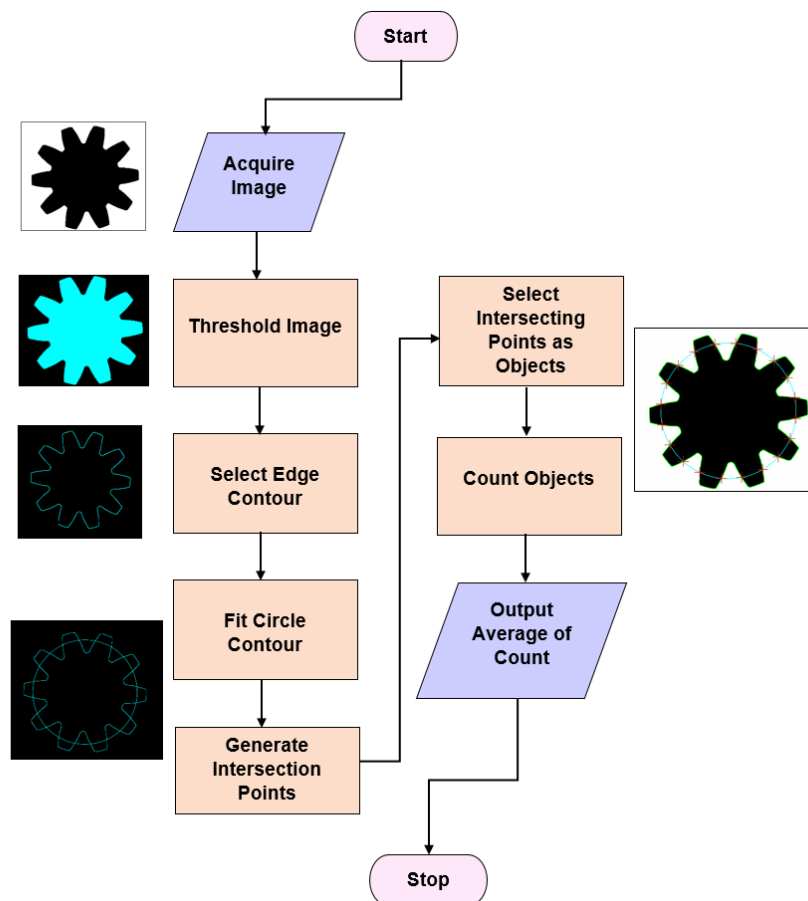


Figure 7.8: Flowchart of tooth number algorithm.

- Threshold the acquired image: The threshold sub-pixel algorithm extracts segments of the input image with sub-pixel accuracy.

- **Select edge contour:** The select contours algorithm selects contours from the input image according to a contour length specified. All contours whose length is far away from the parameter specified are not returned.
- **Fit circle contour:** The fit circle contour algorithm approximates the contours by a circle. The operator returns the area center, and the radius.
- **Intersect contours:** Generates intersecting points of the tooth edge contour and circle contour which, if any, are returned.
- **Select object:** This algorithm selects all the intersecting points generated.
- **Count object:** This algorithm counts the intersecting points and determines as output parameter the average of the counted objects. The average is considered as the output because the number of tooth is twice the number of the intersection points.

7.3.6 The Other Parameters

The above three algorithms calculate the outer diameter, the inner diameter and the number of teeth of the gear to be measured. Using these parameters, all other gear parameters can be calculated. Table 7.1 describes the different gear parameters and the subsequent formulas used to generate the values.

7.4 Inspection Process

To accomplish the desired quality inspection process, the measurement of the gear acquired from the Vision2D application is compared with the measurement of the nominal gear derived from the CMM analysis, within a specified tolerance. The interface of the Vision2D application (Figure 7.9) deals with this process. The inspection process performed uses the following four steps:

- **The standard gear parameters:** The standard gear parameters is set into the Vision2D application for automatic reference. The reference values were obtained from a CMM analysis of a nominal gear.

Table 7.1: The gear nomenclature and formulas

Domination	Symbol	Formula
Module	m	$m = \frac{da}{(z+2)}$
Clearance	c	$c = \frac{((\frac{1}{6}) \times m)}{((\frac{1}{4}) \times m)}$
Pitch diameter	d	$d = m \times z$
Addendum	ha	$ha = m$
Dedendum	hf	$hf = ha + c$
Whole depth	h	$h = ha + hf$
Circular pitch	p	$p = m \times \pi$
Circular tooth thickness	s;e	$s; e = \frac{p}{2}$
Base circular diameter	db	$db = d \times \cos\alpha$
Cordal addendum	hac	$hac = m[1 + (\frac{z}{2})(1 - (\frac{\cos 90}{z}))]$

- The tolerance: The tolerance is set in the Vision2D application. The parameters to be inspected are verified and their allowable tolerances assigned. Each parameter can be assigned unique tolerance values. Alternatively, the same tolerance values can be applied to all parameters.
- Measuring the gear to be inspected: The gear to be inspected is acquired and measured by the Vision2D system, then the calculated parameters are compared with the nominal gear parameters according to the tolerances given.
- Taking an inspection decision: The inspection decision is displayed automatically in the Inspection section. The inspection is accepted if all inspected parameters for the gear satisfy the corresponding parameter conditions from the nominal reference, within the specified tolerances. Otherwise, the inspection is rejected.

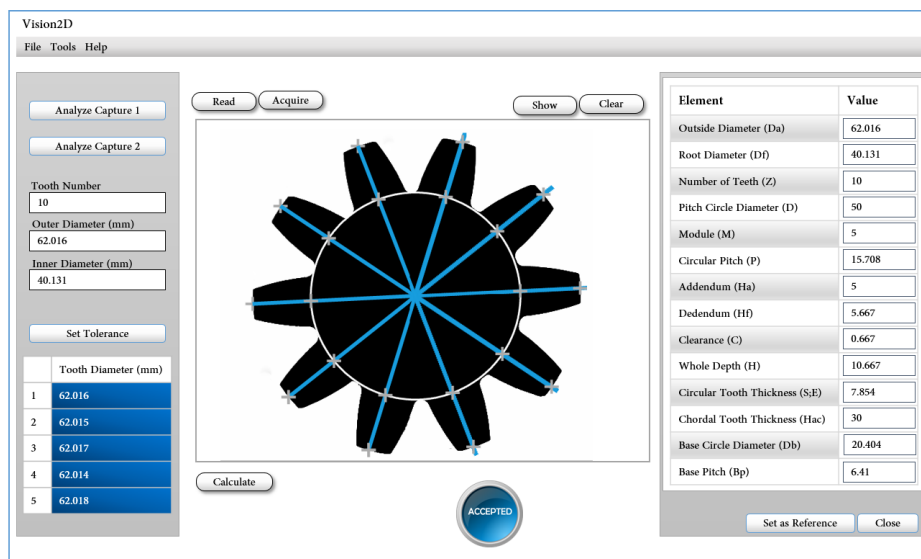


Figure 7.9: The main interface of the Vision2D application.

7.5 Measurement Error and Uncertainty Analysis

The existence of some degree of uncertainty in any given measurement system is caused by different sources or error. Error is the discrepancy between the *"true-value"* and the measured value. Since it is impossible to know the *"true-value"* of a measurement, a measurement made with a much more precise measurement system than the system being tested is taken as the reference measurement.

The quality of the experiment of a measurement system is certain by the minimization or eradication of as many sources of error. Measurement errors are grouped as either random or systematic. Random error usually emerges from unpredictable alterations of dominating quantities. It is almost impossible to require for the random error of measurement, however an increase in the number of experimentation can often times minimize it. A system error emerges from an observable effect of a dominating quantity on a measurement. It is quantifiable. A level of rectification can be applied to require for the effect. Random and systematic errors are related to precision and accuracy respectively. Precision denotes the quality of measurement,

with no attestation that the measurement is right. While accuracy ascertain that, there is an optimal value, normally referenced, to know how distant the feedback is from the optimal value. According to GUM (ISO and OIML, 1995), uncertainty components are grouped into two categories based on their method of evaluation "A" and "B". Both types are different forms to evaluate the uncertainty and are based on probability distributions. Type A standard uncertainty is calculated from series of repeated observations and is the square root of the statistically estimated variance (i.e., the estimated standard deviation). This technique principally encompass random errors. Type B standard uncertainty is also the square root of an estimated variance, but rather than being evaluated by repeated measurement, it is obtained from an assumed probability density function based on the degree of belief that an event will occur. This technique encompasses systematic errors and the other uncertainty factors considered important.

The individual uncertainty components u_i (sometimes of Type A and sometimes of Type B) should be combined using the law of propagation of uncertainties, commonly called the "root-sum-of-squares" or "RSS" method to obtain the combined standard uncertainty, denoted by u_c .

$$u_c = \sqrt{\sum u_i^2} \quad (7.1)$$

However, when this is done, the combined standard uncertainty should be equivalent to the standard deviation of the result, making this uncertainty value correspond with a 68% confidence interval (with a normal distribution). If a wider confidence interval is desired, the uncertainty can be multiplied by a coverage factor (usually $k = 2$ or 3) to provide an uncertainty range that is believed to include the true value with a confidence of 95% (for $k = 2$) or 99,7% (for $k = 3$). This is called expanded uncertainty and is denoted by U_c .

$$U_c = k\sqrt{\sum u_i^2} \quad (7.2)$$

Another possibility is, instead of assuming a normal distribution in all the uncertainties, calculate the coverage factor independently for each uncertainty depending on its specific distribution.

$$U_c = \sqrt{\sum (k_i u_i)^2} \quad (7.3)$$

Table 7.2: Coverture factor for different probability distributions

Rectangular distribution		Normal distribution	
Level of confidence p (%)	Coverture factor k	Level of confidence p (%)	Coverture factor k
57,74	1	68,27	1
95	1,65	90	1,645
99	1,71	95	1,960
100	1,73	95,45	2
		99	2,576
		99,73	3

In this case, Table 7.2 can be used to obtain the parameter k looking for a confidence of 95% that is the usual one in most of the industry processes. As our uncertainties only fall in rectangular or normal distributions, we'll take $k = 1,65$ and $k = 1,96$ respectively.

In this work, the most significant uncertainties (u_i) that have been considered are:

- Resolution uncertainty (Type B)
- Pattern (plate) uncertainty (Type B)
- Calibration uncertainty (Type A)
- Measurement uncertainty (Type A)

7.5.1 Resolution uncertainty

One of the sources of uncertainty of an instrument is the resolution of the device (if it is a digital instrument), or the uncertainty due to the resolution of reading (if it is an analog instrument) that depends on the operator or the way used in the reading.

If the resolution of the indicating device is δx , the input signal value that produces an indication given X can be placed with equal probability

at any point within the interval from $(X - \delta x/2)$ to $(X + \delta x/2)$. The input signal can then be described by means of a rectangular distribution with range δx and standard deviation (typical uncertainty) of:

$$u_r = \frac{\delta x}{2\sqrt{3}} \quad (7.4)$$

Taking into account that the theoretical sub-pixel object space resolution is given by:

$$\delta x = \frac{FOV}{256 * \#pixels} \quad (7.5)$$

where FOV is the Field of View (70mm), #pixels is the number of pixels and each pixel has 8 bits of depth.

7.5.2 Pattern uncertainty

The uncertainty of the pattern should be given by the calibration laboratory, by a formula or simply by its value. In our case, the plate calibration certificate points out that the maximum uncertainty of the plate is $0,15\mu m$. That means an expanded uncertainty with a 100% level of confidence U'_p . The typical uncertainty is obtained by dividing the expanded uncertainty by the coverage factor. In this case $k' = 3$ (normal distribution).

$$u_p = \frac{U'_p}{k'} \quad (7.6)$$

Finally, to obtain the expanded uncertainty with a 95% level of confidence, a $k = 1,96$ should be used.

$$U_p = k u_p \quad (7.7)$$

7.5.3 Calibration uncertainty

In most cases, the best available estimate of the expected value of a quantity that varies randomly (uncertainty Type A), and for which n

independent observations q_k have been obtained under the same conditions of measurement, is the arithmetic mean or average \bar{q} of the n observations. The estimate of variance and its positive square root σ (standard deviation), characterize the variability of the observed values.

$$\sigma = \sqrt{\frac{\sum_{k=1}^n (q_k - \mu)^2}{n - 1}} \quad (7.8)$$

According to statistical theory, the best estimate for Type A standard uncertainty is given by standard deviation of the mean:

$$u_{calib} = \frac{\sigma_{calib}}{\sqrt{n}} = \sqrt{\frac{\sum_{k=1}^n (q_k - \mu_{calib})^2}{n(n - 1)}} \quad (7.9)$$

Knowing the nominal distance between two horizontal points in the plate (2,58065 mm), a set of 18 distance measurements close to 62 mm (roughly the size of the gear) were performed computing its $\mu_{calib} = 65,6610mm$ and $\sigma_{calib} = 0,0017mm$.

If q_0 is the reference value, a calibration correction can also be computed as follows:

$$\Delta q_{corr} = q_0 - \mu_{calib} \quad (7.10)$$

This calibration correction can be applied in two ways. On one hand correcting the value of the measurements, each time a measurement is made, with the deviation value obtained in the calibration correction Δq_{corr} . On the other hand (the chosen one in this work), including as a cause of calibration uncertainty the term of the systematic correction, assuming it is distributed according to a rectangular function ($\frac{\Delta q_{corr}}{\sqrt{3}}$) according to (Sevilla, 2001). This is more comfortable as it has an expression that already introduces this systematic variation, although increases unnecessarily the value of the global uncertainty.

7.5.4 Measurement uncertainty

It is accepted that the variance obtained in the process of calibration be the same as that obtained in the process of usual measurement, so, the uncertainty associated with the measurement process will be the same as u_{calib} with $n = 1$, i.e., $u_m = \sigma_{calib}$.

Before performing measurements, it's important to check the system error measuring the ground-truth nominal sample gear. Figure 7.10 shows the measurement data of different camera exposures of the ground-truth sample gear, in order to check the minimum system error. The minimum error obtained is 0.002 mm at a exposure time of 7500 μs , very coherent to the computed standard uncertainty u_m (see Table 7.4).

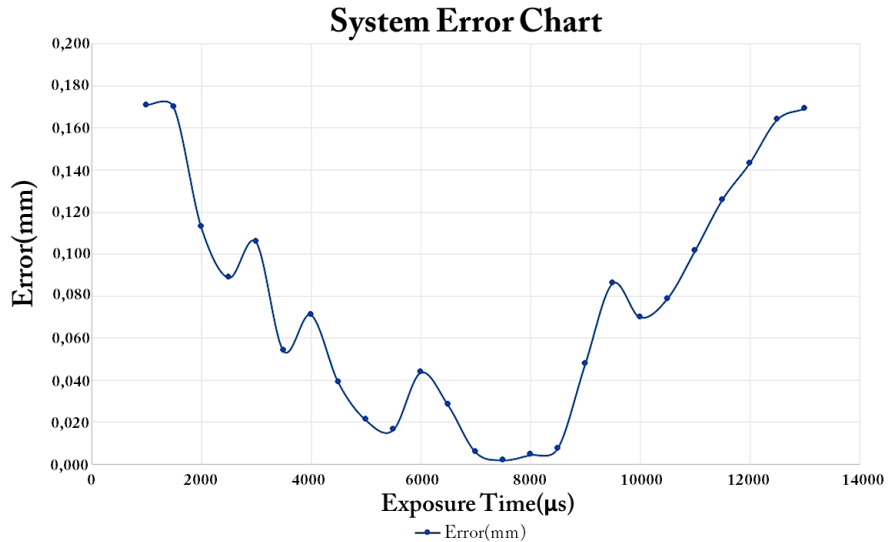


Figure 7.10: Graph to check the minimum system error

A summary of the different uncertainties involved in the combined standard uncertainty is shown in Table 7.3.

Table 7.3: Summary of involved uncertainties

Name	Symbol	Standard uncertainty	Prob. Distr.	Coverture factor	Contribution to expanded uncertainty
		u_i		k_i	U_i
Resolution	u_r	$\frac{FOV}{512\sqrt{3}*\#pixels}$	Rectangular	1,65	$\frac{1,65*FOV}{512\sqrt{3}*\#pixels}$
Pattern	u_p	u_p	Normal	1,96	$1,96u_p$
Calibration	u_{calib}	$\frac{\sigma_{calib}}{\sqrt{n}}$	Normal	1,96	$1,96\frac{\sigma_{calib}}{\sqrt{n}}$
Calibration correction	Δq_{corr}	$\frac{q_0 - \mu_{calib}}{\sqrt{3}}$	Rectangular	1,65	$1,65\frac{q_0 - \mu_{calib}}{\sqrt{3}}$
Measurement	u_m	σ_{calib}	Normal	1,96	$1,96\sigma_{calib}$

Combined uncertainty (u_c)	$u_c = \sqrt{\sum u_i^2}$
Expanded uncertainty (U_c)	$U_c = \sqrt{\sum U_i^2}$

7.6 Validation and Analysis

For the proper verification of the gear system, the developed Vision2D application inspected twelve gear pieces. The inspection process aimed at ascertaining if each of the gear had any defective component. This is to enhance the quality control inspection in the inspection process. The Vision2D application applies the corresponding algorithms to the image processed, and determines if the gear is non-defective or defective. If the image processed meets all the required conditions, the Vision2D application outputs 'accepted', and sends a positive signal to the robot sensor. The robot picks the gear piece from the configuration setup and delivers it to the appropriate section. If the image processed fails the required condition

Table 7.4: Summary of involved uncertainties with numerical values

Name	Symbol	Standard uncertainty (μm)	Prob. Distr.	Coverture factor	Contribution to expanded uncertainty (μm)
Resolution	u_r	0,0322	Rectangular	1,65	0,0531
Pattern	u_p	0,05	Normal	1,96	0,098
Calibration	u_{calib}	0,3966	Normal	1,96	0,7772
Calibration correction	Δq_{corr}	1,7128	Rectangular	1,65	2,8261
Measurement	u_m	1,6824	Normal	1,96	3,2976

Combined uncertainty (u_c)	2,4341 μm
Expanded uncertainty (U_c)	4,4133 μm

set, the Vision2D application outputs 'rejected', and sends a negative signal to the robot sensor. The nominal value acquired from the CMM with the ground-truth sample gear is used to verify the values generated by the Vision2D application. The error margin sets as tolerance of the system is ± 0.020 mm for a gear nominal diameter of 62,014 mm.

In order to compute the uncertainty of the process before the gears measurement, Table 7.3 is filled with numerical values (shown in Table 7.4). This allows to conclude that if a measurement m is made close to 62 mm, and for instance 62,012 mm is obtained, the real value will be:

$$M = (62,012 \pm 0,004mm) \quad (7.11)$$

where the number following the symbol \pm is the numerical value of an expanded uncertainty U_c , determined from a combined standard uncertainty, u_c , and the related coverage factors based on both, rectangular and normal distributions, and defines an interval estimated to have a level of confidence of 95%.

Once the measurement is made, the decision must be made to consider the piece valid or not, according to the value of the nominal size (m_0), the specified nominal tolerance interval (t_0) and the computed expanded uncertainty (U_c). The admissible zone is shown in Figure 7.11 from the next equations:

$$t_{as} = m_0 + t_0 - U_c = 62,014 + 0,020 - 0,004 = 62,030mm \quad (7.12)$$

$$t_{ai} = m_0 - t_0 + U_c = 62,014 - 0,020 + 0,004 = 61,998mm$$

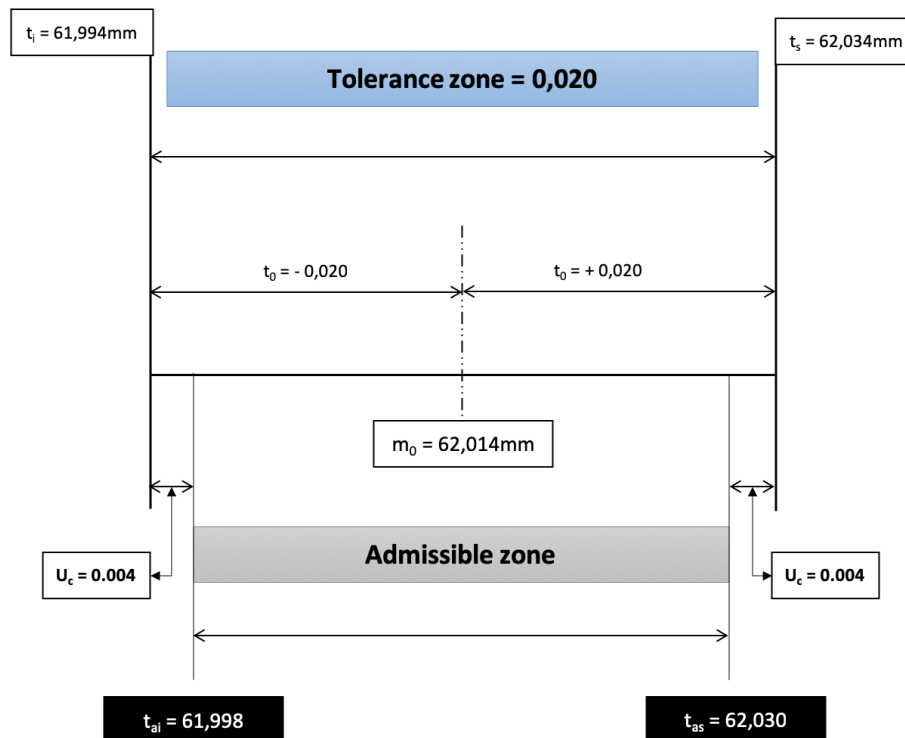


Figure 7.11: Computation of the admissible zone

Table 7.5: Inspection details of accepted Gear 1

Gear Teeth	Outer Diameter (mm)	Error (mm)
1	62,016	0,002
2	62,015	0,001
3	62,017	0,003
4	62,014	0,000
5	62,018	0,004
Average	62,016	0,002

Table 7.6: Inspection details of rejected Gear 12

Gear Teeth	Outer Diameter (mm)	Error (mm)
1	62,065	0,051
2	62,018	0,004
3	62,056	0,042
4	62,019	0,005
5	62,020	0,006
Average	62,036	0,022

Table 7.5 shows the inspection result details of an accepted gear. The Vision2D application inspects and measures each tooth of the gear. It performs the evaluation, and the measured values and difference between the ground-truth value are generated. Vision2D application accepts the gear because of the condition for verification is satisfied.

Table 7.6 shows the verification details of a rejected gear. In this case, the Vision2D application rejects the gear because of the tolerance limit ($16\mu m$), considering the nominal tolerance and the vision system uncertainty, was exceeded.

The inspection result details of all twelve gears and the summary verification chart are shown in Table 7.7 and Fig.7.12 respectively.

Table 7.7: The Inspection Results

Nominal Value m_0 (mm)	62,014		
Tolerance t_0 (mm)	$\pm 0,020$		
Expanded uncertainty U_c (mm)	$\pm 0,004$		
Gear	Outer Diameter (mm)	Error (mm)	Decision
1	62,016	0,002	Accepted
2	62,006	0,008	Accepted
3	62,024	0,010	Accepted
4	62,040	0,026	Rejected
5	62,012	0,002	Accepted
6	62,028	0,014	Accepted
7	61,984	0,030	Rejected
8	62,025	0,011	Accepted
9	62,024	0,010	Accepted
10	62,015	0,001	Accepted
11	62,034	0,020	Rejected
12	62,036	0,022	Rejected

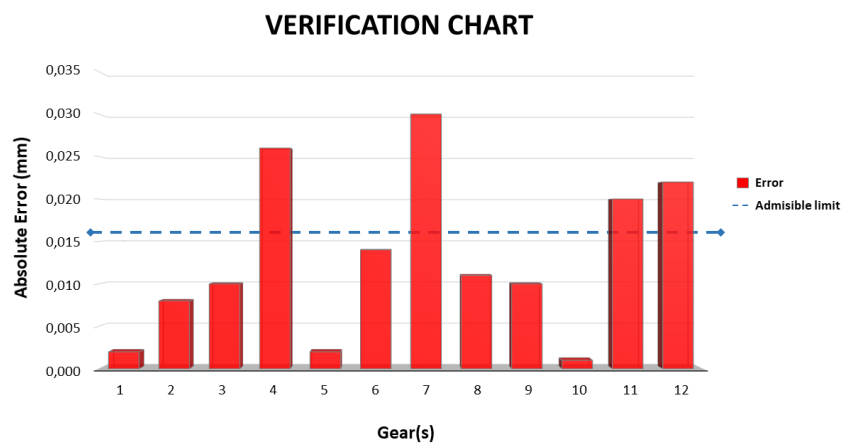


Figure 7.12: The Verification Chart

7.7 Discussion

This chapter further exposes the development of an improved Vision2D for quality control inspection. The experiments carried out with different gears reveal the functionality of the developed Vision2D application taking into account not only the nominal tolerance but also the computed uncertainty of the process. Several emphasized considerations were implemented to better enhance the results generated by the application, as follows:

- The use of a telecentric lens.
- An improved camera configuration and set-up.
- A high-quality system with a very low calibration error result.
- A greater amount of proofs done on an increased number of gear inspections.
- A significantly low tolerance to enhance a limited error-prone system for better quality control inspection
- A methodological study of the uncertainty associated with the process.

The successful implementation of these emphasized considerations and the achievements of the significant uncertainties that have been considered are the contributions that distinguish this chapter.

Part III

Conclusions

Chapter 8

Conclusions

In the case of an industrial inspection process, we were curious to pause at each stage of the inspection to observe the effects of using an optimal algorithm and a not-optimal algorithm to compare the effect on the inspection process of the fabricated piece.

The main conclusions of this dissertation have been to investigate the following research questions associated to each of the identified phases of the optical set-up pipeline:

- The effects of lens misalignment can be highly pronounced. If the lens is not mounted correctly then the result will be an image that is not perfectly focused. If the lens is tilted, part of the image captured by the sensor may be in focus while another part of the image will be blurred. In the first proposal, we present a light alignment algorithm to track and monitor acquired image plane regions to verify an optimal light alignment system.
- Due to the importance and complex nature of an efficient calibration process, several factors are involved for a successful calibration process. Each of these factors play a significant role in determining the accuracy of the error generated. The level of accuracy of the calibration process determines to a large extent the accuracy of the measurement results desired. Proposal 2 has presented the results from this study, in which the effects of the different parameters, such as camera focus, exposure time, calibration plate tilt and number of images, were analyzed to determine how they influence the calibration process. For the camera focus proposal, an algorithm that evaluates focus range in real time is presented. Special attention has been paid

to the focus parameter since currently, the procedure to find the focused image is done visually by the user. However, in this thesis we demonstrate that performing the search for the optimal focus results in lower and statistically different calibration errors, which justifies using this method for use in industrial vision systems.

- As a result of adjustments and motions during a measuring process, it becomes important to have an alignment system to avoid any possible errors that may result from a lack of alignment. In order to obtain the best possible alignment conditions, it is necessary to check if the object to be measured is well placed. In the third proposal, an alignment algorithm was developed and used to track the changes that occur in the image processing. Furthermore, several tilting position of the object was used to verify and authenticate the algorithm. The results shows the efficacy of the algorithm.
- The proposal validation chapter shows experiments in which all the previous proposals were put together so that the impact on each one in both, calibration error and measurement, can be evaluated. The results show that even when visually, an optical set-up can be built and it works, it is worthy to find optimal values in every single pipeline stage.
- Quality control has become a priority in the inspection processes of industrial manufacturing. Machine vision technology provide image-based inspection and analysis for such demanding processes. We present a chapter with the results from the study, in which an improved machine vision application is developed to perform a precise measurement of industrial gears (at sub pixel level), and making a deep study of the uncertainty of the measurement.

8.1 Future research lines

Several research lines are open to continue with this work:

- All proposals of this Thesis have been coded and evaluated separately. The first easiest and fastest work would be to put all proposals together in one single application and enable a GUI to access each one of the algorithms.

-
- The study of more parameters involved in the calibration process like depth-of-field, gamma, ISO, or even those involved in color cameras.
 - The accomplished uncertainty study makes some assumptions or simplifications or does not take into account other uncertainty sources like temperature. A deeper uncertainty study could be done.
 - This Thesis focus on static environments in which the product is not moving. The following work would be the study of advanced inspection and metrology techniques in a dynamic environment as products move over belt system.
 - The effects of vibration in the metrology and high precision evaluations, especially in dynamic environments.

Part IV

Appendices

Appendix A

Optical Set-Up Definitions

A.1 Understanding Focal Length and Field of View

A Fixed Focal Length Lens, also known as a conventional or endocentric lens, is a lens with a fixed Angular Field of View (AFOV). By focusing the lens for different working distances, differently sized Fields of View (FOV) can be obtained, though the viewing angle is held constant. AFOV is typically specified as the full angle (in degrees) associated with the horizontal dimension (width) of the sensor that the lens is to be used with. Fixed Focal Length Lenses should not be confused with Fixed Focus Lenses. Fixed Focal Length Lenses have the ability to be focused for different distances and Fixed Focus Lenses are intended for use at a single, specific working distance. Examples of Fixed Focus Lenses are many Telecentric Lenses and Microscope Objectives. The focal length of a lens defines the lens's angular field of view. For a given sensor size, the shorter the focal length, the wider the angular field of the lens. Additionally, the shorter the focal length of the lens, the shorter the distance needed to obtain the same FOV compared to a longer focal length lens. For a simple, thin convex lens, the focal length is the distance from the back of the lens to the plane of the image formed of an object placed infinitely far in front of the lens. From this definition, it can be shown that the angular field of view of a lens is related to the focal length (Equation A.1), where f is the focal length in millimeters and h is the horizontal dimension of the sensor in millimeters as show in Figure A.1.

$$AFOV(^{\circ}) = 2 \times \tan^{-1}\left(\frac{h}{2f}\right) \quad (\text{A.1})$$

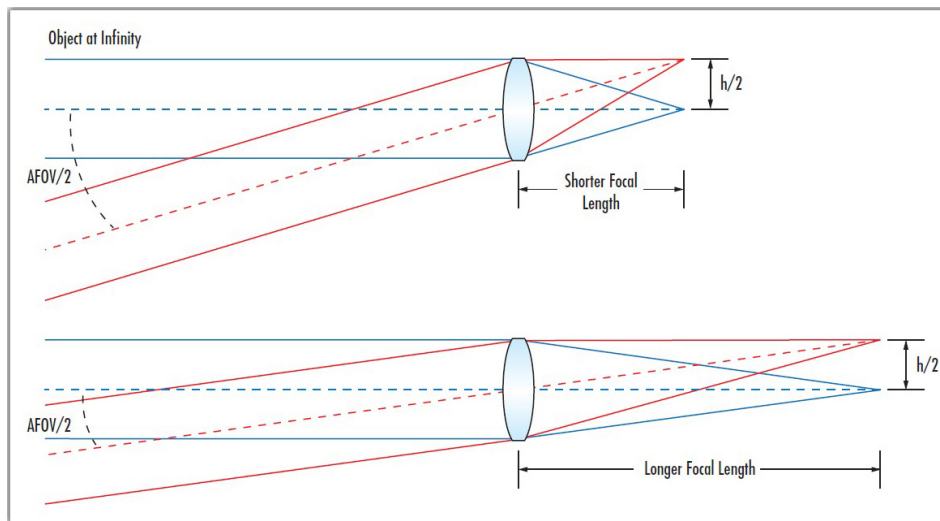


Figure A.1: Focal length of AFOV

When using Fixed Focal Length Lenses, there are three ways to change the field of view of the system (camera and lens):

- The first and often easiest option is to change the working distance from the lens to the object; moving the lens farther away from the object plane increases the field of view.
- The second option is to swap out the lens that is being used with one of a different focal length.
- The third option is to change the size of the sensor that is being used; a larger sensor will yield a larger field of view for the same working distance.

A.2 Working Distance (WD) and Field of View (FOV)

The required distance from an object and the desired field of view (the size of the object with additional buffer space) are typically known quantities. This information can be used to directly determine the required angular field of view via the formulas shown in Equation A.2, where WD is the Working Distance from the lens and AFOV is the Angular Field of View.

$$AFOV(^{\circ}) = 2 \times \tan^{-1}\left(\frac{HorizontalFOV(mm)}{2 \times WD(mm)}\right)$$

or

$$Horizontal\ FOV(mm) = 2 \times WD(mm) \times \tan\left(\frac{AFOV(^{\circ})}{2}\right) \quad (A.2)$$

Once the required AFOV has been determined, the focal length can be approximated using Equation A.1 and the proper lens can be chosen from a lens specification table or datasheet by finding the closest available focal length with the necessary angular field of view for the sensor being used. Alternatively if the sensor has already been chosen, the focal length can be determined directly from the FOV and WD by substituting Equation A.1 in Equation A.2, as shown in Equation A.3,

$$FL = \left(\frac{h \times WD}{HorizontalFOV}\right) \quad (A.3)$$

where, h is the horizontal sensor dimension (number of horizontal pixels multiplied by the pixel size) and FL is the focal length of the lens, both in millimeters; the FOV and WD must be measured in the same unit system.

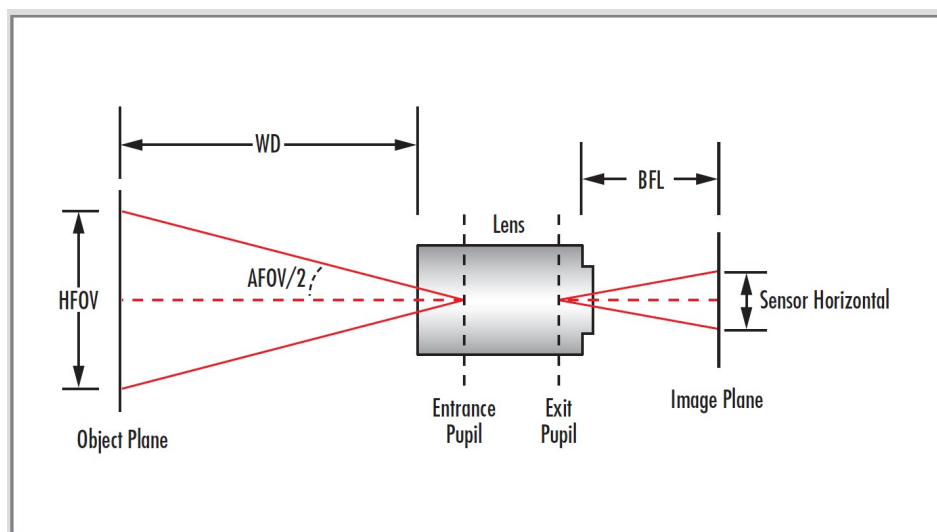


Figure A.2: Relationship between HFOV, sensor size, and WD for a given angular FOV

A.3 Lens Specifications and Resolution

Resolution is a measurement of an imaging system's ability to reproduce object detail and can be influenced by factors such as the type of lighting used, the pixel size of the sensor, or the capabilities of the optics. The smaller the object detail, the higher the required resolution. Dividing the number of horizontal or vertical pixels on a sensor into the size of the object one wishes to observe will indicate how much space each pixel covers on the object and can be used to estimate resolution. However, this does not truly determine if the information on the pixel is distinguishable from the information on any other pixel. As a starting point, it is important to understand what can actually limit system resolution. Figure A.3 shows a pair of squares on a white background. If the squares are imaged onto neighboring pixels on the camera sensor, then they will appear to be one larger rectangle in the image (a) rather than two separate squares (b). In order to distinguish the squares, at least one pixel needs to be between them. This minimum distance is the limiting resolution of the system. The absolute limitation is defined by the size of the pixels on the sensor as well as the number of pixels on the sensor.

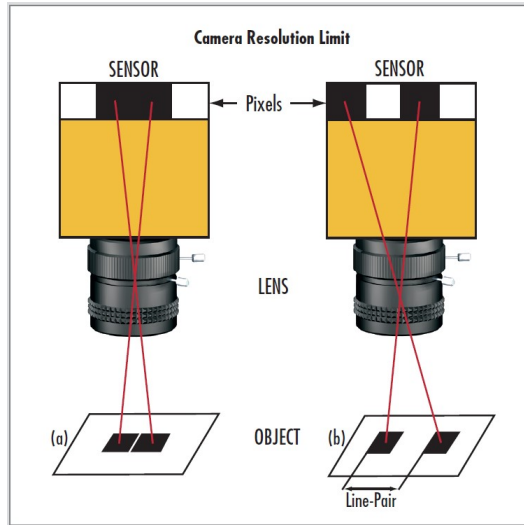


Figure A.3: Resolving two squares. If the space between the squares is too small (a) the camera sensor will be unable to resolve them as separate objects

In order to determine the absolute minimum resolvable spot that can be seen on the object, the ratio of the field of view to the sensor size needs to be calculated. This is also known as the Primary Magnification (PMAG) of the system.

$$PMAG = \left(\frac{\text{sensor size}(mm)}{FOV(mm)} \right) \quad (A.4)$$

The ratio associated with system PMAG allows for the scaling of the imaging space resolution which gives the resolution of the object.

$$\text{object space resolution}(lp/mm) = (\text{image space resolution}(lp/mm) \times PMAG) \quad (A.5)$$

Generally when developing an application, a system's resolution requirement is not given in lp/mm, but rather in microns (μm) or fractions of an inch:

$$\text{object space resolution}(\mu\text{m}) = \left(\frac{\text{pixel size}(\mu\text{m})}{PMAG} \right) \quad (\text{A.6})$$

A.4 Vignetting within a Lens

Vignetting is the result of light rays not making it through the entire lens system to the sensor, due to being blocked by the edges of individual lens elements or mechanical stops. This clipping of rays can be intentional or unintentional, and in some case it is unavoidable. Vignetting is most often seen at or in lower $f/\#$ s, short focal length lenses, or lenses where higher resolutions need to be achieved at a lower cost. Figure A.4 demonstrates clipping as it may occur for the same 16mm lens at different $f/\#$ s ($f/1.8$ and $f/4$). Note the clipping of rays in Figure A.4a, as indicated with red circles; these rays are not able to pass through all of the optics in the lens. Figure A.4b, on the other hand, demonstrates an example without vignetting. The vignetting in Figure A.4a could have several causes, including diameter limitations of the optics or a need to eliminate the rays to block stray light. Vignetting is sometimes purposely included in a lens design to improve overall lens performance or reduce cost.

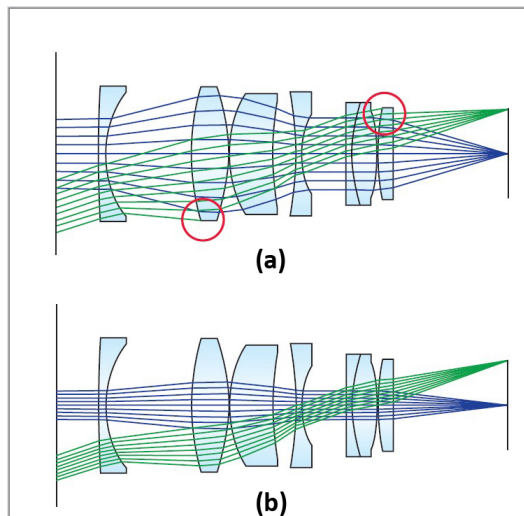


Figure A.4: A 16mm lens design at a) $f/1.8$ and b) $f/4$. At $f/1.8$ vignetting occurs where light rays are clipped by the edges of the lens.

A.5 Depth of Field and Depth of Focus

The Depth of Field (DOF) of a lens is its ability to maintain a desired amount of image quality (spatial frequency at a specified contrast), without refocusing, if the object is positioned closer to and farther from best focus. DOF also applies to objects with complex geometries or features of different heights. As an object is placed closer or farther than the set focus distance of a lens, the object blurs and both resolution and contrast suffer. Because of this, DOF only makes sense if it is defined with an associated resolution and contrast.

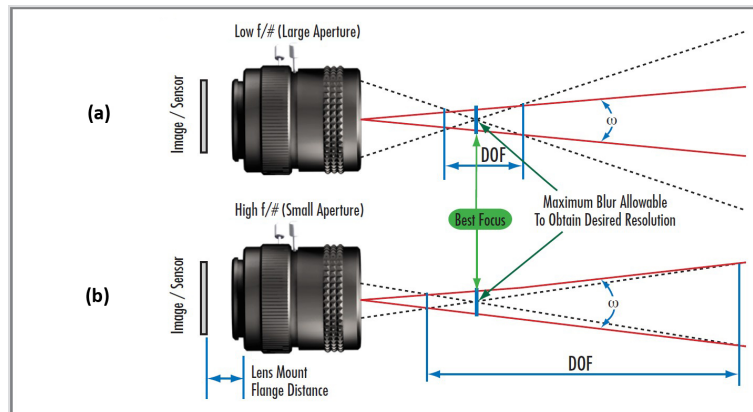


Figure A.5: Geometric representation of DOF for high and low $f/\#$ lenses.

Depth of focus is the image-space complement of depth of field and is related to how the quality of focus changes on the sensor side of the lens as the sensor is moved while the object remains in the same position. Depth of focus dictates how much tip and tilt can be tolerated between the image plane of the lens and the sensor plane itself. As $f/\#$ decreases, so too does the depth of focus, which increases the impact that tilt has on achieving the best focus across the sensor.

A.6 Distortion

The term distortion is often applied interchangeably with reduced image quality. Distortion is an individual aberration that does not technically reduce the information in the image; while most aberrations actually mix information together to create image blur, distortion simply misplaces information geometrically. This means that distortion can actually be calculated or mapped out of an image, whereas information from other aberrations is essentially lost in the image and cannot easily be recreated. Distortion is a monochromatic optical aberration that describes how the magnification in an image changes across the field of view at a fixed working distance; this is critically important in precision machine vision and gauging applications. Distortion is distinct from parallax, which is a change in magnification (field of view) with working distance. It is important to note that distortion varies with wavelength, as shown in Figure A.6, and that when calibrating distortion out of a machine vision system the wavelength of the illumination needs to be taken into account. Curves like the one in Figure A.6 are very helpful in determining how to calibrate out distortion.

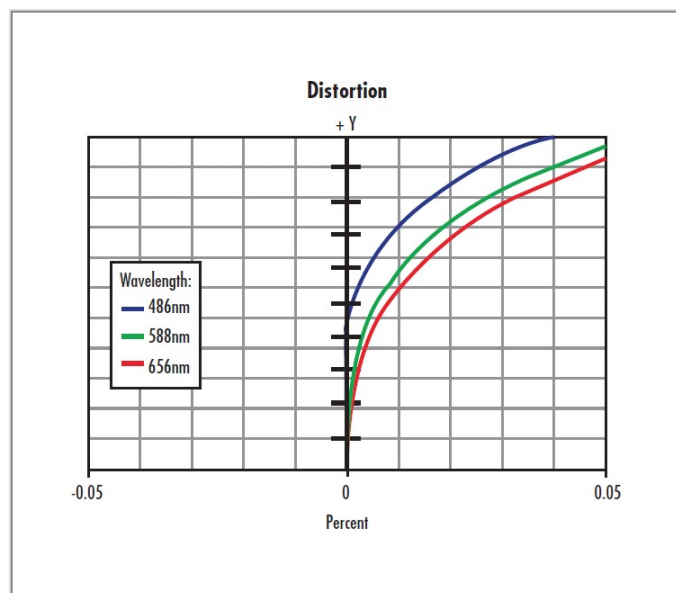


Figure A.6: Distortion plot showing the variance of distortion with respect to wavelength

As with other aberrations, distortion is determined by the optical design of the lens. Lenses with larger fields of view will generally exhibit greater amounts of distortion because of its cubic field dependence. Distortion is a third-order aberration that, for simple lenses, increases with the third power of the field height; this means that larger fields of view (a result of low magnification or short focal length) are more susceptible to distortion than smaller fields of view (high magnification or long focal length). The wide fields of view achieved by short focal length lenses should be weighed against aberrations introduced in the system. On the other hand, telecentric lenses typically have very little distortion: a consequence of the way that they function. It is also important to note that when designing a lens to have minimal distortion, the maximum achievable resolution can be decreased. In order to minimize distortion while maintaining high resolution, the complexity of the system must be increased by adding elements to the design or by utilizing more complex optical glasses.

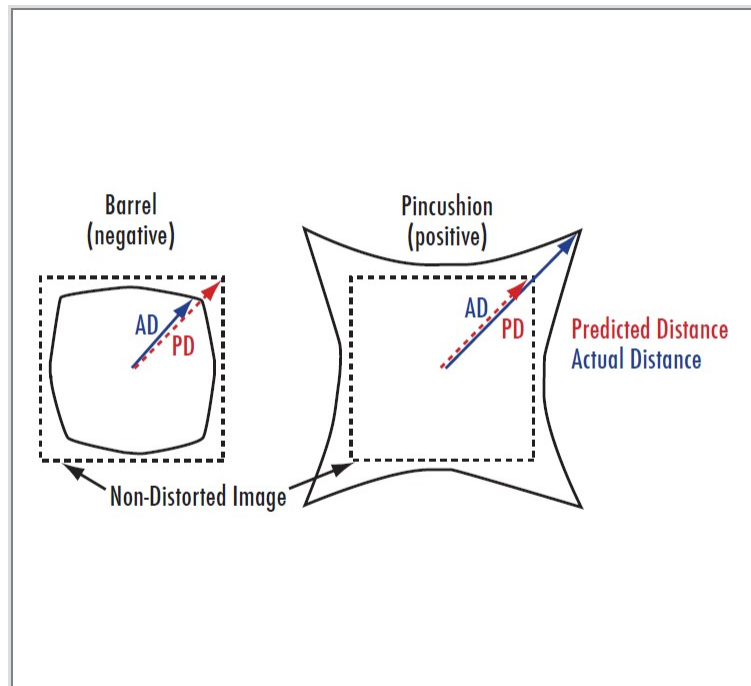


Figure A.7: An illustration of positive and negative distortion

Distortion is typically specified as a percentage of the field height.

Typically, ± 2 to 3% distortion is unnoticed in a vision system if measurement algorithms are not in use. In simple lenses, there are two main types of distortion: positive, barrel distortion, where points in the field of view appear too close to the center; and negative, pincushion distortion, where the points are too far away. Barrel and pincushion refer to the shape a rectangular field will take when subjected to the two distortion types, as shown in Figure A.7. Distortion can be calculated simply by relating the Actual Distance (AD) to the Predicted Distance (PD) of the image using Equation A.7. This is done by using a pattern such as dot target shown in Figure A.8.

$$Distortion(\%) = \left(\frac{AD - PD}{PD} \right) \times 100 \quad (A.7)$$

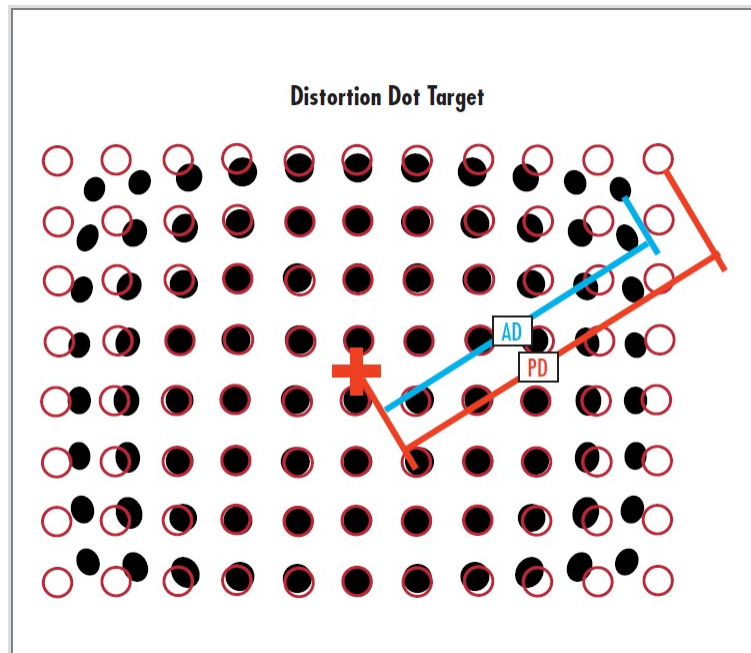


Figure A.8: Calibrated target (red circles) vs. imaged (black dots) dot distortion pattern.

It is important to note that while distortion generally runs negative or positive in a lens, it is not necessarily linear in its manifestation across the

image for a multi-element assembly. Additionally, as wavelength changes, so does the level of distortion. Finally, distortion can be altered with changes in working distance. Ultimately, it is important to individually consider each lens that will be used for a specific application in order to guarantee the highest level of accuracy when looking to remove distortion from a system.

A.7 Telecentric and Perspective Error

Conventional lenses have angular fields of view such that as the distance between the lens and object increases, the magnification decreases. This is how the human vision behaves, and contributes to our depth perception. This angular field of view results in parallax, also known as perspective error, which decreases accuracy, as the observed measurement of the vision system will change if the object is moved (even when remaining within the depth of field) due to the magnification change. Telecentric Lenses eliminate the parallax error characteristic of standard lenses by having a constant, non-angular field of view; at any distance from the lens, a Telecentric Lens will always have the same field of view. Figure A.9 shows the difference between a non-telecentric and a telecentric field of view. A Telecentric Lens's constant field of view has both benefits and constraints for gauging applications. The primary advantage of a Telecentric Lens is that its magnification does not change in respect to depth. Figure A.10 shows two different objects at different working distances, both imaged by a Fixed Focal Length (non-telecentric) Lens (center) and a Telecentric Lens (right). Note that in the image taken with a Telecentric Lens, it is impossible to tell which object is in front of the other. With the Fixed Focal Length Lens, it is quite obvious that the object that appears smaller is positioned farther from the lens. While Figure A.10 is drastic in terms of a working distance shift, it illustrates the importance of minimizing parallax error. Many automated inspection tasks are imaging objects that move through the field of view of an imaging system, and the position of parts is rarely perfectly repeatable. If the working distance is not identical for each object that the lens is imaging, the measurement of each object will vary due to the magnification shift. A machine vision system that outputs different results based on a magnification calibration error (which is unavoidable with a Fixed Focal Length Lens) is a non-reliable solution and cannot be used when high precision is necessary. Telecentric Lenses eliminate the concern about measurement errors that would otherwise occur due to factors such

as a vibrating conveyor or inexact part locations.

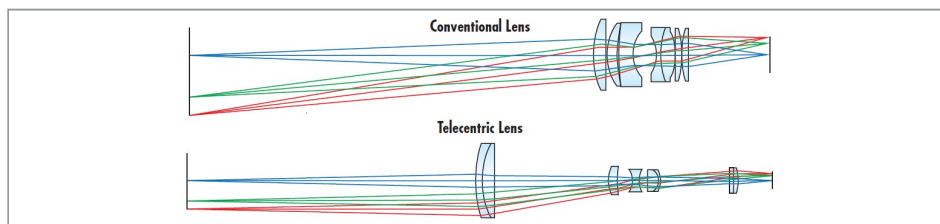


Figure A.9: Field of view comparison of a conventional and Telecentric Lens. Note the conventional lens's angular field of view and the Telecentric Lens's zero angle field of view.



Figure A.10: The angular field of view of the Fixed Focal Length Lens translates to parallax error in the image and causes the two cubes to appear to be different sizes.

A.8 Telecentric Lenses and Depth of Field

It is a common misconception that Telecentric Lenses inherently have a larger depth of field than conventional lenses. While depth of field is still ultimately governed by the wavelength and $f/\#$ of the lens, it is true that Telecentric Lenses can have a larger usable depth of field than conventional lenses due to the symmetrical blurring on either side of best focus. As the part under inspection shifts toward or away from the lens, it will follow the angular field of view that is associated with it. In a non-telecentric lens, when an object is moved in and out of focus, the part blurs asymmetrically due to parallax and the magnification change that is associated with its angular field of view. Telecentric Lenses, however, blur symmetrically since there is no angular component to the field of view. In practice, this means that features such as edges retain their center of mass location; an accurate

measurement can still be made when the object is beyond best focus as long as the contrast remains high enough for the algorithm being used by the machine vision system to function properly. While it may seem counter intuitive, blur can be used advantageously in certain applications with Telecentric Lenses. For example, if a machine vision system needs to find the center location of a pin, as shown in Figure 5.3a, the transition from white to black is quite sharp when the lens is in focus. In Figure 5.3b, the same pin is shown slightly defocused. Looking at a plot of the image gray levels from a line profile taken across the edge of the part, as in Figure 5.4, the slope of the line is much shallower for the slightly defocused image, as the pin edge is spread over more pixels. Due to the symmetric blurring of the Telecentric Lens, this blur is still usable as the centroid has not moved and the amount of sub-pixel interpolation needed is decreased. This reduces sensitivity to grey level fluctuations caused by sensor noise and allows the pin center location to be found more reliably and with higher repeatability.

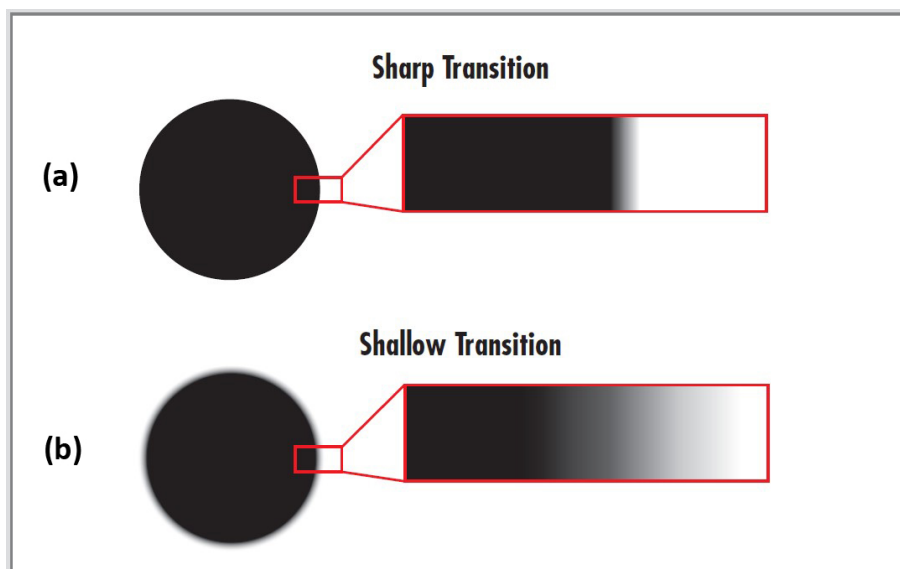


Figure A.11: The same pin imaged both in and out of focus. Note that the transition from white to black covers many more pixels when the lens is slightly out of focus (b), which can be advantageous.

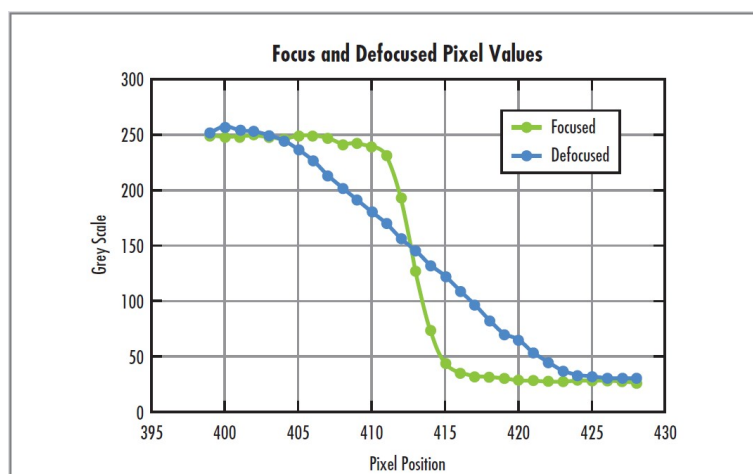


Figure A.12: Plot showing the difference in slope between a focused and defocused edge. The defocused edge takes up many more pixels; finding the edge becomes easier without relying on sub-pixel interpolation.

A.9 Telecentricity and Distortion

Another advantage of using Telecentric Lenses in metrology applications is that Telecentric Lenses typically have lower distortion values than Fixed Focal Length Lenses. Distortion causes the actual position of an object to appear as though it is in a different location, which can further decrease measurement accuracy. Figure A.13a shows jumper pins on a circuit board that has been imaged by a Fixed Focal Length Lens with high distortion. The distortion, coupled with the parallax error inherent to non-telecentric lenses, makes the pins toward the edge of the image appear as though they are bent toward the center. When looking at the same pins with a Telecentric Lens, as in Figure A.13b, it is apparent that the pins are indeed straight. While it is true that distortion can be calibrated out of images to partially improve the accuracy, the parallax is still present and will cause error. The other advantage to not needing to calibrate out the distortion from the Telecentric Lens is that the measurement process can run faster as there is less computing that the software needs to do, reducing CPU load and directly leading to higher system throughput and more parts measured per minute. While the magnitude of the distortion is generally low enough

to not have a significant impact on the measurement of the part under inspection, it is still important to check the distortion specifications of the Telecentric Lens and to properly calibrate the imaging system utilizing the Telecentric Lens.

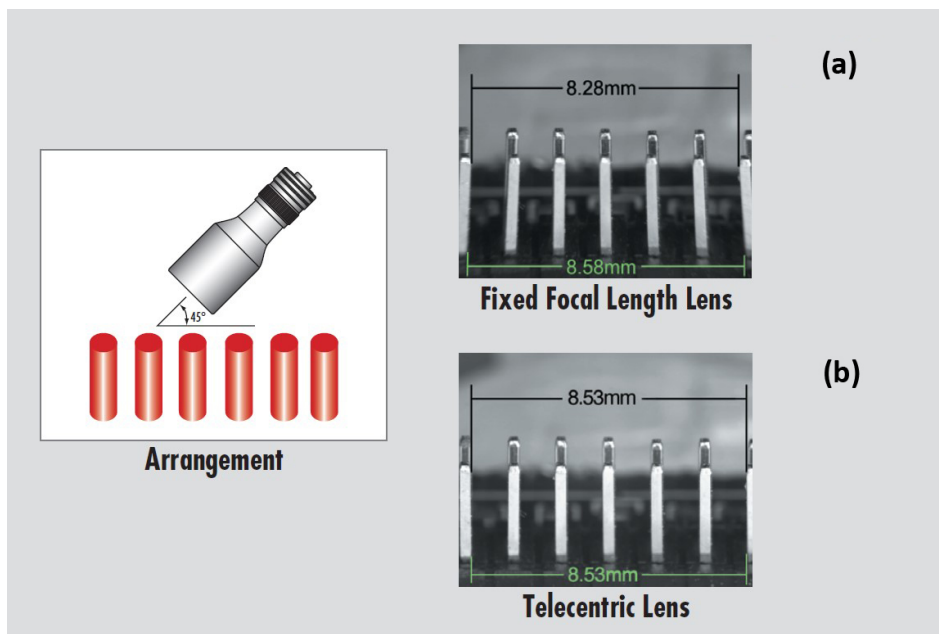


Figure A.13: Comparison of jumpers on a circuit board. a) shows an image that has been taken with a Fixed Focal Length Lens. b) shows an image that has been taken with a Telecentric Lens. Note that the pins do not appear bent in the telecentric image.

In applications where the object plane is tilted, Telecentric Lenses provide a good alternative to Fixed Focal Length Lenses due to their low distortion and invariant magnification. The camera can also be tilted to keep the tilted object in sharp focus; this is called the Scheimpflug condition. The Scheimpflug condition is a way to extend the depth that is being observed by the machine vision system by tilting the object plane and the image plane. If a conventional lens is used this way, it will result in distortion. Telecentric Lenses, however, will not demonstrate distortion, as the magnification does not change with depth.

Appendix B

Generated Publications

Journals

Moru, D. K. and Borro, D. "A machine vision algorithm for quality control inspection of gears". *The International Journal of Advanced Manufacturing Technology*, Vol. 106, N. 1-2, pp. 105-123. January 2020. (Quartil Q2).

Moru, D. K. and Borro, D. "Analysis of different parameters of influence in industrial cameras calibration processes". *Measurement*. (Quartil Q1). (*Submitted in 2020*)

References

- Amarnath, M., Sujatha, C., and Swarnamani, S. “Experimental studies on the effects of reduction in gear tooth stiffness and lubricant film thickness in a spur geared system”. *Tribology international*, Vol. 42, N. 2, pp. 340–352. 2009.
- Bali, A. and Singh, S. N. “A review on the strategies and techniques of image segmentation”. In *Advanced Computing & Communication Technologies (ACCT), 2015 Fifth International Conference on*, pp. 113–120. 2015.
- Baozhang, L. and Yanping, C. “Study on edge subpixel location of ellipse in computer vision measurement”. In *Image and Signal Processing (CISP), 2010 3rd International Congress on*, volume 4, pp. 1684–1688. 2010.
- Batchelor, B. G. “Coming to terms with machine vision and computer vision- they are not the same”. *Advanced imaging*, Vol. 14, N. 1, p. 22. 1999.
- Batchelor, B. G. *Machine vision handbook*. Springer. 2012.
- Beyerer, J., León, F. P., and Frese, C. *Machine vision: Automated visual inspection: Theory, practice and applications*. Springer. 2015.
- Bier, J. “Implementing vision capabilities in embedded systems”. 2011.
- Bin, T., Lei, A., Jiwen, C., Wenjing, K., and Dandan, L. “Subpixel edge location based on orthogonal fourier–mellin moments”. *Image and Vision Computing*, Vol. 26, N. 4, pp. 563–569. 2008.
- Bramberger, M., Pflugfelder, R. P., Maier, A., Rinner, B., Strobl, B., and Schwabach, H. “A smart camera for traffic surveillance”. In *Proceedings*

- of the First Workshop on Intelligent Solutions in Embedded Systems*, pp. 153–164. 2003.
- Chen, A., Gao, C., and He, B. “Influence factors analysis for camera calibration method with planar pattern”. *WIT Transactions on Engineering Sciences*, Vol. 87, pp. 615–622. 02, 2014.
- Chen, G., Guo, Y., Wang, H., Ye, D., and Gu, Y. “Stereo vision sensor calibration based on random spatial points given by cmm”. *Optik*, Vol. 123, N. 8, pp. 731–734. 2012.
- Cheng, H.-D., Jiang, X. H., Sun, Y., and Wang, J. “Color image segmentation: advances and prospects”. *Pattern recognition*, Vol. 34, N. 12, pp. 2259–2281. 2001.
- Chern, N. N. K., Neow, P. A., and Ang, M. H. “Practical issues in pixel-based autofocusing for machine vision”. In *Proceedings 2001 ICRA. IEEE International Conference on Robotics and Automation (Cat. No. 01CH37164)*, volume 3, pp. 2791–2796. 2001.
- Da, F. and Zhang, H. “Sub-pixel edge detection based on an improved moment”. *Image and Vision Computing*, Vol. 28, N. 12, pp. 1645–1658. 2010.
- Dibert, B. and Khan, K. “The embedded vision revolution”. 2013.
- Dowling, K. J., Mueller, G. G., and Lys, I. A. “Systems and methods for providing illumination in machine vision systems”. 2006. US Patent 7,042,172.
- Ekstrom, M. P. *Digital image processing techniques*, volume 2. Academic Press. 2012.
- Elouardi, A., Bouaziz, S., Dupret, A., Lacassagne, L., Klein, J., and Reynaud, R. “A smart sensor for image processing: towards a system on chip”. In *2006 IEEE International Symposium on Industrial Electronics*, volume 4, pp. 2857–2862. 2006.
- Fabijańska, A. “A survey of subpixel edge detection methods for images of heat-emitting metal specimens”. *International Journal of Applied Mathematics and Computer Science*, Vol. 22, N. 3, pp. 695–710. 2012.

- Gadelmawla, E. “A vision system for surface roughness characterization using the gray level co-occurrence matrix”. *NDT & e International*, Vol. 37, N. 7, pp. 577–588. 2004.
- Gadelmawla, E. “Computer vision algorithms for measurement and inspection of external screw threads”. *Measurement*, Vol. 100, pp. 36–49. 2017.
- Gardner, J. “Challenges to embedding computer vision”. 2015.
- Goch, G. “Gear metrology”. *CIRP Annals-Manufacturing Technology*, Vol. 52, N. 2, pp. 659–695. 2003.
- Gregory, R. “Planning a pc-based machine vision system”. 2015.
- Hagara, M. and Kulla, P. “Edge detection with sub-pixel accuracy based on approximation of edge with erf function”. *Radioengineering*, Vol. 20, N. 2, pp. 516–524. 2011.
- Hartley, R. and Zisserman, A. *Multiple view geometry in computer vision*. Cambridge university press. 2003.
- ISO, I. and OIML, B. “Guide to the expression of uncertainty in measurement”. *Geneva, Switzerland*, 1995.
- Jia, Y.-L., Zhang, H.-C., and Jing, Y.-Z. “A modified bresenham algorithm of line drawing [j]”. *Journal of Image and Graphics*, Vol. 1, p. 031. 2008.
- Jurkovic, J., Korosec, M., and Kopac, J. “New approach in tool wear measuring technique using ccd vision system”. *International Journal of Machine Tools and Manufacture*, Vol. 45, N. 9, pp. 1023–1030. 2005.
- Kepf, P. “Important factors when selecting a machine vision lens”. 2016.
- Li, Q., FENG, H.-j., and Xu, Z.-h. “Image pre-processing techniques for auto focusing”. *Opto-electronic Engineering*, Vol. 9, 2004.
- Liu, Z., Li, X., Li, F., and Zhang, G. “Calibration method for line-structured light vision sensor based on a single ball target”. *Optics and Lasers in Engineering*, Vol. 69, pp. 20–28. 2015.
- LIVE, E., Featuring, E., and Qureshi, S. “Implementing vision capabilities in embedded systems”. 2014.

- Malamas, E. N., Petrakis, E. G., Zervakis, M., Petit, L., and Legat, J.-D. “A survey on industrial vision systems, applications and tools”. *Image and vision computing*, Vol. 21, N. 2, pp. 171–188. 2003.
- Malik, A. W., Thörnberg, B., and Kumar, P. “Comparison of three smart camera architectures for real-time machine vision system”. *International Journal of Advanced Robotic Systems*, Vol. 10, N. 12, p. 402. 2013.
- Martin, W. A. “Method and system for assisting security camera focusing”. 2019. US Patent 10,372,016.
- Moru, D. K. and Borro, D. “A machine vision algorithm for quality control inspection of gears”. *The International Journal of Advanced Manufacturing Technology*, Vol. 106, N. 1-2, pp. 105–123. 2020.
- Muruganantham, C., N, J., Ramamoorthy, B., and D., G. “Optimal settings for vision camera calibration”. *The International Journal of Advanced Manufacturing Technology*, Vol. 42, pp. 736–748. 06, 2008.
- Nair, R., Ruhl, K., Lenzen, F., Meister, S., Schäfer, H., Garbe, C. S., Eisemann, M., Magnor, M., and Kondermann, D. “A survey on time-of-flight stereo fusion”. In *Time-of-Flight and Depth Imaging. Sensors, Algorithms, and Applications*, pp. 105–127. Springer. 2013.
- Nalwa, V. S. and Binford, T. O. “On detecting edges”. *IEEE transactions on pattern analysis and machine intelligence*, N. 6, pp. 699–714. 1986.
- Nevatia, R. “Computer vision systems”. In *Computer vision systems: papers from the Workshop on Computer Vision Systems, held at the University of Massachusetts, Amherst, Massachusetts, June 1-3, 1977*, p. 81. 1978.
- Newman, T. S. and Jain, A. K. “A system for 3d cad-based inspection using range images”. *Pattern Recognition*, Vol. 28, N. 10, pp. 1555–1574. 1995.
- Pedreschi, F., Leon, J., Mery, D., and Moyano, P. “Development of a computer vision system to measure the color of potato chips”. *Food Research International*, Vol. 39, N. 10, pp. 1092–1098. 2006.

- Peng, G., Zhang, Z., and Li, W. “Computer vision algorithm for measurement and inspection of o-rings”. *Measurement*, Vol. 94, pp. 828–836. 2016.
- Rodríguez-Vázquez, A., Domínguez-Castro, R., Jiménez-Garrido, F., and Morillas, S. “A cmos vision system on-chip with multicore sensory processing architecture for image analysis above 1,000 f/s”. In *Sensors, Cameras, and Systems for Industrial/Scientific Applications XI*, volume 7536, p. 75360O. 2010.
- San Choi, K., Lam, E. Y., and Wong, K. K. “Automatic source camera identification using the intrinsic lens radial distortion”. *Optics express*, Vol. 14, N. 24, pp. 11551–11565. 2006.
- Sanz, J. L. *Advances in machine vision*. Springer Science & Business Media. 2012.
- Sevilla, L. *Análisis comparativo y propuesta metodológica para la evaluación de incertidumbres en métodos de medida indirecta de ángulos*. Tesis Doctoral, Universidad de Málaga. 2001.
- Shi, Y. and Lichman, S. “Smart cameras: a review”. In *Proceedings of*, pp. 95–100. 2005.
- Shirvaikar, M. V. “An optimal measure for camera focus and exposure”. In *Thirty-Sixth Southeastern Symposium on System Theory, 2004. Proceedings of the*, pp. 472–475. 2004.
- Singh, K. K. and Singh, A. “A study of image segmentation algorithms for different types of images”. *International Journal of Computer Science Issues (IJCSI)*, Vol. 7, N. 5, p. 414. 2010.
- Steger, C., Ulrich, M., and Wiedemann, C. *Machine vision algorithms and applications*. John Wiley & Sons. 2018.
- Szeliski, R. *Computer vision: algorithms and applications*. Springer Science & Business Media. 2010.
- Thomas, A. D., Rodd, M. G., Holt, J. D., and Neill, C. “Real-time industrial visual inspection: A review”. *Real-Time Imaging*, Vol. 1, N. 2, pp. 139–158. 1995.

- Tian, Y. “Autofocus using image phase congruency”. *Optics express*, Vol. 19, N. 1, pp. 261–270. 2011.
- Wang, D., Ding, X., Zhang, T., and Kuang, H. “A fast auto-focusing technique for the long focal lens tdi ccd camera in remote sensing applications”. *Optics & Laser Technology*, Vol. 45, pp. 190–197. 2013.
- Wang, Z., Wu, Z., Zhen, X., Yang, R., and Xi, J. “An onsite structure parameters calibration of large fov binocular stereovision based on small-size 2d target”. *Optik-International Journal for Light and Electron Optics*, Vol. 124, N. 21, pp. 5164–5169. 2013.
- Wolf, W., Ozer, B., and Lv, T. “Smart cameras as embedded systems”. *computer*, N. 9, pp. 48–53. 2002.
- Zhang, B., Bai, L., and Zeng, X. “A novel subpixel edge detection based on the zernike moment”. *Information Technology Journal*, Vol. 9, N. 1, pp. 41–47. 2010.
- Zhang, H., Fritts, J. E., and Goldman, S. A. “Image segmentation evaluation: A survey of unsupervised methods”. *computer vision and image understanding*, Vol. 110, N. 2, pp. 260–280. 2008.
- Zhang, Y., Zhang, Y., and Wen, C. “A new focus measure method using moments”. *Image and Vision computing*, Vol. 18, N. 12, pp. 959–965. 2000.
- Zhang, Z. “A flexible new technique for camera calibration”. *IEEE Transactions on pattern analysis and machine intelligence*, Vol. 22, 2000.